DEVELOPMENT AND APPLICATION OF THE METHOD OF DISTRIBUTED VOLUMETRIC SOURCES TO THE PROBLEM OF UNSTEADY-STATE FLUID FLOW IN RESERVOIRS

A Dissertation

by

SHAHRAM AMINI

Submitted to the Office of Graduate Studies of
Texas A&M University
in partial fulfillment of the requirements for the degree of

DOCTOR OF PHILOSOPHY

December 2007

Major Subject: Petroleum Engineering

DEVELOPMENT AND APPLICATION OF THE METHOD OF DISTRIBUTED VOLUMETRIC SOURCES TO THE PROBLEM OF UNSTEADY-STATE FLUID FLOW IN RESERVOIRS

A Dissertation

by

SHAHRAM AMINI

Submitted to the Office of Graduate Studies of
Texas A&M University
in partial fulfillment of the requirements for the degree of

DOCTOR OF PHILOSOPHY

Approved by:

Co-Chairs of Committee,	Peter P. Valkó
	Thomas A. Blasingame
Committee Members,	Duane A. McVay
	Richard Gibson
Head of Department,	Stephen A. Holditch

December 2007

Major Subject: Petroleum Engineering

ABSTRACT

Development and Application of the Method of Distributed Volumetric Sources to the Problem of Unsteady-State Fluid Flow in Reservoirs. (December 2007)

Shahram Amini

B.S.; M.S., University of Tehran;

M.S., IFP School (ENSPM)

Co-Chairs of Advisory Committee: Dr. Peter P. Valkó
Dr. Thomas A. Blasingame

This work introduces the method of Distributed Volumetric Sources (DVS) to solve the transient and pseudosteady-state flow of fluids in a rectilinear reservoir with closed boundaries. The development and validation of the DVS solution for simple well/fracture configurations and its extension to predict the pressure and productivity behavior of complex well/fracture systems are the primary objectives of this research.

In its simplest form, the DVS method is based on the calculation of the response for a closed rectilinear system to an *instantaneous* change in a rectilinear, uniform volumetric source inside the reservoir. Integration of this response over the time provides us with the solution to a continuous change (constant-rate pressure response). Using the traditional material balance equations and the DVS pressure response of the system, we can calculate the productivity index of the system in both transient and pseudosteady-state flow periods, which enables us to predict the production behavior over the life of the well/reservoir.

Solutions for more complex situations, such as sources with infinite or finite-conductivity (*i.e.*, a fracture), are provided using discretization of the source. This work considers the case of a complex system with a horizontal well intersecting multiple transverse fractures as an example to show the ability (and flexibility) of the new method. The DVS solution method provides accurate solutions for complex well/fracture configurations — which will help engineers to design and implement optimum well completions.

The DVS solutions has been validated by comparing to existing analytical solutions (where applicable), as well as to numerical (simulation) solutions. In all cases the DVS solution was successfully validated — at least in a practical sense — specifically in terms of the accuracy and precision of the DVS solution. As the DVS method is approximate (at early times), there are small discrepancies which are of little or no practical consequence. In terms of computation times, because of its analytic nature, the DVS method is not always optimal in terms of speed for certain problems, but the DVS approach is similar in computation speed with commercial reservoir simulation programs.

DEDICATION

To my parents,
Abbas Amini and Farideh Gorji,
and to my sisters,
Shohreh and Shahla
— for their love and support

ACKNOWLEDGEMENTS

I would like to thank my co-chairs of advisory committee, Dr. Peter P. Valkó and Dr. Thomas A. Blasingame for their guidance and support. I would like also to thank Dr. Duane A. McVay and Dr. Richard Gibson for serving as committee members and for their valuable contributions to this research.

Finally, I appreciate the support and encouragement of all my Iranian friends in the Department of Petroleum Engineering at Texas A&M University. God bless them all.

TABLE OF CONTENTS

Page

CHAPTER I INTRODUCTION 1
1.1 Introduction 1
1.2 Objectives 1
1.3 Statement of the Problem 2
1.4 Deliverables 3
1.5 Organization of the Dissertation 4
CHAPTER II DEVELOPMENT OF THE DVS METHOD 6
2.1 Literature Review 6
2.2 Development of Uniform-Flux Solution 10
2.3 Solution for Infinite-Conductivity Cases 13
2.4 Solution for Finite-Conductivity Cases 14
2.5 Productivity Index Calculation 20
CHAPTER III VALIDATION OF THE MODEL 23
3.1 Introduction 23
3.2 Validation with Pressure Models 23
3.3 Validation with Productivity Index Models 30
CHAPTER IV APPLICATION OF THE NEW TECHNIQUE TO A COMPLEX WELL/FRACTURE CONFIGURATION CASE 34
4.1 Introduction 34
4.2 Formulation of the Problem 34
4.3 Validation Through Simulation 35
4.4 Design and Optimization 38
4.5 Application to Field Examples 48
4.6 Summary 61
CHAPTER V SUMMARY, CONCLUSIONS, AND RECOMMENDATIONS FOR FUTURE WORK 62
5.1 Summary 62
5.2 Conclusions 62
5.3 Recommendations for Future Work 63

Page

NOMENCLATURE 64
REFERENCES 67
APPENDIX A — DEVELOPMENT OF THE SOLUTION 69
APPENDIX B — DIMENSIONLESS PRODUCTIVITY INDEX FROM PRESSURE DATA 76
APPENDIX C — DETAILED RESULTS OF CALCULATION FOR MAXIMUM DIMENSIONLESS PRODUCTIVITY INDEX OF THE EXAMPLE CASE, PROPPANT NUMBER (N_{PROP}) = 0.001 78
APPENDIX D — DETAILED RESULTS OF CALCULATION FOR MAXIMUM DIMENSIONLESS PRODUCTIVITY INDEX OF THE EXAMPLE CASE, PROPPANT NUMBER (N_{PROP}) = 0.01 89
APPENDIX E — DETAILED RESULTS OF CALCULATION FOR MAXIMUM DIMENSIONLESS PRODUCTIVITY INDEX OF THE EXAMPLE CASE, PROPPANT NUMBER (N_{PROP}) = 0.1 101
APPENDIX F — DETAILED RESULTS OF CALCULATION FOR MAXIMUM DIMENSIONLESS PRODUCTIVITY INDEX OF THE EXAMPLE CASE, PROPPANT NUMBER (N_{PROP}) = 1.0 113
APPENDIX G — COMPLETE RESULTS OF FIELD APPLICATION WHELAN GAS FIELD ... 125
APPENDIX H — COMPLETE RESULTS OF FIELD APPLICATION PERCY WHEELER GAS FIELD 129
APPENDIX I— COMPLETE RESULTS OF FIELD APPLICATION APPLEBY NORTH GAS FIELD 133
VITA 137

LIST OF FIGURES

FIGURE Page

2.1 Schematic of the Model. 11

2.2 Discretized of the Rectangular Source. 13

2.3 Example of 1D Flow in the Source. 15

2.4 Example of 2D Flow in the Source. 15

2.5 Schematic of a Discretized 1D Source. 16

2.6 Schematic of a Finite Difference Presentation of a Continuous System. 18

2.7 Example of Discretized 2D Source 19

2.8 Graphical Representation of the **D** Matrix for 2D Flow in Fracture. 20

3.1 Comparison of the DVS Results with Line Source and Cylindrical Source Solutions: Vertical Well in a Bounded Reservoir (In the Box-in-Box Model $w_z=z_e/2$, $w_x = w_y =0.477$ *ft*, and the actual value of z_e is irrelevant) 24

3.2 Comparison of DVS Results with Yildiz's Model for a Partially-Penetrating Vertical Well (Box-in- Box Model),(h, h_p, and h_b are represented by z_e, $2w_z$, and c_z- w_z respectively) 25

3.3 Comparison of DVS Results with Ozkan's and Gringarten's Solutions for a Horizontal Well in a Bounded Reservoir, Uniform Flux Solution (In the Box-in-Box Model $x_{eD}= x_e/w_x$, $y_{eD}= y_e/w_x$, and $L_D= z_e/w_x$) 26

3.4 Comparison DVS Results with Gringarten, Ramey and Raghavan (1974) Solution for a Vertically Fractured Well in a Bounded Reservoir; Uniform Flux Solution ($x_{eD}= x_e/w_x$ in the Box-in-Box Model) 28

3.5 Comparison of DVS Results with Gringarten, Ramey and Raghavan (1974) Solution for a Vertically Fractured Well in Bounded Reservoir; Infinite Conductivity Solution. ($x_{eD}= x_e/w_x$ in the Box-in-Box Model) 28

3.6 Comparison of DVS with Cinco-Ley, Samaniego, and Dominguez (1978) Results for Finite Conductivity Fracture 29

3.7 Distribution of the Contribution of Different Segments to Total Production at Various Times, Finite Conductivity Vertical Fracture of Full Vertical Penetration for Half the Fracture (C_{fD} =1.6 and I_x = 0.25) 29

3.8 Dimensionless Productivity Index of a Vertically Fully Penetrated Fracture as a Function of Fracture Conductivity and Proppant Number (From Economides, Oligney, and Valkó 2002) 32

3.9 Dimensionless Productivity Index of the Example Case Using DVS Method 33

4.1 Schematic of the Model's Building Block. 34

FIGURE Page

4.2 A 3D View of ¼ of the Simulation Model, (Case of 4 Transverse Fractures) 36
4.3 Simulation Output, Well Bottomhole Pressure and Average Reservoir Pressure for Cases of 1 Fracture and 4 Fractures..... 37
4.4 Comparison Between Simulation Results and DVS Method's..... 37
4.5 Distribution of Dimensionless Productivity Index as a Function of Number of Fractures..... 42
4.6 Fracture Contribution to Flow as a Function of Dimensionless Time and Number of Fractures (N_{Prop} = 1.0, $k_x = k_y = k_z$ =1 md).....43
4.7 Fracture Contribution to Flow as a Function of Dimensionless Time and Number of Fractures ($k_x = k_y$ = 1 md, k_z =0.1 md). 43
4.8 Fracture Contribution to Flow as a Function of Dimensionless Time and Number of Fractures ($k_x = k_y$ = 1 md, k_z =0.01 md). 44
4.9 Fracture Contribution to Flow as a Function of Dimensionless Time and Number of Fractures ($k_x = k_y$ = 1 md, k_z =0.001 md).....44
4.10 Maximum Dimensionless Pseudosteady-State Productivity Index as a Function of Number of Fractures and Proppant Number ($k_x = k_y = k_z$ =1 md) 46
4.11 Maximum Dimensionless Pseudosteady-State Productivity Index as a Function of Number of Fractures and Proppant Number ($k_x = k_y$ = 1 md, k_z =0.1 md). 46
4.12 Maximum Dimensionless Pseudosteady-State Productivity Index as a Function of Number of Fractures and Proppant Number ($k_x = k_y$ = 1 md, k_z =0.01 md). 47
4.13 Maximum Dimensionless Pseudosteady-State Productivity Index as a Function of Number of Fractures and Proppant Number ($k_x = k_y$ = 1 md, k_z =0.001 md). 47
4.14 Gas Production Rate as a Function of Production Time, Number of Fractures, and Completion Scheme for Whelan Field (80 Acres Spacing, 250,000 lb Proppant) 52
4.15 Gas Production Rate as a Function of Production Time, Number of Fractures, and Completion Scheme for Percy Wheeler Field (80 Acres Spacing, 250,000 lb Proppant)..... 53
4.16 Gas Production Rate as a Function of Production Time, Number of Fractures, and Completion Scheme for Percy Wheeler Field (80 Acres Spacing, 500,000 lb Proppant)..... 53
4.17 Gas Production Rate as a Function of Production Time, Number of Fractures, and Completion Scheme for Appleby North Field (80 Acres Spacing, 250,000 lb Proppant)..... 54
4.18 Gas Production Rate as a Function of Production Time, Number of Fractures, and Completion Scheme for Appleby Nprth Field (80 Acres Spacing, 500,000 lb Proppant)..... 54
4.19 Average Reservoir Pressure as a Function of Production Time, Number of Fractures, and Completion Scheme for Whelan Field (80 Acres Spacing, 250,000 lb Proppant) 55

FIGURE Page

4.20 Average Reservoir Pressure as a Function of Production Time, Number of Fractures, and Completion Scheme for Percy Whelan Field (80 Acres Spacing, 500,000 lb Proppant) 56
4.21 Average Reservoir Pressure as a Function of Production Time, Number of Fractures, and Completion Scheme for Appleby North Field (80 Acres Spacing, 250,000 lb Proppant)..... 56
4.22 Average Reservoir Pressure as a Function of Production Time, Number of Fractures, and Completion Scheme for Appleby North Field (80 Acres Spacing, 500,000 lb Proppant)..... 57
4.23 Cumulative Gas Production as a Function of Production Time, Number of Fractures, and Completion Scheme for Whelan Field (80 Acres Spacing, 250,000 lb Proppant) 57
4.24 Cumulative Gas Production as a Function of Production Time, Number of Fractures, and Completion Scheme for Whelan Field (80 Acres Spacing, 500,000 lb Proppant) 58
4.25 Cumulative Gas Production as a Function of Production Time, Number of Fractures, and Completion Scheme for Percy Wheeler Field (80 Acres Spacing, 250,000 lb Proppant) 59
4.26 Cumulative Gas Production as a Function of Production Time, Number of Fractures, and Completion Scheme for Percy Wheeler Field (80 Acres Spacing, 500,000 lb Proppant) 59
4.27 Cumulative Gas Production as a Function of Production Time, Number of Fractures, and Completion Scheme for Appleby North Field (80 Acres Spacing, 250,000 lb Proppant)..... 60
4.28 Cumulative Gas Production as a Function of Production Time, Number of Fractures, and Completion Scheme for Appleby North Field (80 Acres Spacing, 500,000 lb Proppant)..... 60

LIST OF TABLES

TABLE Page

3.1 Reservoir/Fluid Properties Used for Example Cases of Chen and Asaad (2003) (Comparison of Different Pseudosteady-State Productivity Index Correlations)..... 30

3.2 Comparison of DVS Results with Various Pseudosteady-State Productivity Index Correlations. 31

4.1 Reservoir, Fracture, and Fluid Characteristic Used for Simulation Model and DVS Calculations. 35

4.2 Reservoir and Proppant Characteristics Used for Case Study. 38

4.3 Range of Variation of Design Parameters. 39

4.4 Table of Mathematically Feasible Fracture Sizes for Example Case. 40

4.5 Locus of Maxima for Example as a Function of Number of Fractures and Permeability Anisotropy (N_{Prop} = 1.0). 42

4.6 Reservoir and Fluid Properties for Example Cases. 48

4.7 Initial Gas-in-Place (G) for Example Cases. 48

4.8 Optimum Fracture Dimensions for Field Cases as a Function of Proppant Used and Number of Fractures. Fully-Penetrating Horizontal Well Contributes to Flow. 49

4.9 Results of Field Case Studies, Average Reservoir Pressure, Gas Production Rate, and Cumulative Gas Production as a Function of the Amount of Proppant, Number of Fractures, and Completion Schemes for Example Cases. 51

CHAPTER I

INTRODUCTION

1.1 Introduction

In this work we present the development and application of a new solution to the problem of unsteady-state flow of a slightly compressible fluid in a rectilinear reservoir. The method of Distributed Volumetric Sources (DVS) is developed to solve problems of transient and pseudosteady-state fluid flow. The basic building block of the method is the calculation of the analytical response of a rectilinear reservoir with closed outer boundaries to an *instantaneous volumetric source*, also shaped as a rectilinear body (a rectilinear geometry is required for the DVS approach). The DVS solution provides the time-derivative of the pressure response to a continuous source in analytical form (*i.e.*, the derivative of the constant rate pressure response function). This result is integrated over time to provide the required pressure response.

The results from the new solution are combined with the traditional material balance equations and are used to predict the production behavior of the system in the form of the dimensionless Productivity Index (PI) — for transient, transition, and pseudosteady-state flow behavior (flow regimes). This approach can be used to design optimal completion schemes for a specific well/reservoir configuration.

The new method has been shown to provide a relatively fast and uniformly robust mechanism to generate pressure transient solutions and well performance predictions whenever complex well/fracture configurations are considered.

1.2 Objectives

The following objectives are proposed for this work:

- To develop the distributed volumetric source (or DVS) method as a solution to the problem of pressure distributions in closed, rectangular reservoirs for the case of a uniform-flux source.
- To develop and validate a series of solutions for pressure behavior of simple and complex well/fracture configurations such as:
  - Unfractured vertical wells.
  - Horizontal wells (uniform-flux and infinite-conductivity).
  - Vertically fractured wells (infinite- and finite-conductivity fractures).
- To generate the transient and pseudosteady-state behavior of the productivity index using the DVS pressure solution and to validate these results with existing models used in production engineering.

This dissertation follows the style and format of the *SPE Journal*.

- To demonstrate the applicability of the new solution method in predicting pressure and production behavior for a complex well/fracture configuration.

  —Horizontal well with multiple transverse fractures, where both horizontal section and fractures contribute to the flow.

- To apply the new method as an optimization tool to obtain the best completion scheme for development of an example case.

1.3 Statement of the Problem

Most of the solutions for flow problems in porous media have been investigated in a similar manner as the classical heat transfer problems — and in fact, many common solutions originated from the heat transfer literature. Along that path, the work of Gringarten and Ramey (1973) is an early application of the Green's (source) function for the problem of unsteady-state fluid flow in a reservoir. They introduced Green's functions for a series of source shapes and boundary conditions and they showed that the point source solution is actually a more general form of the Green's function. Gringarten and Ramey (1973) used the integration of the response for an instantaneous source solution to obtain the response for a continuous source solution. In addition, the application of Newman's (1936) principle in expressing a problem into 3 dimensions as the product of three 1-dimensional solutions is also discussed in their work.

The major disadvantage of this method is the inherent singularity of the solution where the source is placed. Since the source is assumed to have no volume (point, line, or plane source), the source is considered to be at infinite pressure at any time and it is not possible to calculate the exact pressure as a function of time at the point where the source is placed. The solutions provided for finite reservoir cases yield infinite series, which converge very slowly as we approach the coordinates of the source. This makes the process of computation inefficient as we approach the source. To address this problem, we must assume an arbitrary point a certain distance from the source, and compute the solution at that point. The solution obtained by using this method is only a function of the distance from the source, regardless of the coordinates, so it may raise questions as to the reliability of the solution for anisotropic systems and/or complex well completion schemes.

The application of Green's functions was later extended to the case of an unsteady-state pressure distribution for more complex well completion schemes (Gringarten, Ramey, and Raghavan 1974; Cinco-Ley, Samaniego, and Dominguez 1978; Cinco-Ley and Meng 1988; Ozkan 1988). These solutions do not suffer the singularity problem (because the line source solution is integrated over the length or area of the source) but these solutions still require reference points from which to perform calculations. Moreover, the assumption of the source not having a volume has led us to develop different solutions for each special case.

The DVS method was developed to remove this singularity problem and provide a faster and more reliable solution to the problems of transient and pseudosteady-state fluid flow in a reservoir with closed boundaries. In the DVS method, every source, regardless of its size and dimensions, is assumed to contain a volume. In this case, the initial value of pressure in the source is *never infinite*. This assumption provides the opportunity to treat any kind of source in a similar way — in other words, the DVS solution for a uniform-flux source is unique no matter whether it is a point, a vertical or horizontal well with partial penetration, or a well with a vertical fracture.

The main concept in this research is to introduce an instantaneous volumetric source inside the reservoir and then to construct the analytical 3-dimensional response of the system as a product of three 1-dimensional responses based on Newman's principle. This solution approach will yield the well-testing (time) derivative of the response to a continuous source, in an analytical form. This result can be integrated over time to provide the pressure response for a continuous source.

In production engineering application, the productivity of a well is calculated using the pressure response of the reservoir in its pseudosteady-state period. There are numerous studies for different well completion schemes — such as horizontal wells and fractured wells — where correlations for the pseudosteady-state productivity index are provided for specific cases. Most of the models developed for complex well completion schemes use some type of approximation(s) for the productivity index calculation, and as such, have some limitations in practice.

The need for an analytical form of the productivity index (*i.e.*, a solution that is valid for all times) is necessitated by the exploitation of lower quality reservoirs (low- and ultra low-permeability reservoirs to be exact) where transient flow dominates and pseudosteady-state productivity calculations are less applicable in prediction of the production behavior of the reservoir. The DVS method seems able to fill this gap, as it can provide the solution for the productivity index of a general well completion scheme for transient as well as pseudosteady-state flow.

1.4 Deliverables

The general derivation of the DVS method and its application to productivity index calculation are presented in **Chapter II**, **Appendix A,** and **Appendix B**. To demonstrate the effectiveness of the DVS method in the prediction of the pressure and production behavior of different systems, the DVS results have been compared to the existing (analytical) models for the following cases (**Chapter III**):

- Unfractured vertical wells
- Horizontal wells (uniform-flux and infinite-conductivity).
- Vertically fractured wells (infinite- and finite-conductivity fractures).

Comparisons are also made with well-known models for the productivity index: (Chapter III)

- Horizontal wells
- Vertically-fractured wells

Chapter IV provides the application of the new method in the prediction of the behavior of complex well/fracture systems. Specifically, the case of a horizontal well with multiple transverse fractures is studied where both the horizontal well section and fractures contribute to the flow. This case is validated using a commercial reservoir simulator. The DVS and reservoir simulation results compare well, and we note for comparison that the DVS computation times are comparable to the reservoir simulation times. However, the advantage of the DVS method is the "analytic" nature of this method, which means that the DVS method can be used for design, analysis, modeling, and optimization. While not an objective of this dissertation, the DVS method may be useful for developing approximate, closed-form solutions for complex well/fracture systems.

In Chapter IV we provide the results of a study to develop an optimum completion scheme, along with the correlation plots used to assess the optimal well completion scheme. The detailed calculations for cases with different proppant number are provided in **Appendices C through F**. Specifically, the optimum dimensionless productivity index (based on the constant rate DVS method) is integrated with the material balance equation to provide reservoir performance predictions for cases producing at constant bottomhole pressure. The results of three gas field examples are provided in **Appendices G through I**.

A summary of the research results and the conclusions of this work are discussed in **Chapter V**.

1.5 Organization of the Dissertation

The outline of the proposed dissertation is as follows:

- Chapter I — Introduction
  - Introduction
  - Objectives
  - Statement of the Problem
  - Deliverables
- Chapter II — Development of the DVS Method
  - Literature Review
  - Development of Uniform-Flux Solution
  - Solution for Infinite Conductivity Cases
  - Solution for Finite-Conductivity Cases
  - Productivity Index Calculation
- Chapter III — Validation of the Model
  - Comparison with Existing Pressure Models
  - Comparison with Existing Productivity Index Models

- Chapter IV — Application of the New Technique to a Complex Well/Fracture Configuration Case
  - Introduction
  - Formulation of the Problem
  - Validation through Simulation
  - Design and Optimization
  - Application to Field Examples
  - Summary
- Chapter V — Summary, Conclusions, and Recommendations for Future Work
  - Summary
  - Conclusions
  - Recommendations for future work
- Nomenclature
- References
- Appendices
  - Appendix A — Detailed Derivation of the DVS Method
  - Appendix B — Derivation of Productivity Index from Pressure Data
  - Appendix C — Detailed Results of Calculation for Maximum Dimensionless Productivity Index of the Example Case, Proppant Number (N_{prop}) = 0.001
  - Appendix D — Detailed Results of Calculation for Maximum Dimensionless Productivity Index of the Example Case, Proppant Number (N_{prop}) = 0.01
  - Appendix E — Detailed Results of Calculation for Maximum Dimensionless Productivity Index of the Example Case, Proppant Number (N_{prop}) = 0.1
  - Appendix F — Detailed Results of Calculation for Maximum Dimensionless Productivity Index of the Example Case, Proppant Number (N_{prop}) = 1.0
  - Appendix G — Complete Results of Field Application Whelan Gas Field
  - Appendix H — Complete Results of Field Application Percy Wheeler Gas Field
  - Appendix I — Complete Results of Field Application Appleby North Gas Field
- Vita

CHAPTER II

DEVELOPMENT OF THE DVS METHOD

2.1 Literature Review

As noted earlier, Gringarten and Ramey (1973) provided the first application of the Green's function approach to the problem of unsteady-state fluid flow in the reservoirs. The general form of the diffusivity equation is written as:

$$\eta \nabla^2 p(M,t) - \frac{\partial p(M,t)}{\partial t} = 0 \tag{2.1}$$

For production at a prescribed flowrate and homogeneous boundary conditions (constant pressure, constant rate, or a mix of those conditions), They state that the variation of pressure at each point $M(x, y, z)$ and time t can be described using a proper Green's function (if available) as follows:

$$\begin{aligned}\Delta p(M,t) = {} & \frac{1}{\phi c_t} \int_0^t \int_{D_w} q(M_w,\tau) G(M,M_w,t-\tau)\, dM_w\, d\tau \\ & - \eta \int_0^t \int_{S_e} \{ \frac{\partial p(M',\tau)}{\partial n(M')} G(M,M',t-\tau) - p(M',\tau) \frac{\partial G(M,M',t-\tau)}{\partial n(M')} \} dS_e(M')\, d\tau\end{aligned} \tag{2.2}$$

Where

$$\Delta p(M,t) = \int_D p(M',0) G(M,M',\tau)\, dM' - p(M,t) \tag{2.3}$$

And assuming a uniform initial pressure (p_i), we have:

$$\Delta p(M,t) = p_i - p(M,\tau) \tag{2.4}$$

In the equations given above, M' and τ are integration variables; D, D_w, and S_e denote reservoir domain, source domain, and boundaries respectively.

The *instantaneous Green's function* (*i.e.*, the Green's function corresponding to an instantaneous source of unit strength) is written for an infinite one-dimensional, linear reservoir with uniform initial pressure and constant pressure boundaries as follows:

$$G(i,i',t) = \frac{1}{2\sqrt{\pi \eta_i t}} \exp\left[-\frac{(i-i')^2}{4\eta_i t} \right] \tag{2.5}$$

Where the source is assumed to located at point i'. Gringarten and Ramey also showed that the proposed function meets all the properties expected for a Green's function.

As the system is infinite, with only a single instantaneous point source, the first integral of the right hand side of Eq. 2.2 becomes a point and the second integral vanishes. In this case, we can write the following expression for the pressure variation:

$$\Delta p(i,t) = \frac{1}{\phi c_t} G(i,i',t) = \frac{1}{2\phi c_t \sqrt{\pi \eta_i t}} \exp\left[-\frac{(i-i')^2}{4\eta_i t} \right] \tag{2.6}$$

After developing the response for an infinite one-dimensional system with an instantaneous source, Gringarten and Ramey discuss the fact that developing a general solution for a continuous source is possible by integrating the instantaneous source response over time. They also developed solutions for constant rate or constant pressure boundary conditions for finite reservoir systems using the method of images. Gringarten and Ramey (1973) also discussed the applicability of Newman's principle and demonstrated the application of this principle where the solution for a 3-dimensional reservoir system can be obtained as the product of the solutions for three 1-dimensional reservoir systems. They used this approach to generate a series of solutions for different cases of boundary conditions and different source shapes (uniform-flux sources only).

The application of Green's function was later extended by Gringarten, Ramey, and Raghavan (1974) to the case of an unsteady-state pressure distribution created by a vertical well with an infinite conductivity vertical fracture. They generated this solution by dividing the fracture into *M* segments, assuming each segment as a uniform-flux source. Writing the pressure response as the sum of the variations caused by each uniform-flux segment (*i.e.*, the superposition principle) yields:

$$p_i - p(x,y,t) = \frac{1}{\phi c_t} \int_0^t \left\{ \begin{array}{l} \displaystyle\sum_{m=1}^{M} q_m(\tau) \int_{\frac{(m-1)x_f}{M}}^{\frac{mx_f}{M}} \exp\left[-\frac{(x-x_w)^2 + y^2}{4\eta(t-\tau)} \right] dx_w \\ \displaystyle -\sum_{m=1}^{M} q_m(\tau) \int_{-\frac{(m-1)x_f}{M}}^{-\frac{mx_f}{M}} \exp\left[-\frac{(x-x_w)^2 + y^2}{4\eta(t-\tau)} \right] dx_w \end{array} \right\} d\tau \tag{2.7}$$

Assuming an infinite conductivity vertical fracture leads to the condition where the pressure must be constant along the fracture-face (which is in contact with the reservoir). Equating the pressure response caused by each uniform-flux segment, and imposing the constant rate constraint implies that:

$$\begin{cases} \Delta p(\dfrac{2j-1}{2M}x_f,0,t) = \Delta p(\dfrac{2j+1}{2M}x_f,0,t),\ j=1,M-1 \\ 2\sum_{m=1}^{M} q_m(\dfrac{x_f}{M})h = q_f \end{cases} \tag{2.8}$$

Gringarten, Ramey, and Raghavan (1974) provided the solution to the system of equations (which yields the pressure distribution and the contribution of each segment to the total flow) for two conditions — one early-time condition where the assumption of uniform-flux fracture is valid, and a late-time condition where the contributions from each segment (q_m) are stabilized (*i.e.*, no longer a function of time).

As an aside, they also provided the solution for a uniform-flux fracture in a finite reservoir with no-flow boundary. They also showed that the solution to pressure behavior for an infinite-conductivity fracture in the same closed boundary reservoir can be calculated at the point $x = 0.732\ x_f$ of the uniform-flux case.

Following this effort, Cinco-Ley, Samaniego, and Dominguez (1978) developed the solution for a well with a finite-conductivity vertical fracture in an infinite-acting reservoir using the discretized fracture approach and application of the Green's function for the pressure solution for the reservoir. Equating the pressure and flow between the reservoir and the fracture leads to a system of equations that can be solved using the discretization of Eq. 2.8 in both space and time.

Later, Cinco-Ley and Meng (1988) introduced a more general solution for the pressure transient behavior of a finite-conductivity hydraulic fracture in a dual-porosity medium in the Laplace domain. They used the application of the source and Green's function in calculation of the fracture pressure (Eq. 2.9) in combination with a pressure drop function for calculation of pressure losses because of the fluid flow in the finite-conductivity vertical fracture (Eq. 2.10).

$$p_{fD}(x_D,t_{Dxf}) = \frac{1}{4}\int_0^{t_D}\int_{-1}^{1} q_{fD}(x',\tau)\frac{\exp\left[-\dfrac{(x_D-x')^2}{4(t_{Dxf}-\tau)}\right]}{(t_{Dxf}-\tau)}dx'd\tau \tag{2.9}$$

$$p_{wD}(t_{Dxf}) - p_{fD}(x_D,t_{Dxf}) = \frac{\pi}{(k_f b_f)_D}\left[x_D - \int_0^{x_D}\int_{-1}^{1} q_{fD}(x'',t_{Dxf})dx''dx'\right] \tag{2.10}$$

It should be noted that Eq. 2.10 *is derived assuming incompressible flow in the fracture* — which was shown by Cinco-Ley, Samaniego, and Dominguez (1978) to be valid for practical values of production time.

Using the Laplace transform of the Eq. 2.10 and discretization of the integrals in the space, Cinco-Ley and Meng (1988) developed the following result:

$$\bar{p}_{wD}(s)-\frac{1}{2}\sum_{i=1}^{n}\bar{q}_{fDi}(s)\int_{x_{Di}}^{x_{Di+1}}[K_0(x_{Dj}-x')\sqrt{sf(s)}+K_0(x_{Dj}+x')\sqrt{sf(s)}]dx' \\ +\frac{\pi}{(k_f b_f)_D}\sum_{i=1}^{j-i}[\frac{(\Delta x)^2}{2}+(x_{Dj}-i\Delta x)]\bar{q}_{fDj}(s)+\frac{(\Delta x)^2}{8}\bar{q}_{fDj}(s)=\frac{\pi}{(k_f b_f)_D s}x_{Dj} \tag{2.11}$$

Combining Eq. 2.11 with the identity for the sum of dimensionless rates to be equal to unity, and writing this identity in the form of the Laplace transform yields:

$$\sum_{i=1}^{n}\bar{q}_{fDi}(s)=\frac{1}{s} \tag{2.12}$$

Combining Eq. 2.11 and Eq. 2.12 leads to a system of (n+1) equations and (n+1) unknowns — which represents the contribution of flow from each fracture segment to the total flow and the dimensionless wellbore pressure.

A new form of the point source solution was introduced by Ozkan (1988) where he developed a point source solution in Laplace domain in order to remove the limitations of the Gringarten and Ramey (1973) model in considering the wellbore storage and skin effects. Obtaining the solution for a dual-porosity medium was made possible using this new solution in Laplace domain. The Ozkan's source function approach lets the user obtain solutions for a wide variety of complex well and/or fracture configurations, but this approach is limited to the infinite conductivity and uniform-flux cases.

Yildiz and Bassiouni (1991) developed the transient pressure solution for a partially-penetrating well using the combination of Laplace transformation and the method of separation of variables. The solution is expressed in the form of infinite Fourier-Bessel series in the Laplace space.

Azar-Nejad, Tortike, and Farouq-Ali (1996a, 1996b, 1996c) studied the steady-state and transient potential distribution around sources with a finite length using the point source solution (developed by Muskat), for the cases of uniform flux and uniform potential (infinite conductivity). They introduced the Discrete Flux Element (DFE) method similar to the discretization of source used by Gringarten, Ramey, and Raghavan (1974) and Cinco-Ley, Samaniego, and Dominguez (1978) to model the infinite and finite-conductivity fractures, respectively. Azar-Nejad, Tortike, and Farouq-Ali (1996a, 1996b, 1996c) applied their model to predict the productivity index for partially-penetrated vertical wells as well as horizontal wells. The method was then extended to wells with irregular geometries to evaluate the effect of the well path on productivity index of such wells.

The estimation of the productivity performance for well/fracture systems has been subject of numerous studies. Some of these studies are reviewed for this work to illustrate the methods used and to provide a basis for comparing the results from our new DVS method to the results which can be obtained from the existing models.

Babu and Odeh (1989) developed a general, approximate method for prediction of the productivity of a horizontal well in a rectilinear reservoir of closed or constant pressure boundary. The Babu-Odeh solution uses a Fourier series solution for the rate-dependent pressure solution and this result requires several simplifying assumptions in order to obtain an expression for the pseudosteady-state productivity for a horizontal well in an anisotropic homogeneous medium. In such cases, the Babu-Odeh solution is very similar to the results developed for a vertical well. Babu and Odeh (1989) report an estimated error of 3 to 10 percent, depending on the penetration ratio of the well.

Goode and Kuchuk (1991) introduced another solution for productivity of a horizontal well in a reservoir with no-flow and constant-pressure boundaries. Their solution is expressed in the form of an infinite series and a simplified solution for a "short" horizontal well was presented in their study.

Chen and Asaad (2005) developed a rigorous solution for estimation of the productivity of horizontal wells as well as fractured wells for both uniform-flux and uniform-pressure (infinite conductivity). They presented a rigorous (analytical) solution as well as simplified forms (for estimating the productivity index for the various wellbore conditions).

Economides, Oligney, and Valkó (2002) present a discussion regarding the optimal design of a hydraulic fracture treatment job. They present graphs describing how the *dimensionless productivity index* can change as a function of fracture conductivity, proppant number, and the penetration ratio — for a system consisting of a fully-penetrating vertical fracture in a square (closed) reservoir.

Meyer and Jacot (2005) provide a new solution methodology for the estimation of the pseudosteady-state productivity index based on a formulation which uses a reservoir/fracture "domain resistivity" concept. This solution is capable of accounting for piece-wise continuous linearly-varying fracture conductivity, which enables us to consider the effects of skin, proppant tail-ins, over-flushing, and chocked flow.

2.2 Development of Uniform-Flux Solution

The first step of our approach is to develop the pressure response of a rectilinear reservoir with closed boundaries for an instantaneous withdrawal from the source. The porous media is assumed to be an anisotropic, homogeneous reservoir (shaped like a box). The "box" is oriented in line with the three principal directions of the permeability field. The source is assumed to be a smaller rectilinear box with

its surfaces parallel to the reservoir boundaries. The "source box" is assumed to have the same properties as the reservoir. The schematic of the basic DVS system is shown in **Fig. 2.1**.

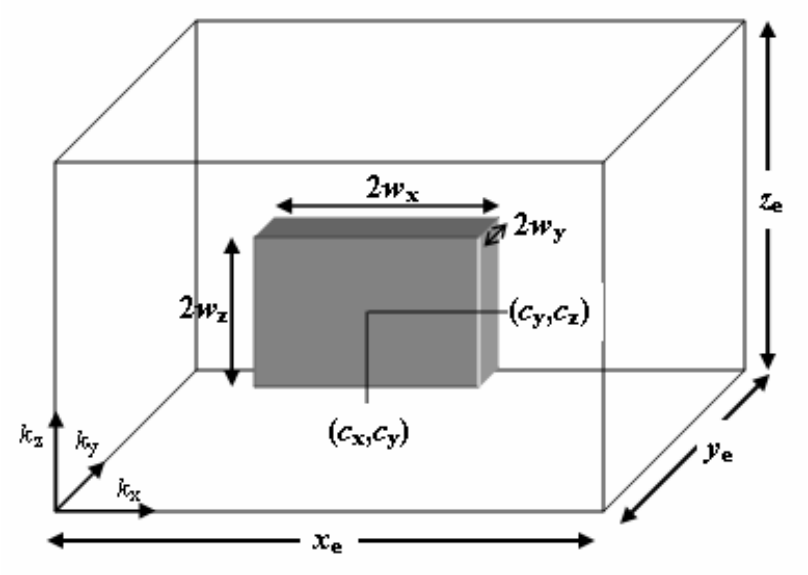

Figure 2.1 — Schematic of the Model.

The instantaneous (unit) withdrawal is distributed uniformly in the volume of the source. This assumption is unique to the DVS model and is the fundamental characteristic of this approach.

As shown in Fig. 2.1, the model is described with the following parameters:

- Reservoir dimensions in the *x*, *y*, and *z* directions respectively (x_e, y_e, z_e).
- Reservoir permeability in principal axes (k_x, k_y, k_z).
- Coordinates of the center point of the source (c_x, c_y, c_z).
- The half-lengths of the source in the *x*, *y*, and *z* directions respectively (w_x, w_y, w_z).

The pressure response for an instantaneous source at any point (x_D, y_D, z_D) is referred to in dimensionless form as $p_{\delta D}(box-pars; x_D, y_D, z_D, t_D)$. For this "box-in-box" method. the *box-pars* variable contains all the parameters needed to properly describe the reservoir model.

For an anisotropic, homogeneous reservoir with an internal source, the diffusivity equation can be written as:

$$\eta_x \frac{\partial^2 p}{\partial x^2} + \eta_y \frac{\partial^2 p}{\partial y^2} + \eta_z \frac{\partial^2 p}{\partial z^2} + \frac{1}{\phi c_t} Q(x, y, z, t) = \frac{\partial p}{\partial t} \tag{2.13}$$

Where the following initial and boundary conditions are used in this work:

Initial Condition (IC): (uniform pressure in the reservoir system)

$$p(x,y,z,0) = p_i \tag{2.14}$$

Boundary Conditions (BC):

$$\begin{aligned}
\left.\frac{\partial p}{\partial x}\right|_{x=0} &= \left.\frac{\partial p}{\partial x}\right|_{x=x_e} = 0 \\
\left.\frac{\partial p}{\partial y}\right|_{y=0} &= \left.\frac{\partial p}{\partial y}\right|_{y=y_e} = 0 \\
\left.\frac{\partial p}{\partial z}\right|_{z=0} &= \left.\frac{\partial p}{\partial z}\right|_{z=z_e} = 0
\end{aligned} \tag{2.15}$$

Where

$$\eta_i = \frac{k_i}{\phi\mu c_t},\ i = x, y, \text{ and } z \tag{2.16}$$

And $Q(x,y,z,t)$ in **Eq. 2.13** is the source function — which, for the instantaneous source, is written as:

$$\begin{aligned}
Q(x,y,z,t) = \frac{qB}{8w_x w_y w_z}\delta(t)&[H(x-c_x-w_x)-H(x-c_x+w_x)] \\
&\times[H(y-c_y-w_y)-H(y-c_y+w_y)] \\
&\times[H(z-c_z-w_z)-H(z-c_z+w_z)]
\end{aligned} \tag{2.17}$$

$\delta(t)$ and $H(x)$ in Eq. 2.17 represent the Dirac delta function and the Heaviside unit-step function, respectively. The homogeneity of the diffusivity equation and its boundary conditions dictates that the 3D pressure derivative solution can be obtained using Newman's principle (a product of three 1D solutions.

$$p_{\delta D}(x_D, y_D, z_D, t_D) = X(x_D, t_D)Y(y_D, t_D)Z(z_D, t_D) \tag{2.18}$$

In Eq. 2.18, the *X*, *Y*, and *Z* terms represent the solutions of 1D problems (in *X*, *Y*, and *Z*) with the source distributed along a finite section of the "linear" reservoir. The detailed derivation of the DVS solution is provided in Appendix A. The final form of 1D solution is written as:

$$\begin{aligned}
I(i_D, t_D) = 1 + \sum_{n=1}^{\infty} &\frac{[\sin(n\pi(i_D - c_{iD} + w_{iD})) - \sin(n\pi(i_D - c_{iD} + w_{iD}))]}{n\pi w_{iD}}\cos(n\pi i_D) \\
&\times\exp\left[-n^2\pi^2\frac{k_i}{k}\left(\frac{i_e}{L}\right)^2 t_D\right]
\end{aligned} \tag{2.19}$$

To obtain the response of the reservoir for a *continuous unit source*, distributed uniformly in the small (source) box, we numerically integrate the pressure derivative solution over time:

$$p_{uD}(x_D, y_D, z_D, t_D) = \int_0^{t_D} p_{\delta D}(x_D, y_D, z_D, \tau) d\tau \tag{2.20}$$

To obtain the wellbore flowing pressure, we can calculate $p_{uD}(x_D, y_D, z_D, t_D)$ *at the geometric center of the well*. Since the solution is not singular, we do not have to select an arbitrary surface point (as is ordinarily done with Green's function solutions).

2.3 Solution for Infinite-Conductivity Cases

In the cases where we have an infinite or finite conductivity condition (*e.g.*, horizontal wells and wells with hydraulic fractures) we must divide the source into *n* uniform-flux segments as prescribed in (Gringarten, Ramey, and Raghavan 1974; Cinco-Ley, Samaniego, and Dominguez 1978; Cinco-Ley and Meng 1988). **Fig. 2.2** shows an example of how the source in Fig. 2.1 can be discretized into 9 segments.

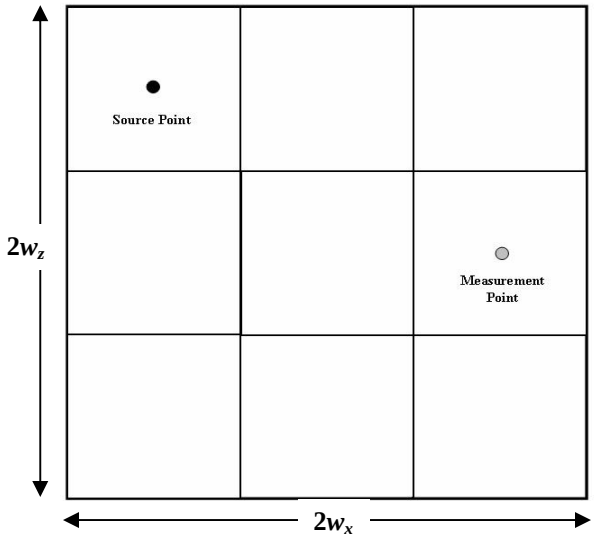

Figure 2.2 — Discretization of the Rectangular Source.

For a source with an infinite conductivity, our primary assumption is that of a uniform pressure over the source. Knowing that the pressure at each segment of the source is defined as the sum of the pressure drops for the other segments (*i.e.*, the superposition of pressure effects), we can write:

$$p_{Di} = \sum_{j=1}^{n} q_{Dj} p_{Di,j} \tag{2.21}$$

In Eq. 2.21, q_{Dj} represents the source strength of the segment j and $p_{Di,j}$ represents the dimensionless pressure calculated at the center of segment i as if the source is put in the segment j. Fig. 2.2 presents an example of how $p_{D1,6}$ is calculated. The pressure $p_{Di,j}$ can be calculated using the uniform flux solution for a continuous source as introduced in Section 2.2. The problem can be written in the matrix form as:

$$[\mathbf{A}]\cdot\mathbf{q}-\mathbf{b}=\mathbf{0} \tag{2.22}$$

We use the notation **A** to describe these ($n \times n$) matrices containing $p_{Di,j}$ terms as its elements. **q** is the vector of source strengths and **b** is the vector where its elements are all equal to $p_{D,wf}$ (the wellbore flowing pressure) since all dimensionless pressures are equal because of the infinite conductivity assumption. The calculation procedure for cases with an infinite conductivity source is as follows:

1. Divide the source into proper number of segments (n)
2. Construct the matrix of $p_{Di,j}$ terms for the series of dimensionless time values as discussed in Section 2.2 and Appendix A. At this stage we should have m matrices of size ($n \times n$) where m represents the number of time steps at which we would like to calculate the pressure responses.
3. For each time step, calculate the source strength vector as the normalized sum of the columns of the pseudo-inverse of its corresponding **A** matrix.
4. Calculate the dimensionless pressure using Eq. 2-21.

In the cases where we use infinite- or finite- conductivity sources, we assume *pseudosteady-state flow in the source* — which means that there is no accumulation of mass in the source. This enables us to solve the **A** matrix independently for each time step.

2.4 Solution for Finite-Conductivity Cases

For the cases with a finite conductivity source we use the same approach as the infinite conductivity source case except that we now have to introduce another term to account for the pressure drop between source segments (because of the finite conductivity of the source term). The matrix notation for this system is given by:

$$[\mathbf{A}+\mathbf{C}]\cdot\mathbf{q}-\mathbf{b}=\mathbf{0} \tag{2.23}$$

The $(i,j)^{th}$ element of the **C** matrix describes the pressure drop in the fracture between the center of the i^{th} source and the wellbore reference point due to the j^{th} inflow. It contains — as a factor — the conductivity of the well. The vector **b** contains the unknown pressure drawdown at the wellbore reference point. The system of equations is augmented with the identity that the sum of strengths should be equal to one. The calculation procedures are similar to what we presented in Section 2.2.

To calculate the pressure drop matrix we consider two cases:

- The case where the fluid flow in the source can be assumed to be 1D (*e.g.*, for the case of a vertical well with vertically fully penetrating fracture or a horizontal well with a longitudinal fracture), and
- The case where the flow is considered 2D (*e.g.*, for the case of a vertical well with partially penetrated fracture or a horizontal well with a transverse fracture).

Examples of 1D and 2D flow geometries are shown in **Figs. 2.3** and **2.4**,respectively.

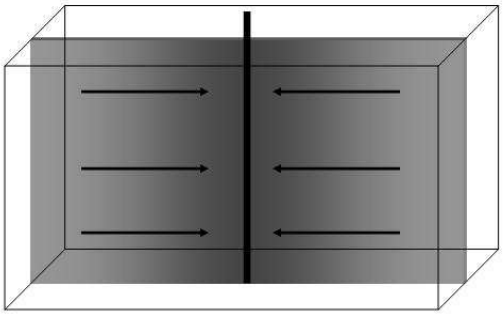

Figure 2.3 — Example of 1D Flow in the Source.

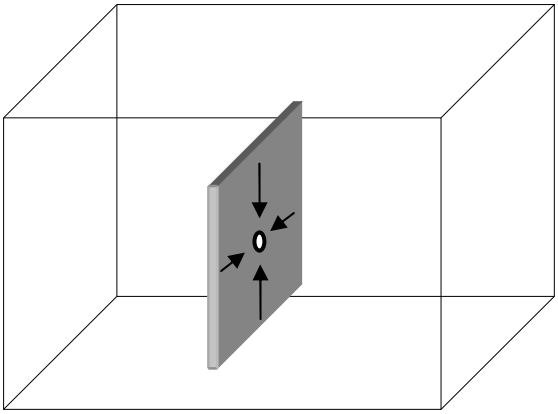

Figure 2.4 — Example of 2D Flow in the Source.

For the case of 1D flow we consider a source discretized by *n* segments in the primary direction of flow, as shown in **Fig. 2.5**. Because of our assumption of pseudosteady-state flow in the source, we can express the pressure drop between center point of each segment and the reference wellbore pressure using Darcy's Law.

For example, in Fig. 2.5 we have discretized the source into 6 segments, and the wellbore is located in the middle of the segments 3 and 4.

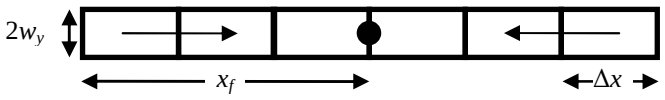

Figure 2.5 — Schematic of a Discretized 1D Source.

The pressure drop is given as:

$$p_i - p_{wf} = \frac{\mu}{2w_y hk_f}\int_{x_i}^{x_{wf}} q dx \tag{2.24}$$

Since each segment is assumed to be a uniform-flux source, the rate at each segment is a *linear function of length*. Therefore we can integrate over each segment from the center of i^{th} segment to wellbore by summing over each segment in the path. For the case shown in Fig. 2.5 (for i= 1 to 3), we can write (numbering from left to right):

$$p_1 - p_{wf} = \frac{\mu}{2w_y 2w_z k_f}\left[\frac{3q_1}{8}\Delta x + \frac{2q_1+q_2}{2}\Delta x + \frac{2q_1+2q_2+q_3}{2}\Delta x\right] = \frac{\mu\Delta x}{2w_y 2w_z k_f}\left[\frac{19q_1}{8} + \frac{3q_2}{2} + \frac{q_3}{2}\right] \tag{2.25}$$

$$p_2 - p_{wf} = \frac{\mu}{2w_y 2w_z k_f}\left[\frac{4q_1+3q_2}{8}\Delta x + \frac{2q_1+2q_2+q_3}{2}\Delta x\right] = \frac{\mu\Delta x}{2w_y 2w_z k_f}\left[\frac{3q_1}{2} + \frac{11q_2}{8} + \frac{q_3}{2}\right] \tag{2.26}$$

$$p_3 - p_{wf} = \frac{\mu}{2w_y 2w_z k_f}\left[\frac{4q_1+4q_2+3q_3}{8}\Delta x\right] = \frac{\mu\Delta x}{2w_y 2w_z k_f}\left[\frac{q_1}{2} + \frac{q_2}{2} + \frac{3q_3}{8}\right] \tag{2.27}$$

Eqs. 2.25 to 2.27 can be written in dimensionless form as:

$$p_{D,wf} - p_{D1} = \frac{2kLx_f}{4nw_y w_z k_f}\left[\frac{19q_{D1}}{8} + \frac{3q_{D2}}{2} + \frac{q_{D3}}{2}\right] \tag{2.28}$$

$$p_{Dwf} - p_{D2} = \frac{2kLx_f}{4nw_y w_z k_f}\left[\frac{3q_{D1}}{2} + \frac{11q_{D2}}{8} + \frac{q_{D3}}{2}\right] \tag{2.29}$$

$$p_{Dwf} - p_{D3} = \frac{2kLx_f}{4nw_y w_z k_f}\left[\frac{q_{D1}}{2} + \frac{q_{D2}}{2} + \frac{3q_{D3}}{8}\right] \tag{2.30}$$

As For this example, for the finite conductivity vertical fracture represented by n = 6 source boxes first we

construct the **C** matrix as:

$$\mathbf{C} = \frac{2kLx_f}{4nw_y w_z k_f}\mathbf{D} \tag{2.31}$$

In which **D** is a coefficient matrix which contains the following elements:

$$\mathbf{D} = \begin{bmatrix} \frac{19}{8} & \frac{3}{2} & \frac{1}{2} & 0 & 0 & 0 \\ \frac{3}{2} & \frac{11}{8} & \frac{1}{2} & 0 & 0 & 0 \\ \frac{1}{2} & \frac{1}{2} & \frac{3}{8} & 0 & 0 & 0 \\ 0 & 0 & 0 & \frac{3}{8} & \frac{1}{2} & \frac{1}{2} \\ 0 & 0 & 0 & \frac{1}{2} & \frac{11}{8} & \frac{3}{2} \\ 0 & 0 & 0 & \frac{1}{2} & \frac{3}{2} & \frac{19}{8} \end{bmatrix} \tag{2.32}$$

The three zeros present in the first row of matrix **D** signify that segments 4 to 6 do not contribute to the pressure losses in the fracture from segment 1 to the wellbore reference point because those segments are located in the other wing of the source. For a source of this kind with *n* segments, the general definition of the non-zero elements of the **D** matrix are:

$$d_{i,j} = \begin{cases} j - \frac{5}{8}, j = i \\ i - \frac{1}{2}, \text{Otherwise} \end{cases}, i = 1, \frac{n}{2}, j = 1, \frac{n}{2} \tag{2.33}$$

Eq. 2.33 gives us the value of the upper-left quarter of **D** matrix. The lower-right quarter is the mirror inverse of the upper-left one and the other parts are equal to zero.

The **C** matrix given above contains the generalized dimensionless fracture conductivity, which is defined as:

$$C_{fD,gen} = \frac{k_f (2w_y)(2w_z)}{k\ Lx_f} \tag{2.34}$$

Where the term $k_f (2w_y)(2w_z)$ can be considered as a generalized conductivity expressed with the cross sectional area available for flow in the fracture. After construction of the **C** matrix, the calculation procedure to obtain strengths and the dimensionless pressure is the same as discussed in Section 2.3.

For the case of 2D flow in the source, a finite-difference formulation can be applied to solve the flux problem within the source. Discretizing Darcy's law as shown in **Fig. 2.6**, we have:

$$q_{i,j} = \frac{k_f 2w_z}{\mu}\left[\frac{\Delta y}{\Delta x}(p_{i-1,j} + p_{i+1,j} - 2p_{i,j}) + \frac{\Delta x}{\Delta y}(p_{i,j-1} + p_{i,j+1} - 2p_{i,j})\right] \tag{2.35}$$

Or in dimensionless format, **Eq. 2.35** becomes:

$$q_{Di,j} = \frac{k_f 2w_z}{kL}\left[\frac{\Delta y}{\Delta x}(p_{Di-1,j} + p_{Di+1,j} - 2p_{Di,j}) + \frac{\Delta x}{\Delta y}(p_{Di,j-1} + p_{Di,j+1} - 2p_{Di,j})\right] \tag{2.36}$$

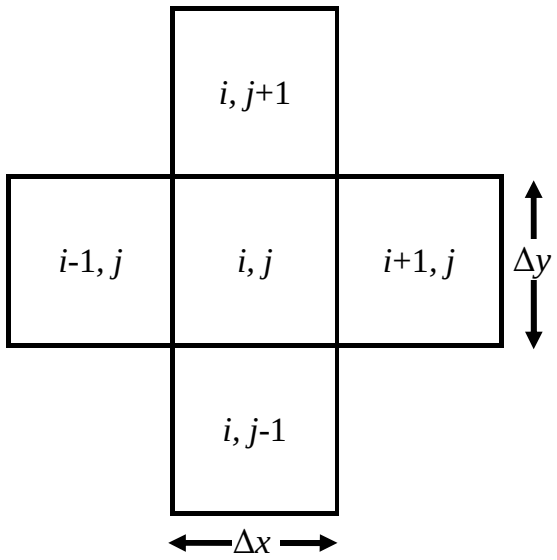

Figure 2.6 — Schematic of a Finite Difference Presentation of a Continuous System.

Where the terms $q_{i,j}$ and $q_{Di,j}$ represent the net production and dimensionless production from the block (*i*, *j*) respectively. Writing similar equations for each segment of the source and arranging these into a matrix form gives us:

$$M.p_D = q_D \tag{2.37}$$

$$p_D = M^{-1}q_D \tag{2.38}$$

Eq. 2.38 shows how the dimensionless pressure drops are determined by segments' strengths. This indicates that the **C** matrix in this case is actually the inverse of matrix **M**. It should be noted that for the special case of the horizontal well with transverse fracture, the well block pressure calculated by this method has to be "corrected" to flowing wellbore pressure using Peaceman (1978) formula.

The dimensionless form of the Peaceman (1978) formula (which relates the wellbore pressure with the grid pressure) is given by:

$$p_{D,Extra} = \frac{1}{2\pi}\frac{kL}{2w_y k_f}\ln[0.14\frac{\sqrt{\Delta x^2 + \Delta z^2}}{r_w}] \tag{2.39}$$

Where Δx and Δz represent the well block size in the x and z directions, respectively. **Fig. 2.7** shows an example of a finite conductivity source divided into 9 segments with the wellbore located in the 5th segment.

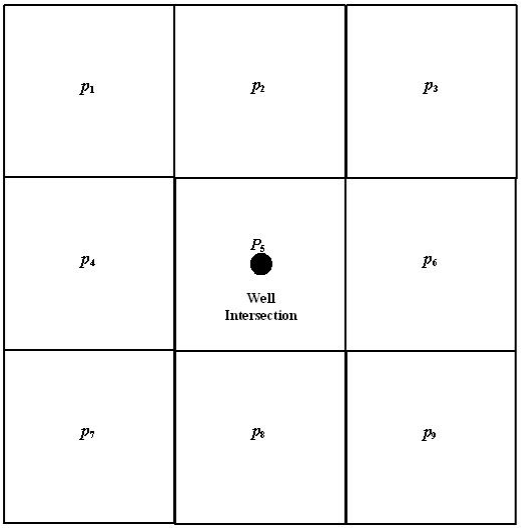

Figure 2.7 — Example of a Discretized 2D Source.

An example of the **D** matrix for the discretized source, as shown in Fig. 2.7, is given by:

$$\mathbf{D} = \begin{bmatrix} 0.875 & 0.375 & 0.250 & 0.375 & 0.000 & 0.125 & 0.250 & 0.125 & 0.125 \\ 0.375 & 0.583 & 0.375 & 0.167 & 0.000 & 0.167 & 0.125 & 0.083 & 0.125 \\ 0.250 & 0.375 & 0.875 & 0.125 & 0.000 & 0.375 & 0.125 & 0.125 & 0.250 \\ 0.375 & 0.167 & 0.125 & 0.583 & 0.000 & 0.083 & 0.375 & 0.167 & 0.125 \\ 0.000 & 0.000 & 0.000 & 0.000 & 0.000 & 0.000 & 0.000 & 0.000 & 0.000 \\ 0.125 & 0.167 & 0.375 & 0.083 & 0.000 & 0.583 & 0.125 & 0.167 & 0.375 \\ 0.250 & 0.125 & 0.125 & 0.375 & 0.000 & 0.125 & 0.875 & 0.375 & 0.250 \\ 0.125 & 0.083 & 0.125 & 0.167 & 0.000 & 0.167 & 0.375 & 0.583 & 0.375 \\ 0.125 & 0.125 & 0.250 & 0.125 & 0.000 & 0.375 & 0..250 & 0.375 & 0.875 \end{bmatrix} \tag{2.40}$$

Fig. 2.8 is a graphical representation of the **D** matrix with the colors, in gray scale, showing the coefficients schematically for the example described above (black represents the largest value and white

represents the zero coefficient). We note that all of the elements of the row corresponding to the well block are equal to zero, which indicates that there is no pressure drop — other than the correction using Peaceman formula (which relates the wellbore and block pressures).

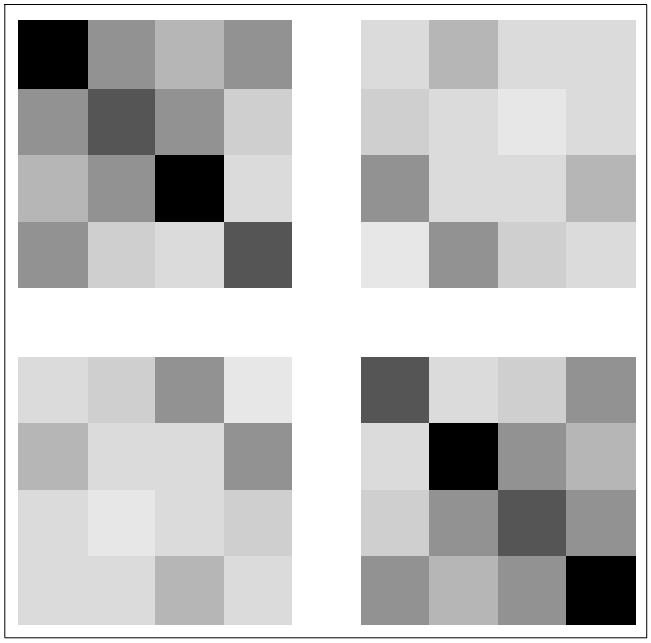

Figure 2.8 — Graphical Representation of the **D** Matrix for 2D Flow in Fracture

2.5 Productivity Index Calculation

Apart from the well-test analysis applications, use of the new solution in the prediction of productivity behavior for a well/fracture system is considered in this work. We cast the results into a transient/pseudo-steady-state productivity index form and then we compare these results with the well-known productivity models for different well/fracture systems.

The application of DVS method is *not* limited to prediction of the pressure behavior of well/fracture configurations. The pressure data calculated from the DVS method can be used to predict the productivity index (PI) behavior of the system. The productivity index and in particular, the pseudosteady-state productivity index of a system is a measure of the *capability* of the system to produce the fluid from a reservoir. Comparison of pseudosteady-state productivity indexes of two completion schemes can be used to establish which completion drains the reservoir most efficiently.

The definition of dimensionless productivity index of a system using the dimensionless pressure and time data as it is discussed by Ramey and Cobb (1971), and the dimensionless productivity index is stated as:

$$J_D = \frac{1}{p_{D,trad} - 2\pi t_{DA}} \tag{2.41}$$

The detailed derivation of Eq. 2.41 is presented in Appendix B. We note that although Eq. 2.41 is derived for the case of a constant production rate, this solution has also been proved to be correct for a system producing at a constant wellbore pressure condition. To compute the variable-rate performance as a function of time (constant flowing pressure case), we use the following procedure:

1. Calculate the average reservoir pressure and flowing pressure. Starting from zero time, the average reservoir pressure is equal to the initial pressure (*i.e.*, uniform pressure initial condition).
2. Assuming the productivity index is constant for the chosen time interval, we can calculate the corresponding flowrate of the system using Eq. 2.42:

   $$q_i = J_i(p_{avg,i} - p_{wf}) \tag{2.42}$$

   Assuming that the flowrate is constant over a given time interval, we can calculate the incremental cumulative production over that time interval as the rate multiplied by the time interval. For the (total) cumulative production profile, we simply add the incremental cumulative production values.

3. The average reservoir pressure for the $(i+1)^{th}$ time interval can then be calculated by subtracting Δp_i from the pressure of the i^{th} time interval. For the pseudosteady-state flow assumption, this Δp_i represents the reduction in the average reservoir pressure of the system due to the fluid withdrawal during the i^{th} time interval, and Δp_i is calculated using the material balance equation as:

   $$\Delta p_i = \frac{\Delta N_p B}{\phi A h c_t} = \frac{q_i B \Delta t_i}{\phi A h c_t} \tag{2.43}$$

Steps 1–4 are repeated for each time interval — which yields the calculated flowrate profile as a function of time. For gas reservoirs, a similar procedure can be followed using the gas material balance equation for a volumetric dry gas reservoir and the gas inflow performance equation, which are given by:

$$\frac{p}{z} = \frac{p_i}{z_i}\left[1 - \frac{G_p}{G}\right] \tag{2.44}$$

$$q = \frac{1}{1424}\frac{1}{T}\sqrt{k_x k_y}\, h\, J_D\,[m(p_{avg}) - m(p_{wf})] \tag{2.45}$$

Where in Eq. 2.45 q represents the gas production rate in MSCF/D and T is reservoir temperature in °R. Eq. 2.44 is known as the material balance equation for a volumetric gas reservoir and Eq. 2.45 represents the inflow performance of a gas well. $m(p)$ is the pseudopressure function, which is defined as:

$$m(p) = 2\int_{p_i}^{p} \frac{p}{\mu z} dp \tag{2.46}$$

Where μ and z are the gas viscosity and the gas compressibility, respectively. The subscript i represents the reference pressure of which we integrate the pseudopressure function and it is chosen arbitrarily, typically the reference pressure is the base pressure or the pressure at standard conditions.

At each time step, *assuming the average pressure is constant for that time step*, we calculate the production rate at that time step using the dimensionless productivity index and the calculated pseudopressure values. Knowing the rate, we can calculate the cumulative gas production and the new average pressure. This is an iterative process for the gas case since the compressibility factor (z) and gas viscosity (μ) are functions of pressure, but usually the convergence is quite fast because of the small changes in pressure incurred at each time step.

CHAPTER III

VALIDATION OF THE MODEL

3.1 Introduction

To show the applicability of the new DVS method, results of this method are validated using comparisons with existing solutions for several simple well configurations (*e.g.*, vertical well with full and partial penetration, horizontal well, and fractured wells with finite- and infinite-conductivity fractures). In this effort we not only validate the pressure response, but we also validate the productivity index function using the existing models. All procedures discussed in Chapter II were programmed in the MATHEMATICA (Version 5.2, Wolfram Research Inc. 2005) programming/computation language.

3.2 Validation with Pressure Models

Fully Penetrating Vertical Well

For this case we have two well-known representations — the line source and the cylindrical source solutions. Both solutions can be combined with the method of images (Raghavan 1993) to produce bounded reservoir responses. Also, it is well-known that the medium-late time solution is not sensitive to the actual source geometry (*i.e.*, the transition period between which neither the source nor the boundaries control the pressure response). In **Fig. 3.1** we provide a comparison between the results of the line- and cylinder-source solutions and the DVS method solution. Except at very early times, we note very good agreement between the DVS solution and the line- and cylinder-source solutions.

To represent the actual well by a box source, we have to define the w_x and w_y parameters, which are the widths of the hypothetical source box. Detailed numerical experimentation has revealed that the following relation provides the best results:

$$w_x = w_y = 1.4444\, r_w \tag{3.1}$$

We note that in Fig. 3.1, the DVS solution is much closer to the cylindrical source solution than to the line source solution, suggesting that the DVS is something of an approximation for a cylinder, but not a line.

Partially Penetrated Vertical Well

Using the solution proposed by Yildiz and Bassiouni (1991) for the transient pressure behavior of a partially penetrated vertical well as our reference for comparison to the DVS solution, we present the comparison of their solution and the DVS solution in **Fig. 3.2**. We note differences only in the early behavior — which are due to source size, the location of the observation point, and (ultimately) the nature of the flow in the near vicinity of the well.

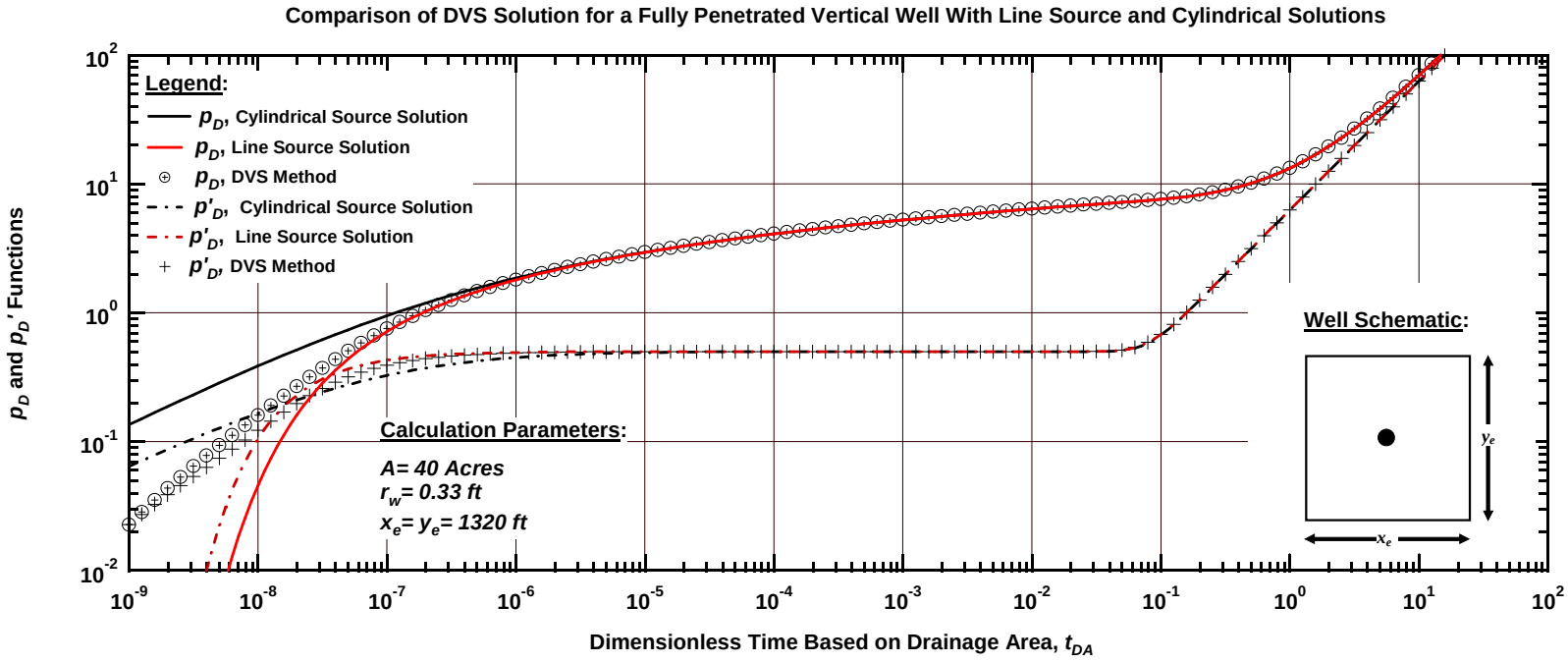

Figure 3.1 — Comparison of the DVS Results With Line Source and Cylindrical Source Solutions: Vertical Well in a Bounded Reservoir (In the Box-in-Box Model $w_z=z_e/2$, $w_x = w_y = 0.477$ *ft*, and the actual value of z_e is irrelevant)

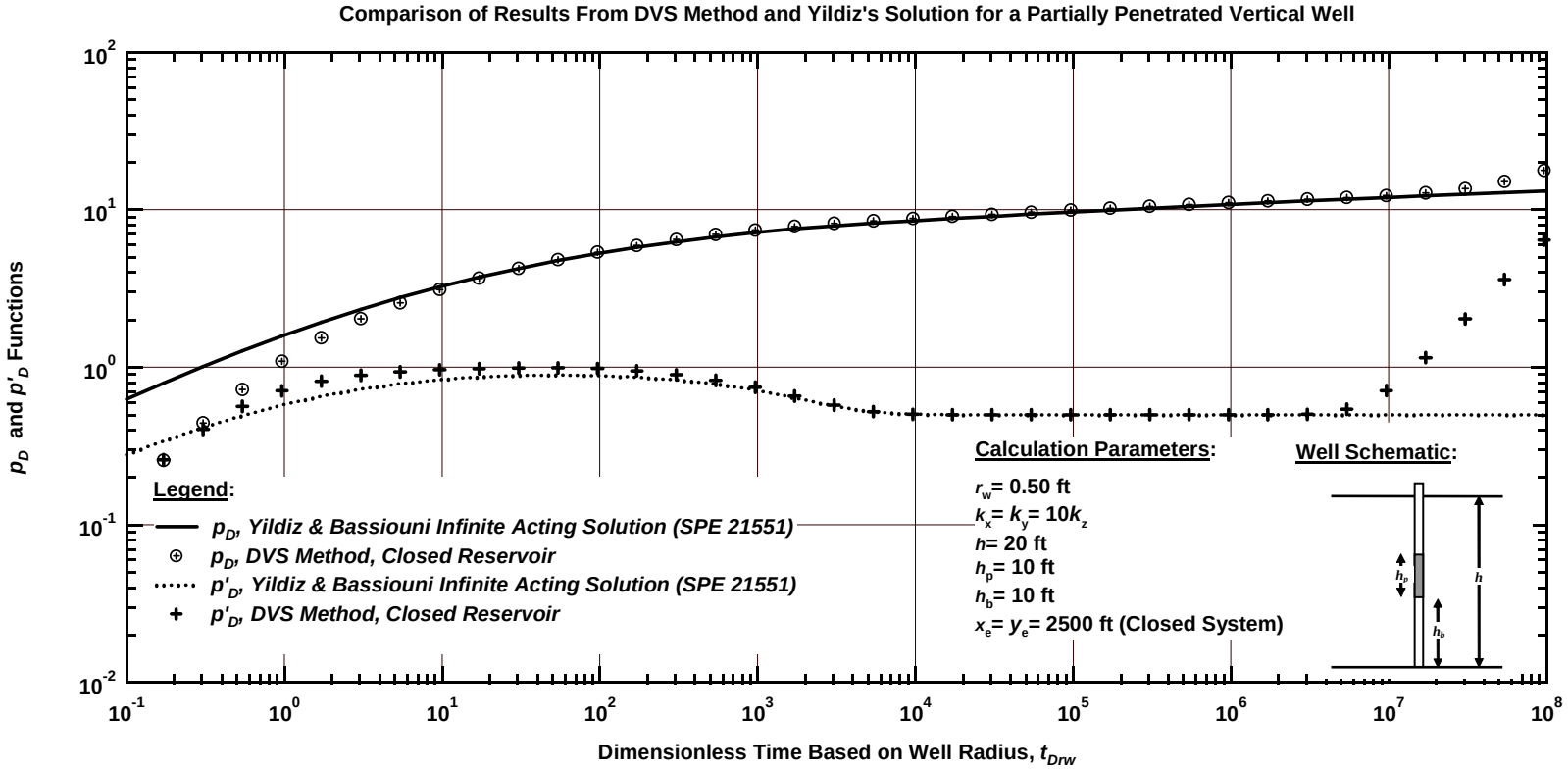

Figure 3.2 — Comparison of DVS Results with Yildiz's Model for a Partially-Penetrating Vertical Well (Box-in-Box Model), h, h_p, and h_b are represented by z_e, $2w_z$, and c_z- w_z respectively.

Differences observed at late times are due to the effect of boundaries imposed on the DVS solution. Recalling that the Yildiz and Bassiouni (1991) solution is only valid for transient flow, it would be far from trivial to develop a method-of-images solution for a boundary case using this solution. We recorded the computation times for each solution computed on a typical desktop computer with Pentium IV processor — the DVS solution required 1.23 seconds, compared to 436.1 seconds for the Yildiz-Bassiouni solution.

Uniform Flux Horizontal Well

Ozkan (1988) presented a method to compute the performance of a horizontal well and specifically, he developed a series solution in Laplace domain for a fracture with uniform flux and adjusted the solution to obtain the performance of a horizontal well. In this work we used the results given in Table 2.6.2 of Ref. 6 for comparison purposes.

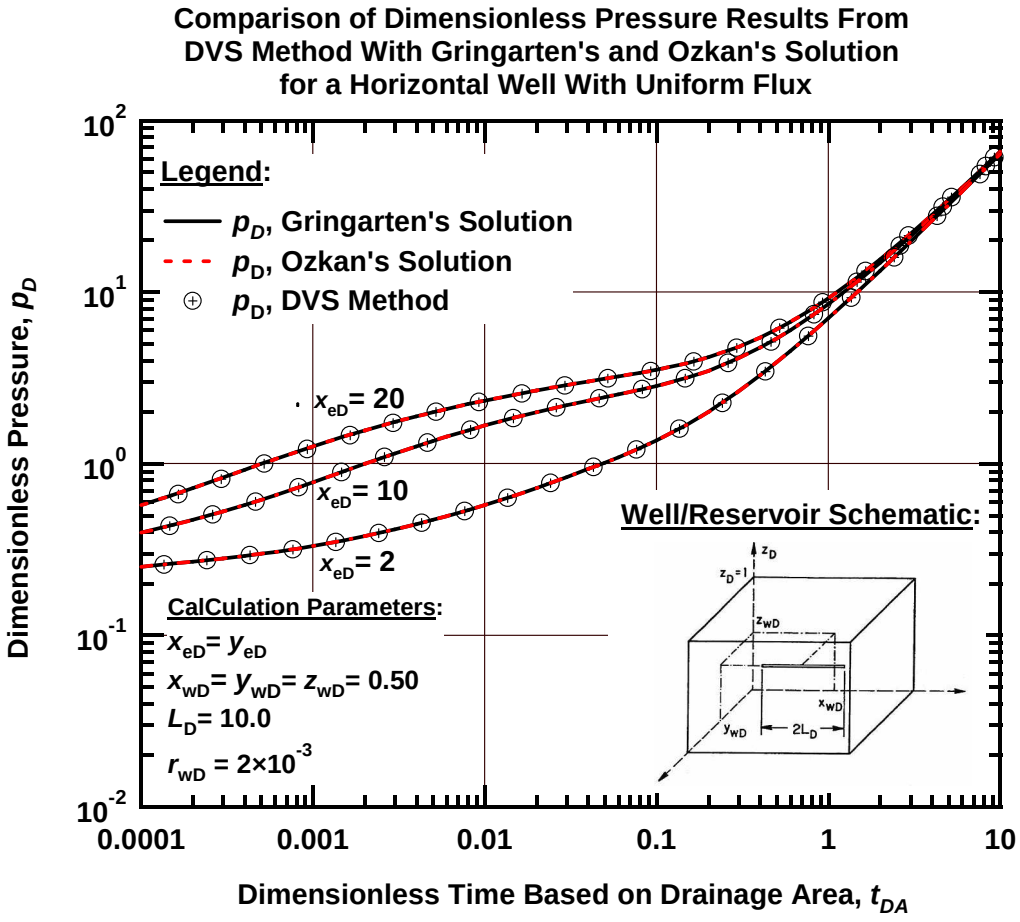

Figure 3.3 — Comparison of DVS Results with Ozkan's and Gringarten's Solutions for a Horizontal Well in a Bounded Reservoir, Uniform Flux Solution (In the Box-in-Box Model $x_{eD}= x_e/w_x$, $y_{eD}= y_e/w_x$, and $L_D= z_e/w_x$).

Fig. 3.3 shows the graphical presentation of the solutions by Gringarten, Ramey and Raghavan (1974) and Ozkan (1988) compared to the DVS for the case of uniform flux horizontal well with various horizontal penetrations. For the DVS represen-tation of the horizontal well, Eq. 3.1 is used to obtain the w_y and w_z widths of the source box. The data given in Ozkan (1988) omits the very early time period of the solution, so we do not observe any differences between the DVS solution and the reference solutions.

Fully Penetrating Vertical Fracture (*Uniform-Flux and Infinite-Conductivity Fracture*)

In **Figs. 3.4 and 3.5** we present the results of the widely accepted Gringarten, Ramey and Raghavan (1974) (Green's function) solution for the case of vertical well with a fully-penetrating vertical fracture along with our DVS results for the uniform flux fracture case (Fig. 3.4) and the infinite conductivity fracture case (Fig. 3.5). The DVS solution results presented in Fig. 3.4 are calculated with a single uniform box source (the w_y width is selected to be "sufficiently small" ($10^{-6}y_e$.) as to not distort the solution). The DVS solution results presented in Fig. 3.5 were obtained using the uniform-flux solution with the "equivalent observation point" ($0.732\ x_f$) for the infinite conductivity fracture case. For these particular cases, the analytical and DVS results are indistinguishable.

The computation times for these cases are as follows:

- DVS Method:
  - —Uniform-flux fracture (84.73 seconds).
  - —Infinite conductivity fracture (542 seconds).
- Gringarten Solution:
  - —Uniform-flux fracture (520.1 seconds).
  - —Infinite conductivity fracture (815.1 seconds).

Fully Penetrating Vertical Fracture (*Finite-Conductivity Fracture*)

As a natural progression, we need to compare our new DVS solution to the case of a vertical well with a finite-conductivity vertical fracture in an infinite acting reservoir. The reference solution for this case is given by Cinco-Ley, Samaniego, and Dominguez (1978) — and we also note that we will require a "discretized" fracture solution for this case due to the finite conductivity of the fracture (*i.e.*, the fracture has to be treated as a separate "reservoir to account for the non-trivial pressure drop in the fracture). The comparison of results is presented in **Fig. 3.6**. For the DVS solution we divided the fracture into 32 segments. From Fig. 3.6 we note a very good comparison of the DVS solution and the results of Cinco-Ley, Samaniego, and Dominguez (1978) — except at early times where the source of the volume affects the solution.

In **Fig. 3.7** we present the distribution of the *computed* source strengths along the lateral coordinate in *one fracture wing*. For pseudosteady-state (late times), the stabilized strength distribution profiles computed by the DVS method are somewhat similar to the "U-shaped" distributions shown by Cinco-Ley, Samaniego, and Dominguez (1978) We believe that this is a relatively minor issue, and that the DVS solution is validated for this case, except at very early times. For comparison, the DVS solution required a computational time of 689 seconds and their solution required a computational time of 9632 seconds.

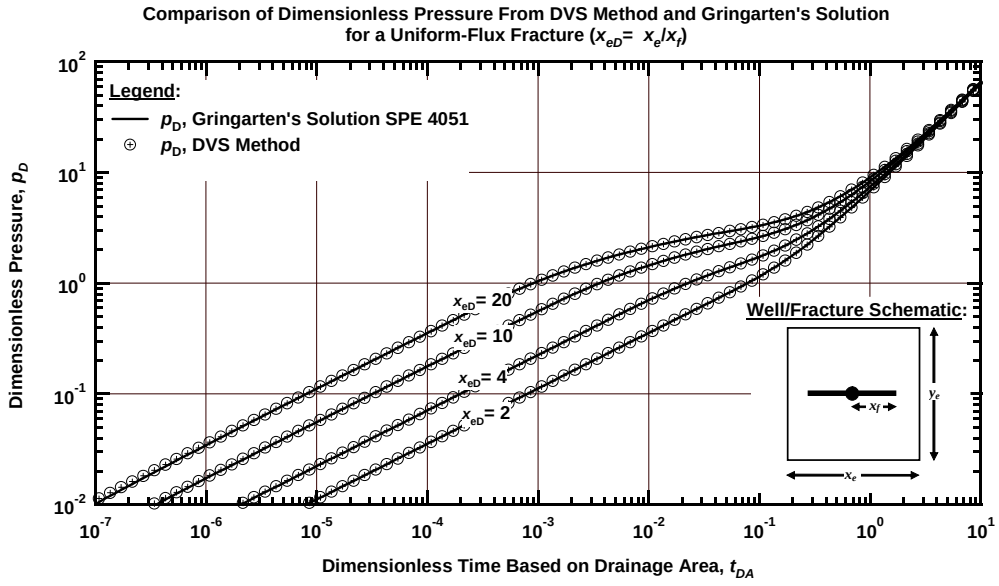

Figure 3.4 — Comparison DVS Results with Gringarten, Ramey and Raghavan (1974) Solution for a Vertically Fractured Well in a Bounded Reservoir; Uniform Flux Solution ($x_{eD}= x_e/w_x$ in the Box-in-Box Model).

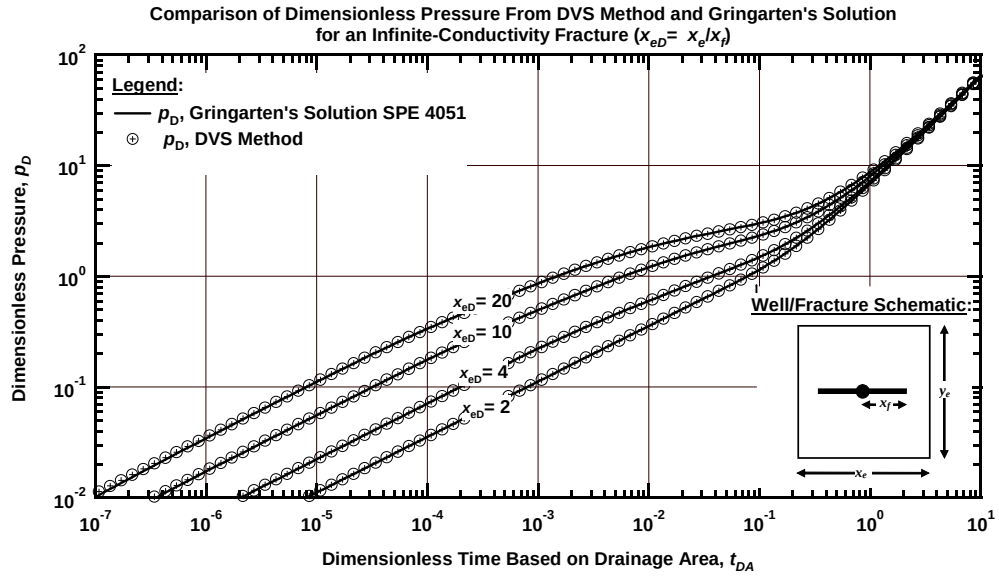

Figure 3.5 — Comparison of DVS Results with Gringarten, Ramey and Raghavan (1974) Solution for a Vertically Fractured Well in Bounded Reservoir; Infinite Conductivity Solution. ($x_{eD}= x_e/w_x$ in the Box-in-Box Model).

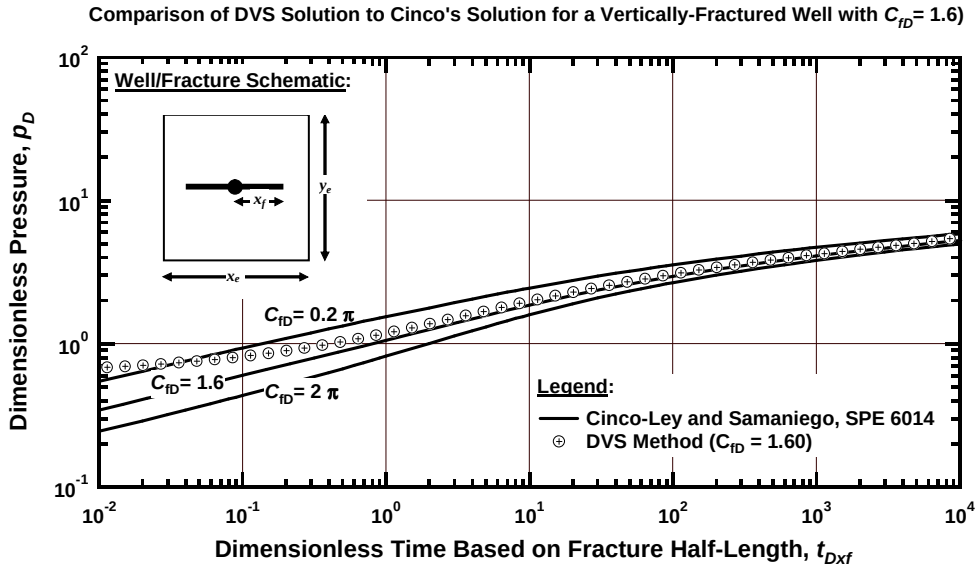

Figure 3.6 — Comparison of DVS with Cinco-Ley, Samaniego, and Dominguez (1978) Results for Finite Conductivity Fracture.

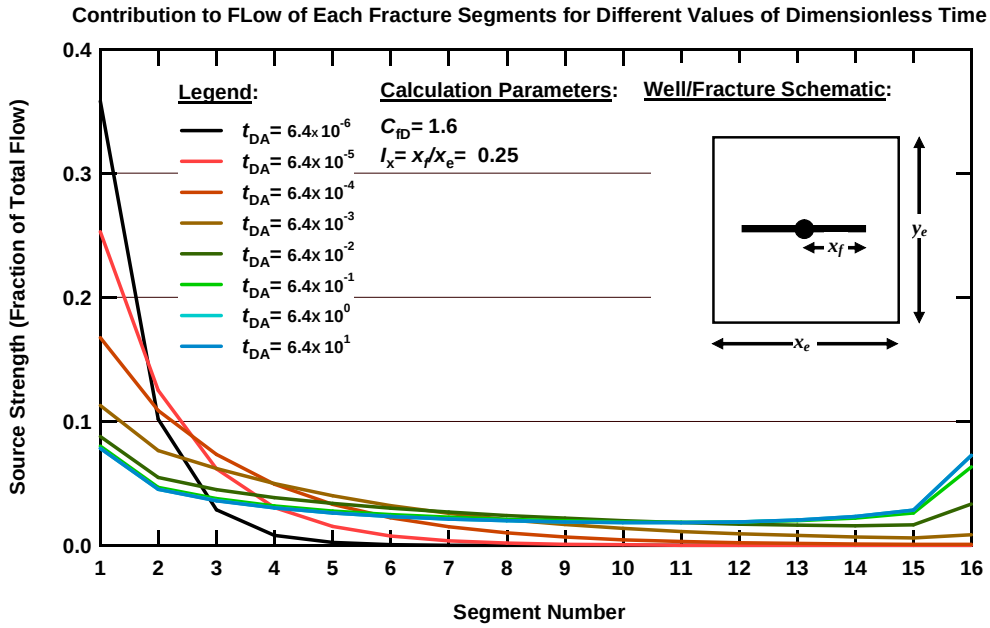

Figure 3.7 — Distribution of the Contribution of Different Segments to Total Production at Various Times, Finite Conductivity Vertical Fracture of Full Vertical Penetration for Half the Fracture (C_{fD} =1.6 and I_x = 0.25, n = 32).

3.3 Validation with Productivity Index Models

The results of our DVS method can be used to calculate the transient as well as the pseudosteady-state productivity index for a given well/reservoir configuration. The method of calculation for the dimensionless productivity index (J_D) is provided in Appendix B. To validate the applicability and reliability of the results obtained from the DVS method for the case of a horizontal well, we used the work of Chen and Asaad (2003). They validated their work using the results taken from Babu and Odeh (1989) and from Goode and Kuchuck (1991) for the case of horizontal well. Chen and Asaad later extended their correlation to fractured wells. We compare our DVS results for the examples A1, B1, and B2 given by Chen and Asaad (2003). **Table 3.1** provides the reservoir/fluid properties used for the calculation and **Table 3.2** present the results of our comparative study.

Table 3.1 — Reservoir/Fluid Properties Used for Example Cases of Chen and Asaad (2003) (Comparison of Different Pseudosteady-State Productivity Index Correlations).

Reservoir/Fluid Properties	Unit	A1	B1	B2
Drainage Length in x, $2x_e$	ft	2640	2000	4000
Drainage Length in y, $2y_e$	ft	2640	4000	2000
Formation thickness, h	ft	45	100	200
Horizontal well length, L_h	ft	1475	1000	1000
Well location in x, x_w	ft	1320	1250	1500
Well location in y, y_w	ft	1320	3000	1000
Well location in z, z_w	ft	22.5	50	150
Wellbore radius, r_w	ft	0.33	0.25	0.25
Formation volume Factor, B	RB/STB	1.05	1	1
Fluid viscosity, μ	cp	7.5	1	1
Horizontal permeability in x, k_x	md	350	200	100
Horizontal permeability in y, k_y	md	350	200	100
Vertical permeability, k_z	md	70	50	20

From Table 3.2 we can see that for this case (a horizontal well), we have obtained excellent agreement between the results of different methods (our DVS solution, the Chen and Asaad (2003) solution, and the Babu and Odeh (1989) solution). This agreement is consistent for both the uniform-flux and infinite-conductivity horizontal well cases. Further to this effort, we compared our DVS solution with the Chen and Asaad (2003) solution for the case of a vertically-fractured well (uniform flux and infinite conductivity cases are considered). We do note that for case B2 the difference between solution results rises to around 10 percent (compared to less than 1 percent difference for all of the other cases). We suspect that the discrepancy is due to the approximations used in the Chen and Asaad (2003) formulation, which tend to show higher error in cases where the horizontal penetration of the vertical fracture is relative small.

Table 3.2 — Comparison of DVS Results with Various Pseudosteady-State Productivity Index Correlations.

Case		Method	PI (STB/D/psi) A1	B1	B2
Horizontal Well	**Uniform Flux**	Babu-Odeh[11]	11.40	41.50	31.90
		Chen-Assad[13] Simple	11.45	41.79	32.21
		Chen-Assad[13] Full	11.44	41.66	33.26
		DVS	11.44	41.68	33.35
		Goode-Kuchuk[12]	13.00	N/A	N/A
	Infinite Conductivity	Chen-Assad[13] Simple	12.99	43.75	32.94
		Chen-Assad[13] Full	12.99	43.61	34.84
		DVS	12.75	43.23	34.86
Fractured Well	**Uniform Flux**	Chen-Assad[13] Simple	14.10	56.63	73.36
		DVS	14.07	56.40	79.09*
	Infinite Conductivity	Chen-Assad[13] Simple	16.51	60.30	77.29
		DVS	16.10	59.35	87.16*

The production behavior of a vertical well with finite-conductivity fracture has been discussed extensively in Economides, Oligney, and Valkó (2002). They provide practical guidelines on how to design a fracture treatment which should yield the maximum productivity index. **Fig. 3.8a** provides a "zoom view" of the dimensionless productivity index for a system consisting of a vertically fractured well with full vertical penetration varies as a function of fracture conductivity and the proppant number (here noted as N_p, N_{Prop} elsewhere). The "full view" is presented in **Fig. 3.8b**. Fig. 3.8a and 3.8b are provided as "design charts" to obtain the optimum fracture (*i.e.*, the highest productivity index) for a constant fracture volume (which is represented by the proppant number).

To validate the results obtained from the DVS method for the case of a well with a finite-conductivity vertical fracture, we *assume* a proppant number of 0.1. The proppant number is a measure of the fracture volume (Eq. 3.2), and the fracture conductivity is a measure of the ratio of fracture length over fracture width (Eq. 3.3).

$$C_{fD} = \frac{k_f w_y}{k w_x} \tag{3.2}$$

$$N_{prop} = \frac{2kfV_{fracture,2-wings}}{kV_{reservoir}} \tag{3.3}$$

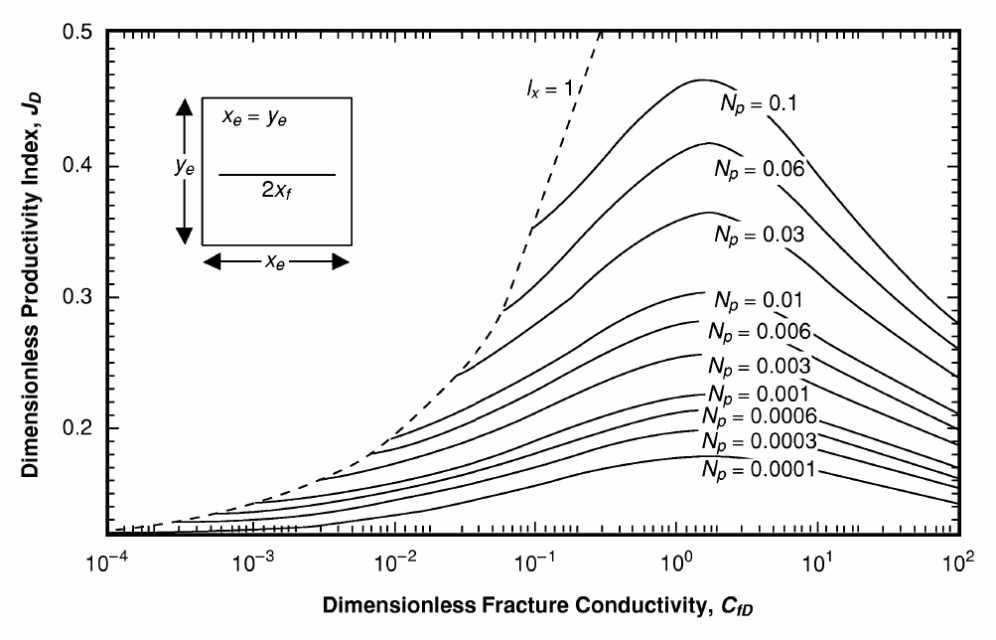

Figure 3.8a — (zoom view) Dimensionless Productivity Index of a Vertically Fully Penetrated Fracture as a Function of Fracture Conductivity and Proppant Number (From Economides, Oligney, and Valkó 2002).

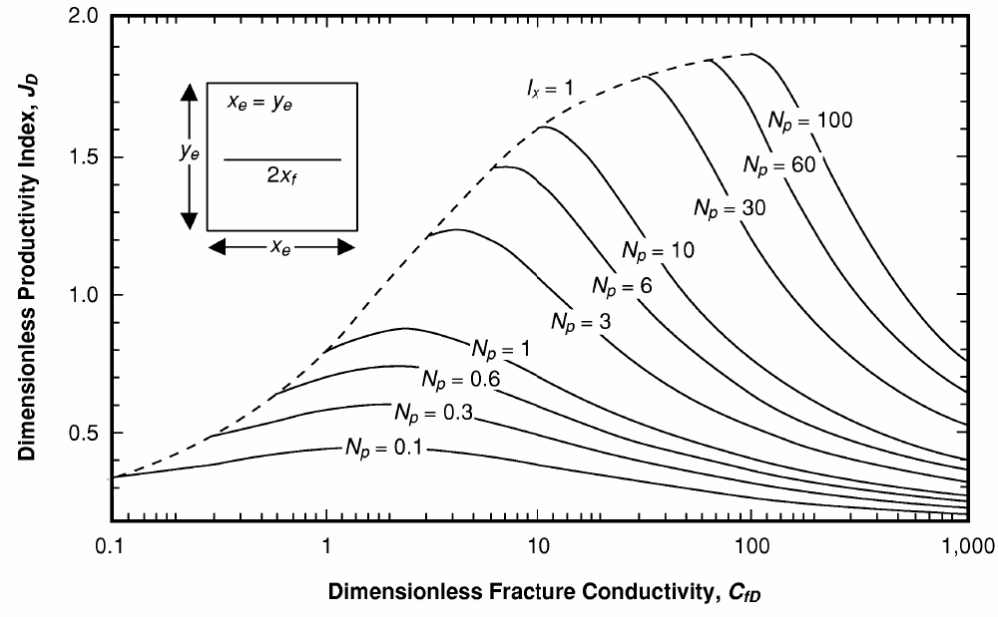

Figure 3.8b — Dimensionless Productivity Index of a Vertically Fully Penetrated Fracture as a Function of Fracture Conductivity and Proppant Number (From Economides, Oligney, and Valkó 2002).

Using the assumed values of the proppant number and the fracture conductivity, we can calculate the corresponding fracture half-length. For this example case the lateral penetration ratio is 0.25, which means the fracture length is half the reservoir length. The value of maximum dimensionless productivity index for this case occurs at the fracture conductivity of 1.6 and it is equal to 0.467.

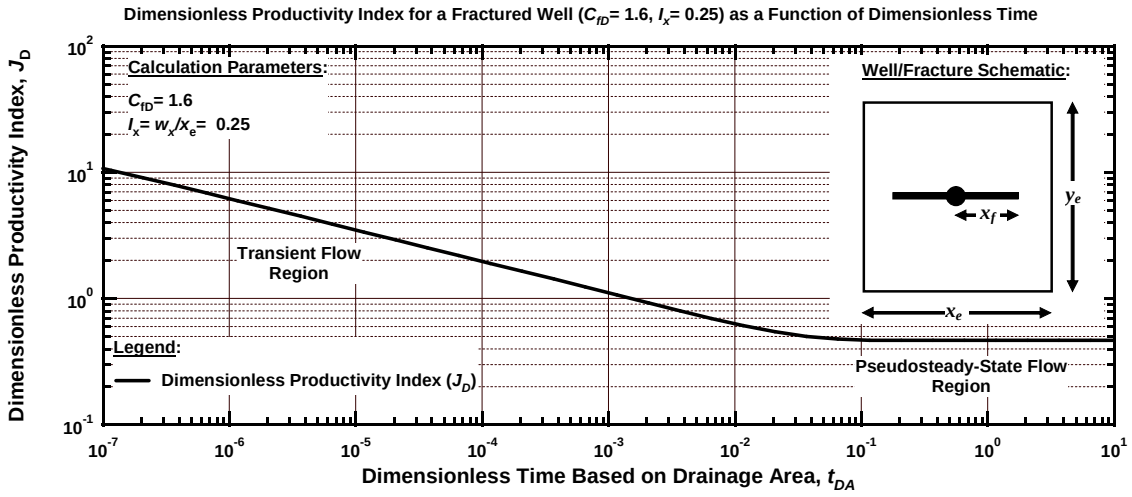

Figure 3.9 — Dimensionless Productivity Index of the Example Case Using DVS Method.

Fig. 3.9 shows the results of an analog case generated using the DVS method. We note that during pseudosteady-state, the calculated dimensionless productivity index is equal to 0.467 which corresponds *exactly* with the value defined by the correlation shown in Fig. 3.8. This comparison confirms the validity of the DVS results for applications such as this (*e.g.*, fractured wells). Another advantage of the DVS method is its ability to very accurately model the productivity index during transient as well as the pseudosteady-state flow.

From Fig. 3.9 we note that the character of the dimensionless productivity index for all flow regimes: transient, transition, and pseudosteady-state. Such plots may also be useful for performance predictions.

CHAPTER IV

APPLICATION OF NEW TECHNIQUE TO A COMPLEX WELL/FRACTURE CONFIGURATION CASE

4.1 Introduction

In this chapter, we apply the DVS method to a case of complex well/fracture completion scheme and we demonstrate the utility of the DVS in a production optimization approach. The case considered in this demonstration is that of a horizontal well with multiple transverse fractures in which both the horizontal well and the fractures contribute to production. We first discuss the formulation of the problem and the construction of the reservoir model using the DVS method. To the best of our knowledge, no analytical solution exists for this particular case, so we utilize a commercial reservoir simulator to compare our results. The results of our optimization and our sensitivity analysis approach are presented in detail and discussed in this chapter. We also apply the computation procedure described in Chapter II to forecast the production performance for the well/fracture completion scheme being considered.

4.2 Formulation of the Problem

The challenge we pose for this Chapter is to use the DVS method to systematically assess the various horizontal well/fracture completion schemes that could be used to develop a rectangular reservoir (of the size $x_e \times y_e \times z_e$). In this case, transverse fractures (orthogonal to the horizontal well) will be used, but the horizontal well is assumed open to flow over the entire reservoir length (*i.e.*, the fractures and the horizontal well both contribute to production).

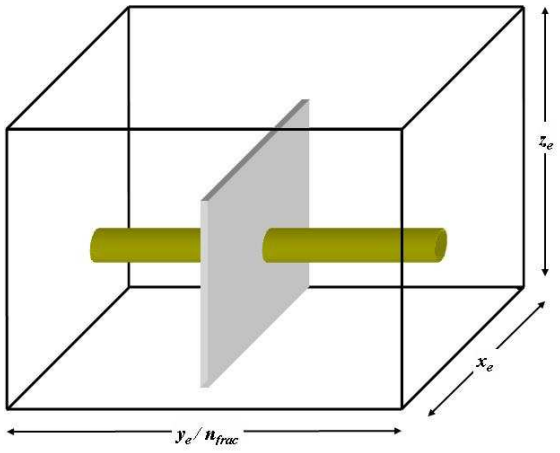

Figure 4.1 — Schematic of the Model's Building Block.

The schematic for this system is presented in **Fig. 4.1**, which shows a schematic of the building block of the model (we can add more fractures to this configuration). We assume that any/all fractures have the same size ($2w_x \times 2w_y \times 2w_z$) and are located symmetrically (central to the horizontal well) for the sake of

simplicity. The variable n_{frac} represents the number of transverse fractures and, in principle could be any integer from 1 to ∞, but for this study, we limit the number of fractures from 1 to 5. We assume the total system is composed of n_{frac} building blocks connected together in the y direction. Lastly we assume the fractures to be of finite-conductivity and the horizontal well to of infinite-conductivity.

As we discussed in Chapter II, the entire source should be divided into sub-sources for cases of finite- and/or infinite-conductivity sources. In this case, we divide the individual fractures into $(2n_x + 1)$ by $(2n_z + 1)$ segments and the horizontal well into $2n_h$ segments. Because the fractures are assumed to be of finite conductivity, the **C** matrix is only calculated for the fracture sub-sources. We also incorporate Peaceman's correction (Peaceman 1978) to account for 2D flow in the fracture.

4.3 Validation Through Simulation

To validate the model, we used the CMG (Version 2005.10, Computer Modeling Group Ltd.) commercial reservoir simulator to simulate a rectangular reservoir of the size (1320×1320×100 ft), with horizontal permeability of 1 md and permeability anisotropy (k_v/k_h) equal to 0.1. The individual fractures are of the size ($1000 \times 0.01 \times 80$ ft) and have permeabilities of 10,000 md. For our validation, we consider the case of 1 fracture and the case of 4 fractures. Lastly, the horizontal well penetrates the entire reservoir width. **Table 4.1** presents the reservoir, fracture, and fluid characteristics used for both the simulation model and the DVS calculations.

Table 4.1 — Reservoir, Fracture, and Fluid Characteristic Used for Simulation Model and DVS Calculations.

Reservoir Characteristics:

x_e = 1320 ft
y_e = 1320 ft
z_e = 100 ft
k_x = 1 md
k_y = 1 md
k_z = 0.1 md
ϕ= 10 percen t

Fracture Characteristics:

w_x = 500 ft
w_y = 0.01 ft
w_z = 40 ft
k_x = 10,000 md

Fluid Characteristics:

μ= 1.011 cp
$c_t = 1.35 \times 10^{-5}$ psi^{-1}

well Characteristics:

r_w= 0.3 ft
L_h = 1320 ft

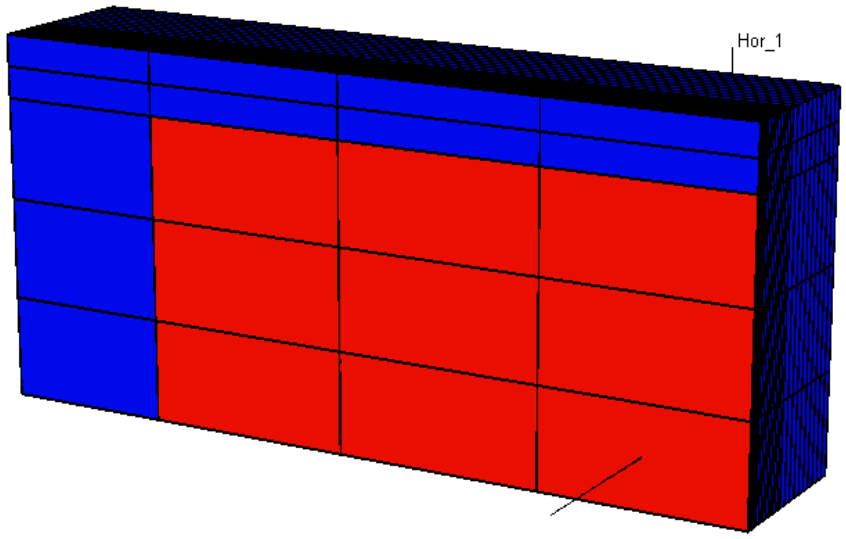

Figure 4.2 — A 3D View of ¼ of the Simulation Model, (Case of 4 Transverse Fractures).

We have assumed a (7×75×9) grid for simulation model, 1/4 of which is shown in **Fig. 4.2**. The horizontal well is defined at the center of the reservoir and is open to flow over the reservoir length — the fractures are intersected by the horizontal well at the center of the fractures. The "wellbore blocks" (where the horizontal well intersects the fracture) are also refined locally in a (7×7) grid in order to reduce effect of the block size.

The simulations were performed assuming a constant production rate — in particular, we specified the production rate at 5 stock-tank barrels per day (STB/D) in order to avoid any significant changes in simulation results because of changes in fluid properties in the 1000 day production period (this is a constant compressibility or "black oil" reservoir model, the basis for most analytical solutions).

From the report of pressures (bottomhole flowing pressure and average reservoir pressure) as functions of production time (see **Fig. 4.3**), we compute the dimensionless productivity index from the simulation data. **Fig. 4.4** provides a comparison of dimensionless productivity index calculated from simulation and the results from our DVS method, plotted as a function of production time. We note that the results of the DVS method and the simulation compare very well during the transition and pseudosteady-state flow regimes. At early times these results differ — our interpretation of this difference is that the two models consider the fluid storage in the fracture differently. There may also issues of gridding, but our contention is that the "pseudosteady-state storage" concept used to model the fracture behavior in the DVS solution

may not be sufficient to address the early time flux distribution in a finite-conductive vertical fracture (see Fig. 3.6 for comparison). Regardless, we accept that this issue may be significant for some cases.

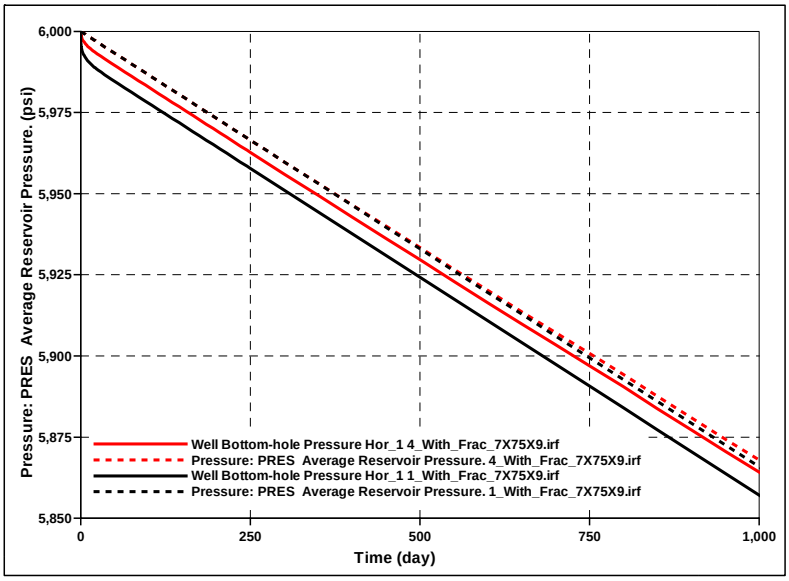

Figure 4.3 — Simulation Output, Well Bottomhole Pressure and Average Reservoir Pressure for Cases of 1 Fracture and 4 Fractures.

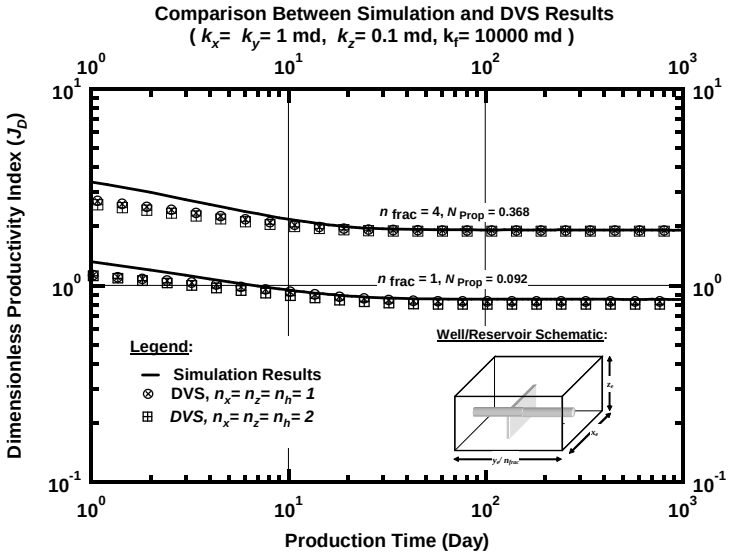

Figure 4.4 — Comparison Between Simulation Results and DVS Method's.

The computational "run time" for the numerical simulation case was about 32 seconds, while for this case, the DVS method required 292 seconds. We believe that if the DVS method were programmed into a more traditional programming language (other than MATHEMATICA), then the computational times for the DVS method would improve substantially. We recognize the implication that, for this case, the numerical simulation model is substantially faster than our DVS method, but we believe that there is a balance of speed and potential accuracy in the DVS method.

For the DVS method we considered only two cases of grid sizes, $n_x = n_z = n_h = 1$, and 2. Our investigations showed that the dimensionless productivity index for pseudosteady-state flow does change as the number of segments change, but in most cases this change is negligible (less than 0.1 percent when n_x, n_z, and n_h are equal to 2). We note that the CPU computation times increase *quadratically* as n_x, n_z, and n_h increase, and based on this observation we elected to use $n_x = n_z = n_h = 2$ (which yields 25 blocks for each fracture source and 4 block for the horizontal section).

4.4 Design and Optimization

The DVS method has been shown to predict the productivity index behavior of complex well/fracture completion schemes with reasonable (*i.e.,* practical) accuracy. Considering the semi-analytical nature of the method, we could (and should) use the DVS method as an optimization/screening tool to evaluate different well design and completion scenarios for reservoir development applications. To illustrate this premise, we provide a demonstration application of DVS method to optimize production for an example case.

Table 4.2 — Reservoir and Proppant Characteristics Used for Case Study.

Reservoir Characteristics:

x_e = 1320 ft
y_e = 1320 ft
z_e = 100 ft
k_x = 1 md
k_y = 1 md
k_z = 1, 0.1, 0.01, 0.001 md

Proppant Characteristics:

d_p = 0.005 ft
ρ_p = 2.83
ϕ_p = 35 percent
k_f = 10,000 md

Table 4.2 provides the characteristics of the reservoir and the fracture proppant we will use for our example case. The challenge we face is how to find the best completion schemes in term of number and size of fractures. The "best" completion scheme will be defined as that which provides us the maximum

dimensionless productivity index (production potential), for a constant proppant volume. In other words an optimum design is sought for the constant proppant number (N_{Prop}).

For estimating the optimal design parameters, we develop numerous "scenario" cases. The objective is to maximize the dimensionless productivity index achieved during the pseudosteady-state flow period. Specifically, we will generate production performance cases using the DVS method for different numbers of fractures and different values of the proppant number. Our strategy is to fix the proppant number (as we fix the amount of proppant for fracturing) and the fracture half-width (as an integer multiple of proppant diameter), we can then obtain a series of fractures with the same volume and width.

Table 4.3 — Range of Variation of Design Parameters.

Fracture Half-Width (w_x)	= $1d_p$ to $10d_p$
N_{Prop}	= 0.001, 0.01, 0.1, 1.0
Number of Fractures	= 1 to 5

Table 4.3 presents the ranges of the parameters we utilize in this study. Based on the definition of the proppant number and the given values of the proppant numbers, the equivalent proppant weights used in this study are 1,000, 10,000, 100,000, and 1,000,000 lb, respectively. Unlike the previous studies we do not consider the dimensionless fracture conductivity (C_{fD}) directly, but rather through the use of its component variables and the definition of the proppant number. In this study we vary the fracture dimensions to maintain a constant fracture volume.

All of the results in this study consider the case of a proppant number equal to 1.0 since this is an optimal value that can be achieved in practice. Additional cases ($N_{prop} \leq 1.0$) are presented in Appendices C to F. In **Table 4.4** we present the mathematically feasible fracture sizes which correspond to the fracture volume that can be generated by 1,000,000 lb of proppant. In **Table 4.5** we present corresponding values of the dimensionless productivity index (pseudosteady-state flow) as a function of number of fractures and permeability anisotropy to illustrate the flow contribution for each configuration. From Table 4.5 it is clear that there is no basis for the perception that a fully-penetrating fracture (vertical or horizontal well) should yield the maximum productivity. Although it is correct that a fully-penetrating vertical fracture does yield higher productivity for cases with higher permeability contrast, for some cases maximum productivity is achieved via a partially-penetrating fracture.

Fig. 4.5 shows the distribution of the dimensionless productivity index (pseudosteady-state flow) as a function of number of fractures for the case of a homogeneous reservoir ($k_x = k_y = k_z$ =1 md). From Fig. 4.5 we note that an optimal fracture half-width does exist for a given number of fractures, there are also sub-optima, in which the productivity index is not significantly different than maximum. These sub-optimal half-widths may in fact be easier to implement in practice, so a firm criteria for the what is optimal remains in question, and the engineer is encouraged to use Fig. 4.5 (and others like it) as guides, not as an absolute design requirement.

Table 4.4 — Table of Mathematically Feasible Fracture Sizes for Example Case (N_{Prop} = 1.0).

n_{frac}	w_x	w_y	w_z	n_{frac}	w_x	w_y	w_z
1	660.0	0.033	50.0	3	660.0	0.025	22.0
1	622.3	0.035	50.0	3	242.0	0.030	50.0
1	641.1	0.035	48.5	3	451.0	0.030	26.8
1	660.0	0.035	47.1	3	660.0	0.030	18.3
1	544.5	0.040	50.0	3	207.4	0.035	50.0
1	602.3	0.040	45.2	3	433.7	0.035	23.9
1	660.0	0.040	41.3	3	660.0	0.035	15.7
1	484.0	0.045	50.0	3	181.5	0.040	50.0
1	572.0	0.045	42.3	3	420.8	0.040	21.6
1	660.0	0.045	36.7	3	660.0	0.040	13.8
1	435.6	0.050	50.0	3	161.3	0.045	50.0
1	547.8	0.050	39.8	3	410.7	0.045	19.6
1	660.0	0.050	33.0	3	660.0	0.045	12.2
2	660.0	0.017	50.0	3	145.2	0.050	50.0
2	544.5	0.020	50.0	3	402.6	0.050	18.0
2	602.3	0.020	45.2	3	660.0	0.050	11.0
2	660.0	0.020	41.3	4	660.0	0.008	50.0
2	435.6	0.025	50.0	4	544.5	0.010	50.0
2	547.8	0.025	39.8	4	602.3	0.010	45.2
2	660.0	0.025	33.0	4	660.0	0.010	41.3
2	363.0	0.030	50.0	4	363.0	0.015	50.0
2	511.5	0.030	35.5	4	511.5	0.015	35.5
2	660.0	0.030	27.5	4	660.0	0.015	27.5
2	311.1	0.035	50.0	4	272.3	0.020	50.0
2	485.6	0.035	32.0	4	466.1	0.020	29.2
2	660.0	0.035	23.6	4	660.0	0.020	20.6
2	272.3	0.040	50.0	4	217.8	0.025	50.0
2	466.1	0.040	29.2	4	438.9	0.025	24.8
2	660.0	0.040	20.6	4	660.0	0.025	16.5
2	242.0	0.045	50.0	4	181.5	0.030	50.0
2	451.0	0.045	26.8	4	420.8	0.030	21.6
2	660.0	0.045	18.3	4	660.0	0.030	13.8
2	217.8	0.050	50.0	4	155.6	0.035	50.0
2	438.9	0.050	24.8	4	407.8	0.035	19.1
2	660.0	0.050	16.5	4	660.0	0.035	11.8
3	660.0	0.011	50.0	4	136.1	0.040	50.0
3	484.0	0.015	50.0	4	398.1	0.040	17.1
3	572.0	0.015	42.3	4	660.0	0.040	10.3
3	660.0	0.015	36.7	4	121.0	0.045	50.0
3	363.0	0.020	50.0	4	390.5	0.045	15.5
3	511.5	0.020	35.5	4	660.0	0.045	9.2
3	660.0	0.020	27.5	4	108.9	0.050	50.0
3	290.4	0.025	50.0	4	384.5	0.050	14.2
3	475.2	0.025	30.6	4	660.0	0.050	8.3

Table 4.4 — Continued.

n_{frac}	w_x	w_y	w_z
5	660.0	0.007	50.0
5	435.6	0.010	50.0
5	547.8	0.010	39.8
5	660.0	0.010	33.0
5	290.4	0.015	50.0
5	475.2	0.015	30.6
5	660.0	0.015	22.0
5	217.8	0.020	50.0
5	438.9	0.020	24.8
5	660.0	0.020	16.5
5	174.2	0.025	50.0
5	417.1	0.025	20.9
5	660.0	0.025	13.2
5	145.2	0.030	50.0
5	402.6	0.030	18.0
5	660.0	0.030	11.0
5	124.5	0.035	50.0
5	392.2	0.035	15.9
5	660.0	0.035	9.4
5	108.9	0.040	50.0
5	384.5	0.040	14.2
5	660.0	0.040	8.3
5	96.8	0.045	50.0
5	378.4	0.045	12.8
5	660.0	0.045	7.3
5	87.1	0.050	50.0
5	373.6	0.050	11.7
5	660.0	0.050	6.6

Table 4.5 — Locus of Maxima for Example as a Function of Number of Fractures and Permeability Anisotropy (N_{Prop} = 1.0).

n_{frac}	w_x	w_y	w_z	k_v/k_h	$J_{D,\,pss,\,max}$, 1 fracture	$J_{D,\,pss,\,max}$, Total	Fracture Contribution
1	547.80	0.050	39.76	1.000	1.7435	1.7435	0.3242
2	438.90	0.050	24.81	1.000	0.9374	1.8748	0.4239
3	402.60	0.050	18.03	1.000	0.6989	2.0968	0.5065
4	384.45	0.050	14.16	1.000	0.5886	2.3544	0.5645
5	373.56	0.050	11.66	1.000	0.5229	2.6144	0.6072
1	547.80	0.050	39.76	0.100	1.1816	1.1816	0.4971
2	438.90	0.050	24.81	0.100	0.6882	1.3764	0.6286
3	207.43	0.035	50.00	0.100	0.5304	1.5912	0.7197
4	155.57	0.035	50.00	0.100	0.4605	1.8420	0.7758
5	124.46	0.035	50.00	0.100	0.4178	2.0890	0.8126
1	435.60	0.050	50.00	0.010	0.8423	0.8423	0.7268
2	217.80	0.050	50.00	0.010	0.5705	1.1410	0.8374
3	170.82	0.043	50.00	0.010	0.4758	1.4275	0.8820
4	155.57	0.035	50.00	0.010	0.4258	1.7032	0.9042
5	124.46	0.035	50.00	0.010	0.3939	1.9696	0.9216
1	435.60	0.050	50.00	0.001	0.7070	0.7070	0.8810
2	217.80	0.050	50.00	0.001	0.5324	1.0648	0.9320
3	170.82	0.043	50.00	0.001	0.4570	1.3711	0.9513
4	155.57	0.035	50.00	0.001	0.4137	1.6547	0.9607
5	124.46	0.035	50.00	0.001	0.3859	1.9294	0.9680

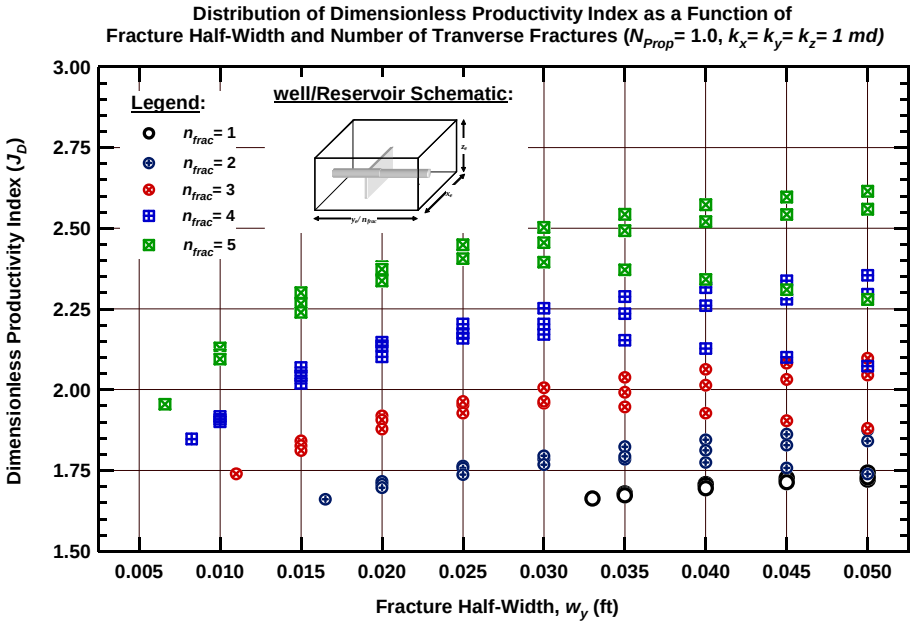

Figure 4.5 — Distribution of Dimensionless Productivity Index as a Function of Number of Fractures (N_{Prop} = 1.0, $k_x = k_y = k_z$ =1 md).

In **Figs. 4.6 to 4.9** we present the fracture contributions to flow (as a fraction of total flow) shown as a function of dimensionless time and the number of fractures for the N_{Prop} = 1.0 case, as well as for different permeability anisotropy ratios (k_v/k_h).

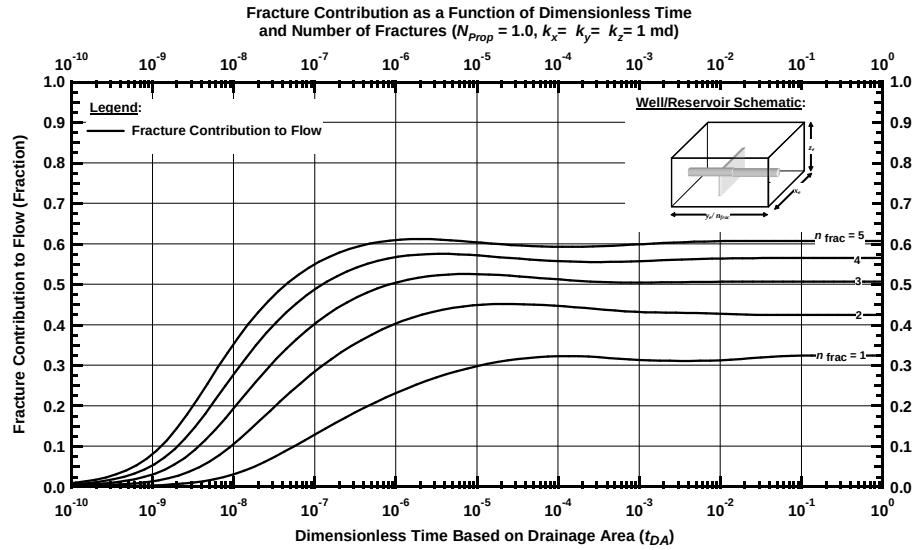

Figure 4.6 — Fracture Contribution to Flow as a Function of Dimensionless Time and Number of Fractures (N_{Prop} = 1.0, $k_x = k_y = k_z$ =1 md).

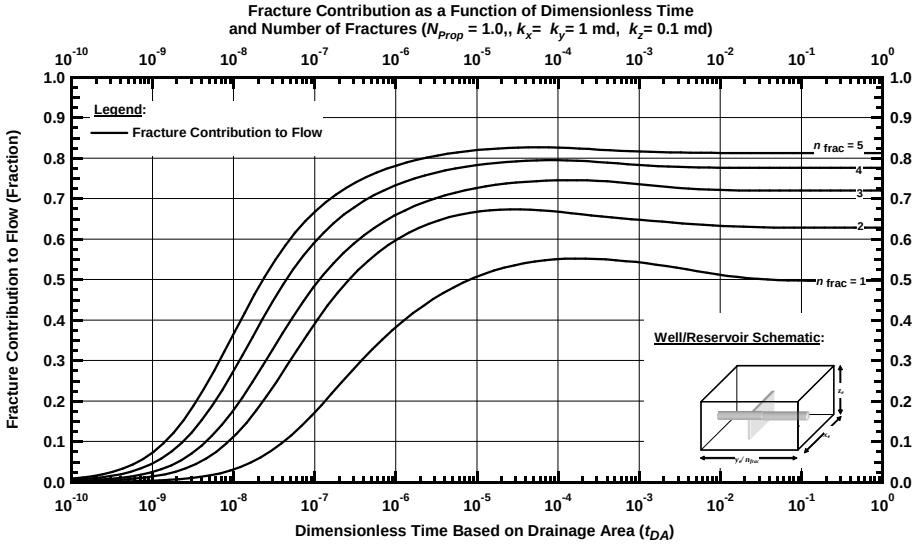

Figure 4.7 — Fracture Contribution to Flow as a Function of Dimensionless Time and Number of Fractures (N_{Prop} = 1.0, $k_x = k_y$ = 1 md, k_z = 0.1 md).

For all cases shown in Figs. 4.6 to 4.9 the early-time production is dominated by the horizontal well, the fracture contribution increases during the transient flow period and then stabilizes during the pseudosteady-state flow period. We also note that the fracture contribution increases as the permeability anisotropy increases (which is logical as less fluid would be produced by the horizontal well for such cases). Obviously, the fracture contribution to flow increases with the number of fractures — each fracture simply adds to the fracture contribution.

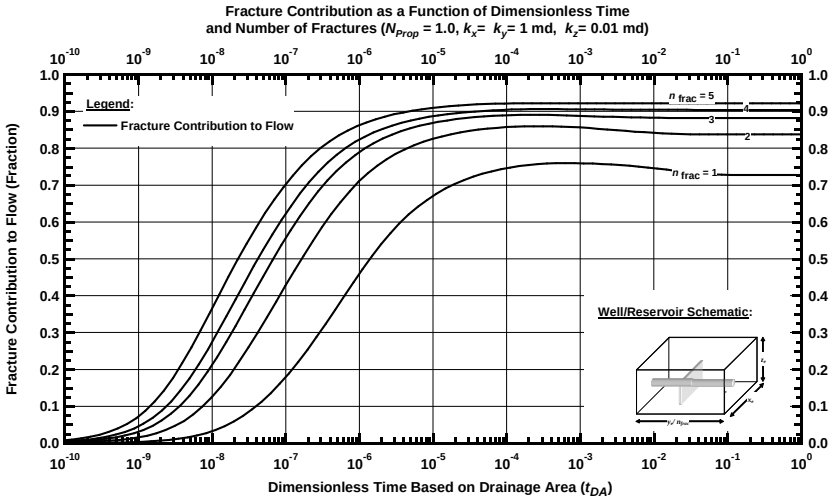

Figure 4.8 — Fracture Contribution to Flow as a Function of Dimensionless Time and Number of Fractures (N_{Prop} = 1.0, k_x = k_y = 1 md, k_z = 0.01 md).

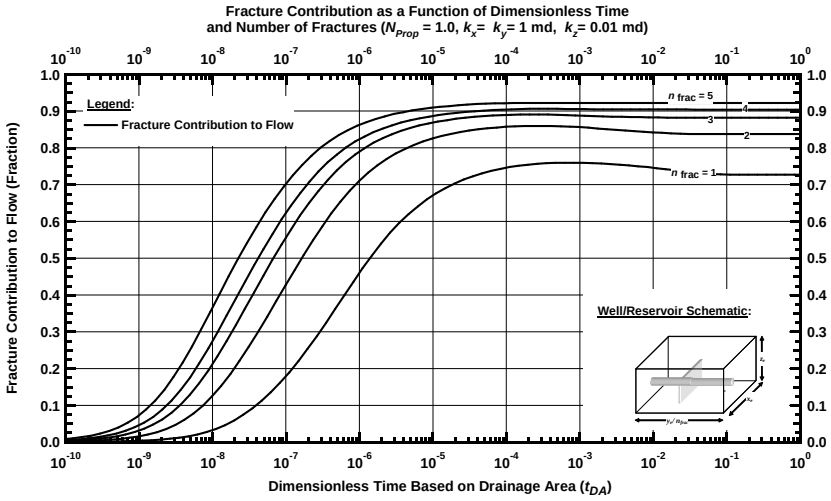

Figure 4.9 — Fracture Contribution to Flow as a Function of Dimensionless Time and Number of Fractures (N_{Prop} = 1.0, k_x = k_y = 1 md, k_z = 0.001 md).

In **Figs. 4.10 to 4.13** we present the behavior of the maximum dimensionless productivity index versus the number of fractures, for various cases of the proppant number and a specific case of permeability anisotropy. We note that the dimensionless pseudosteady-state productivity index ($J_{D,\,pss\,,Max}$) *decreases* as the anisotropy ratio *increases* — this phenomenon is observed for cases. This behavior is more severe for cases with a lower proppant number. Decreasing productivity as a consequence of increased anisotropy can be attributed to the fact that the production in the horizontal section decreases as the anisotropy increases, as discussed by Mukherjee and Economides (1991). If there is sufficient proppant to achieve an efficient (*i.e.*, high conductivity) fracture, then the lost productivity of the horizontal section would be compensated for by the increased fracture contribution.

For the specific case of proppant numbers of 1.0 and 0.001, we note a reduction of 59.5 and 26.2 percent in $J_{D\,,pss,\,Max}$. For the cases of 1 and 5 fractures (and a proppant number equal to 1.0), we have 87.3 and 83.8 percent loss compared to the same cases for a proppant number equal to 0.001. These cases illustrate the need (if not the absolute requirement) to maximize proppant volume (and proppant placement) for cases of high permeability anisotropy.

From Figs. 4.10 to 4.13 we note that $J_{D\,,pss,\,Max}$ increases as the number of fractures increase — and that this behavior is consistent for every case. We also note that the size of the increase in well productivity depends directly on the amount of proppant used.

An interesting outcome of this study is that the selection of an optimal well completion is clearly a function of all of the major variables — proppant number, number of fractures, and permeability anisotropy. In isolation — for example, the maximizing number of fractures would seem to always be the best choice. However, the issue of permeability anisotropy, which is obviously fixed by nature in practice, changes the perception that more fractures is always better (see Fig. 4.8 (k_v/k_h = 0.01) and Fig. 4.9 (k_v/k_h = 0.001), where the profiles essentially flat (*i.e.*, the number of fractures does not significantly influence the $J_{D,pss,Max}$ function).)

The impact of this "sensitivity study" is that any well/fracture design must be considered in terms of the objectives (maximize production performance) and the practical limitations of the system (permeability anisotropy and fracture treatment size). We can design the optimal fracture treatment — there will always be a clear best case(s), but can we delivery said treatment to the formation? This work provides the means to design optimal treatments for complex well/fracture configurations, but the engineer must consider any and all practical limitations of this design for implementation in the field.

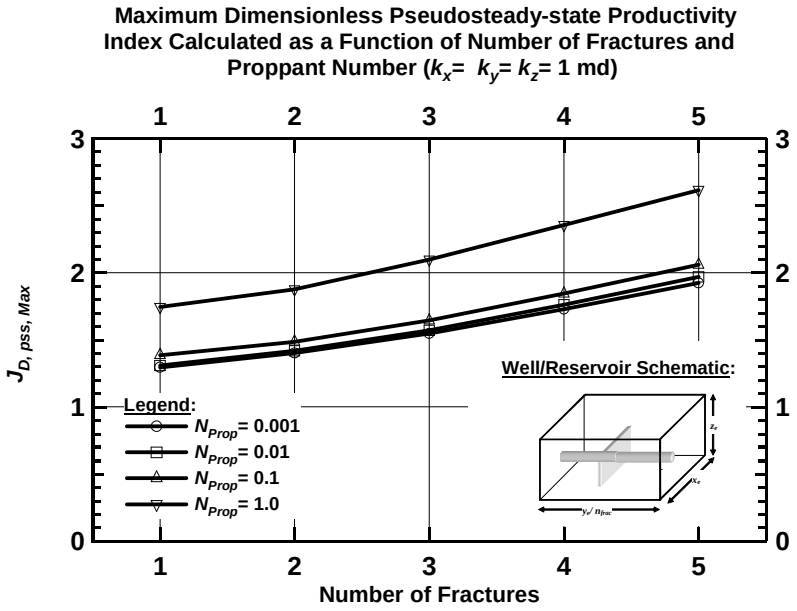

Figure 4.10 — Maximum Dimensionless Pseudosteady-State Productivity Index as a Function of Number of Fractures and Proppant Number ($k_x = k_y = k_z$ =1 md).

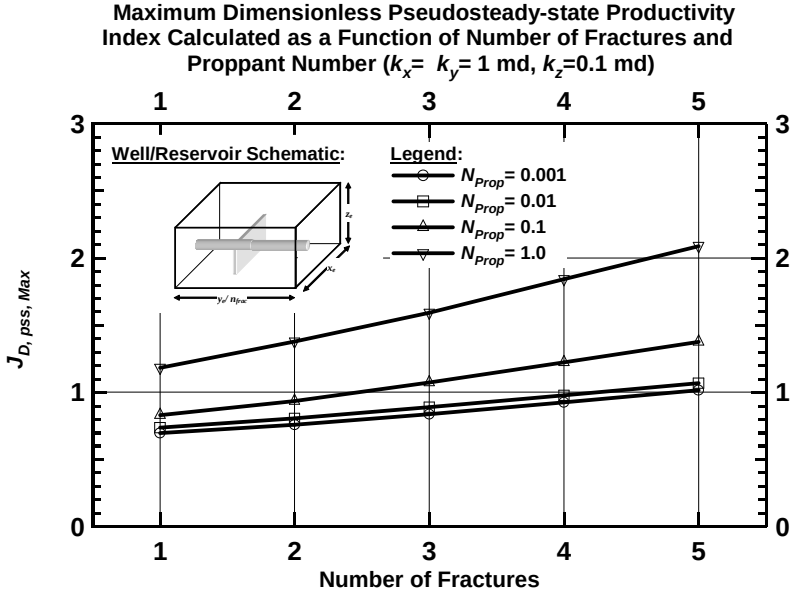

Figure 4.11 — Maximum Dimensionless Pseudosteady-State Productivity Index as a Function of Number of Fractures and Proppant Number ($k_x = k_y$ = 1 md, k_z =0.1 md).

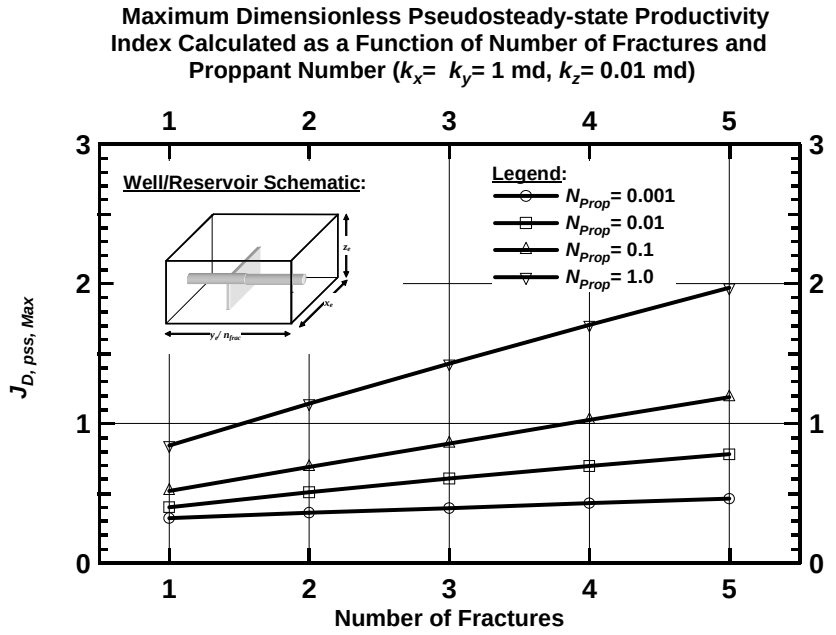

Figure 4.12 — Maximum Dimensionless Pseudosteady-State Productivity Index as a Function of Number of Fractures and Proppant Number ($k_x = k_y = 1$ md, $k_z = 0.01$ md).

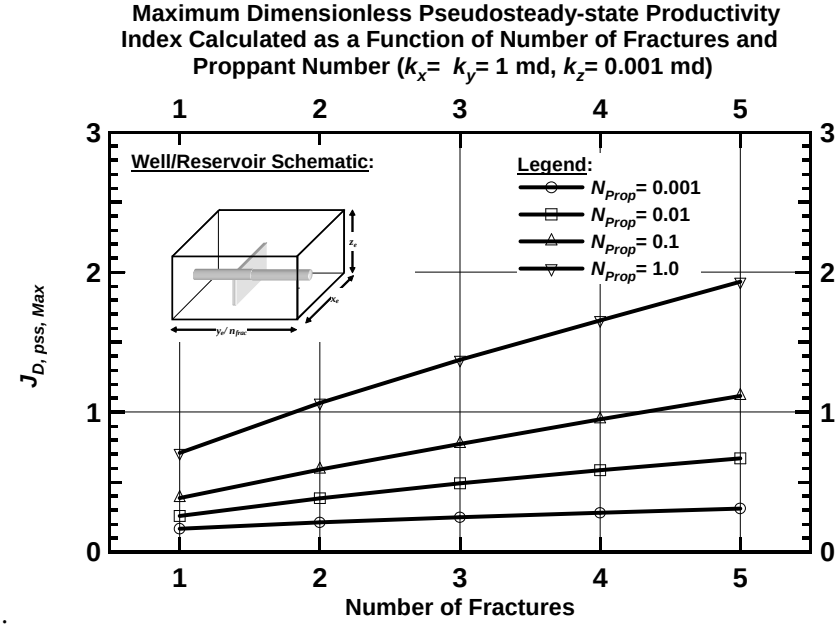

Figure 4.13 — Maximum Dimensionless Pseudosteady-State Productivity Index as a Function of Number of Fractures and Proppant Number ($k_x = k_y = 1$ md, k_z =0.001 md).

4.5 Application to Field Examples

To demonstrate the DVS method in a practical example, we have chosen to estimate the productivity behavior of the well/fracture system producing at a constant bottomhole pressure (using the procedure given in Chapter II) for example gas field cases from East Texas (USA). The reservoir and fluid data for these cases are taken from Magalhaes, Zhu, Amini, and Valko (2007). The field examples were chosen because these are low- to very-low permeability reservoirs, and a complex completion scheme of a horizontal well with multiple (transverse) fractures are considered the ideal completion scheme for this kind of reservoir. The reservoir and fluid properties for the gas field examples are shown in **Table 4.6**.

Table 4.6 — Reservoir and Fluid Properties for Example Cases.

	Whelan	**Percy Wheeler**	**Appleby North**
Net Pay (ft)	200	200	60
Horizontal Permeability (md)	0.9	0.05	0.01
Porosity (percent)	8.8	10.3	8.8
Initial Pressure (psia)	3500	3000	2800
Reservoir Temperature(°F)	220	245	254
Gas Gravity	0.63	0.62	0.61

The following assumptions are applied to all of the field cases:

- A vertical to horizontal permeability ratio (*i.e.*, k_v/k_h) of 0.10.
- A well spacing of 80 acres.
- A constant bottomhole pressure of 500psia.

We used the correlations given in the Lee, Rollins, and Spivey (2003) text to estimate gas properties such as compressibility factor, viscosity, and formation volume factor. Gas-in-place estimates were calculated for each field using the given reservoir properties and the drainage area. The gas-in-place (G) estimates for these cases are summarized in **Table 4.7**:

Table 4.7 — Initial Gas-in-Place (G) for Field Cases.

Field	***G*** **(BCF)**
Whelan	11.907
Percy Wheeler	11.495
Appleby North	2.706

The proppant properties for this study are taken from Tables 4.2 and 4.3 and the cases of 250,000 and 500,000 lb of proppant were used.

For consistency, our study considers 1,000 days of production. For each scenario, we consider the case where both the horizontal well and fractures contribute to flow, and the case where only the fractures contribute to flow. Up to five fractures are considered for each case. In **Table 4.8** we present the optimum fracture dimensions and the corresponding maximum dimensionless productivity index ($J_{D,\ pss,ma}$) for each field case — based on 500,000 or 250,000 lb of proppant and in terms of the number of fractures.

Table 4.8 — Optimum Fracture Dimensions for Field Cases as a Function of Proppant Used and Number of Fractures. Fully-Penetrating Horizontal Well Contributes to Flow.

Field, Proppant Weight (lb)	n_{frac}	w_x	w_y	w_z	$J_{D,\ pss,max}$, Total
Whelan 500,000	1	108.8	0.0500	100.0	0.667
	2	60.5	0.0450	100.0	0.793
	3	40.3	0.0450	100.0	0.938
	4	34.0	0.0400	100.0	1.086
	5	27.2	0.0400	100.0	1.231
Whelan 250,000	1	54.4	0.0500	100.0	0.625
	2	32.0	0.0425	100.0	0.734
	3	21.3	0.0425	100.0	0.856
	4	16.0	0.0425	100.0	0.982
	5	10.9	0.0500	100.0	1.105
Percy Wheeler 500,000	1	738.9	0.0100	73.7	1.266
	2	602.8	0.0100	45.1	1.519
	3	648.2	0.0050	56.0	1.817
	4	602.8	0.0050	45.1	2.094
	5	575.6	0.0050	37.8	2.344
Percy Wheeler 250,000	1	738.9	0.0050	73.7	1.015
	2	602.8	0.0050	45.1	1.230
	3	557.5	0.0050	32.5	1.436
	4	136.1	0.0050	100.0	1.651
	5	108.8	0.0050	100.0	1.876
Appleby North 500,000	1	933.5	0.0194	30.0	3.149
	2	933.5	0.0097	30.0	4.074
	3	933.5	0.0065	30.0	5.261
	4	933.5	0.0050	29.2	6.468
	5	933.5	0.0039	30.0	7.612
Appleby North 250,000	1	933.5	0.0097	30.0	3.015
	2	933.5	0.0050	29.2	3.754
	3	933.5	0.0032	30.0	4.672
	4	933.5	0.0024	30.0	5.570
	5	933.5	0.0019	30.0	6.398

It can be seen from Table 4.8 that for higher permeability reservoirs, then full penetration in vertical direction (*i.e.*, $w_z \rightarrow h/2$) is most likely to yield the optimum productivity index. Similarly, for the lower permeability reservoirs the tendency changes toward extension in the horizontal direction (*i.e.*, $w_x \rightarrow x_e/2$).

For the case of Wheeler field the optimum results are achieved by fractures with partial penetration in both directions (except for the cases with 250,000 lb of proppant and 4 and 5 fractures). This observation of vertical penetration being required in "high" permeability reservoirs is due primarily to the fact that the given amount of proppant is not sufficient to achieve efficient fractures. For the lowest permeability case (Appleby North), we observe that the optimum productivity is achieved by fractures which fully penetrate the reservoir in both directions (vertical and horizontal) — even in this case, where the amount of proppant is insufficient to yield a fracture with the width of at least a single proppant diameter.

Table 4.9 presents our final results for each field case (in terms of performance at 1000 says of production) as a function of the amount of proppant and the number of fractures (for the case where the horizontal well and fractures contribute to flow, and the case where only the fractures contribute to flow). Specifically, Table 4.9 contains the average reservoir pressure, the gas production rate, and the cumulative gas production at 1000 days of production. For reference, the complete set of results is provided for each field in Appendices G through I.

The work presented in the remainder of this section is provided to support the observations thus far, and to provide a "time-dependent" view of the performance for these cases. As noted above, the details and the complete suite of results for these examples are given in Appendices G through I.

Table 4.9 — Results of Field Case Studies, Average Reservoir Pressure, Gas Production Rate, and Cumulative Gas Production as a Function of the Amount of Proppant, Number of Fractures, and Completion Schemes for Example Cases.

Field, Proppant Weight (lb)		Fracture + Horizontal Well			Fracture Only		
	n_{frac}	p_{avg} (psia)	q_g (MMSCFD)	G_p (BCF)	p_{avg} (psia)	q_g (MMSCFD)	G_p (BCF)
Whelan 500000	1	560.2	0.59	10.05	817.9	1.73	9.15
	2	535.4	0.40	10.13	620.6	0.95	9.84
	3	519.3	0.26	10.19	554.4	0.55	10.07
	4	510.4	0.16	10.22	526.7	0.33	10.16
	5	505.7	0.10	10.23	513.7	0.20	10.21
Whelan 250000	1	573.3	0.68	10.00	923.2	2.04	8.78
	2	545.9	0.49	10.10	674.7	1.20	9.65
	3	526.4	0.33	10.16	582.6	0.73	9.97
	4	514.6	0.21	10.20	541.2	0.45	10.11
	5	507.7	0.13	10.23	520.1	0.27	10.19
Percy Wheeler 500000	1	1811.4	2.62	4.49	2089.2	2.26	3.40
	2	1667.9	2.77	5.05	1833.3	2.67	4.40
	3	1577.5	2.82	5.41	1709.5	2.79	4.89
	4	1511.8	2.84	5.67	1629.8	2.83	5.20
	5	1464.2	2.84	5.86	1575.1	2.85	5.42
Percy Wheeler 250,000	1	1976.6	2.45	3.84	2275.4	1.96	2.68
	2	1860.7	2.62	4.29	2029.2	2.44	3.63
	3	1761.3	2.74	4.68	1878.1	2.65	4.22
	4	1660.4	2.78	5.08	1725.6	2.76	4.82
	5	1572	2.82	5.43	1622	2.81	5.23
Appleby North 500000	1	1862.8	0.45	0.89	2089.9	0.34	0.67
	2	1761.6	0.48	0.99	1869.8	0.45	0.89
	3	1660.8	0.52	1.09	1717.4	0.52	1.04
	4	1565.6	0.56	1.19	1599.4	0.56	1.15
	5	1483	0.59	1.27	1505.6	0.59	1.25
Appleby North 250000	1	1911.3	0.45	0.85	2146.1	0.34	0.62
	2	1834.7	0.48	0.92	1951.8	0.44	0.81
	3	1758.9	0.52	1.00	1824.7	0.51	0.93
	4	1682.1	0.56	1.07	1724.7	0.56	1.03
	5	1613.6	0.59	1.14	1644.2	0.59	1.11

Fig. 4.14 presents the computed gas production rate as a function of production time for the Whelan field, where each fracture stimulation consists of 250,000 lbs of proppant. The Whelan field has the highest permeability of our field cases (0.10 md). In Fig. 4.14 we can distinguish two distinct flow periods — the first flow period is the transient flow period (which has very little rate decline). The second flow period is that of pseudosteady-state or boundary-dominated flow, and we note a much steeper rate decline due to the influence of the reservoir boundaries.

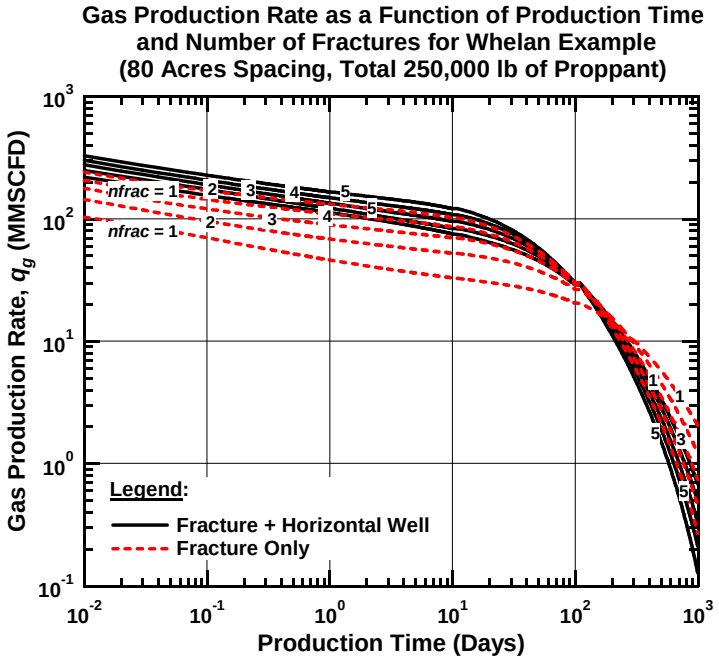

Figure 4.14 — Gas Production Rate as a Function of Production Time, Number of Fractures, and Completion Scheme for Whelan Field (80 Acres Spacing, 250,000 lb Proppant).

For other two field cases (Percy Wheeler and Appleby North), the 1,000 day production period is not sufficient time for the reservoir to produce under boundary-dominated flow conditions, even for the cases of 500,000 lb of proppant (large, highly conductive fractures). **Figs. 4.15** to **4.18** present the gas rate profiles for the Percy Wheeler and Appleby North fields, respectively for the cases of 250,000 and 500,000 lb of proppant. For production at 1,000 days, we note that the Percy Wheeler field case shows evidence of the start of the boundary-dominated flow, but for the Appleby North field case we can only observe the *transition* into boundary-dominated flow.

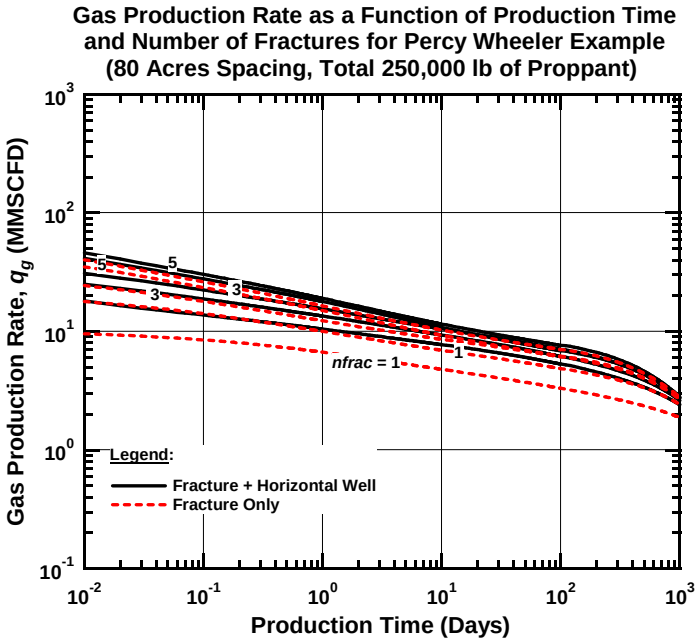

Figure 4.15 — Gas Production Rate as a Function of Production Time, Number of Fractures, and Completion Scheme for Percy Wheeler Field (80 Acres Spacing, 250,000 lb Proppant).

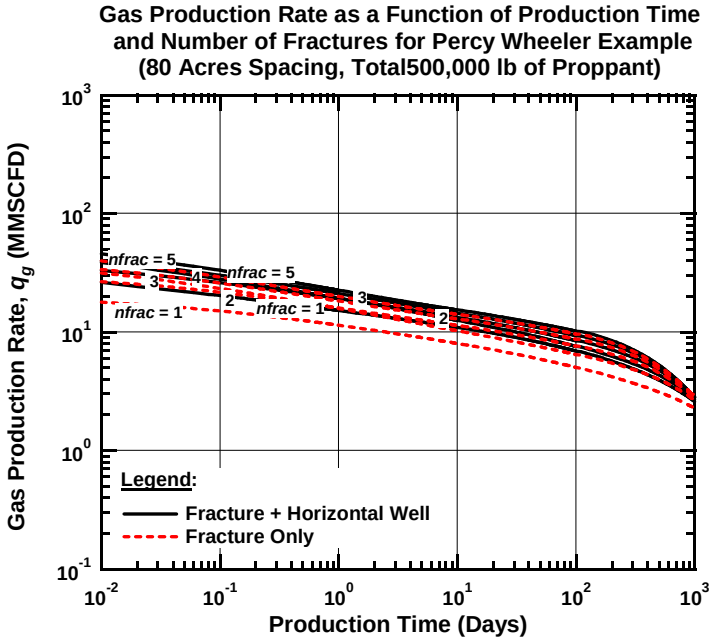

Figure 4.16 — Gas Production Rate as a Function of Production Time, Number of Fractures, and Completion Scheme for Percy Wheeler Field (80 Acres Spacing, 500,000 lb Proppant).

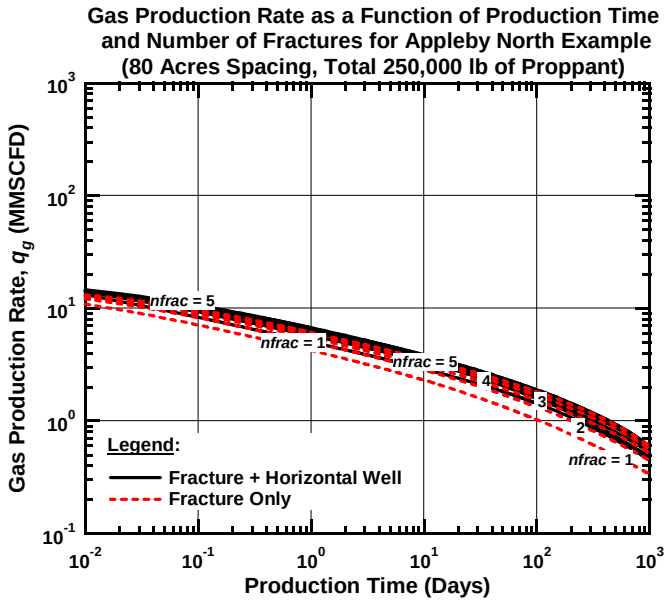

Figure 4.17 — Gas Production Rate as a Function of Production Time, Number of Fractures, and Completion Scheme for Appleby North Field (80 Acres Spacing, 250,000 lb Proppant).

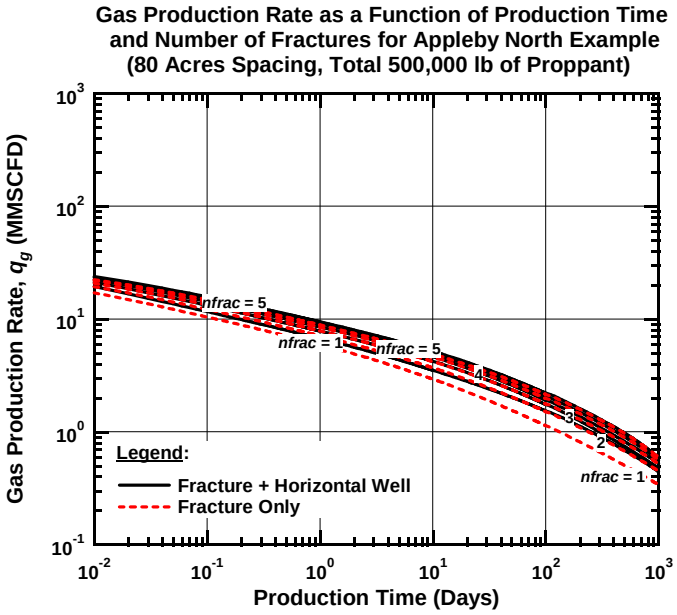

Figure 4.18 — Gas Production Rate as a Function of Production Time, Number of Fractures, and Completion Scheme for Appleby North Field (80 Acres Spacing, 500,000 lb Proppant).

In **Figures 4.19** to **4.22** we present the computed average reservoir pressure profiles (versus production) time for the Whelan and Appleby North fields, for cases of 250,000 or 500,000 lb of proppant. These comparisons are provided to illustrate the influence of the number of fractures, the proppant used, and the fractures themselves (comparisons of "fracture + horizontal well" and "fracture only" performance). The primary discriminator for these cases is actually reservoir permeability (Whelan field (0.9 md) and Appleby North field (0.01 md)) — ultimately, permeability will be the most influential variable for these presentations of computed average reservoir pressure.

The "steepness" of the average pressure decline could be construed as an indicator of the most efficient depletion (*i.e.*, the most rapid recovery). In such a case, the "fracture only" cases for the Whelan field comparison (Figs. 4.19 and 4.20) would appear to be the least "efficient" (as would be expected) — however; it is our contention that increasing the stimulation (proppant) volume for the "fracture only" cases may yield faster depletion, but poor economics. The most obvious conclusion that can be drawn from Figs. 4.19 and 4.20 is that the 1 and 2 fracture cases (within the "fracture only" cases) are by far the least efficient — hence, the observation that more fractures would always be better is certainly supported by these cases, but again, economic (rather than just technical) aspects must be considered to justify such a claim. As for the Appleby North field cases (Figs. 4.21 and 4.22) the comparison of average reservoir pressure with time merely confirmed that these cases are not in full depletion.

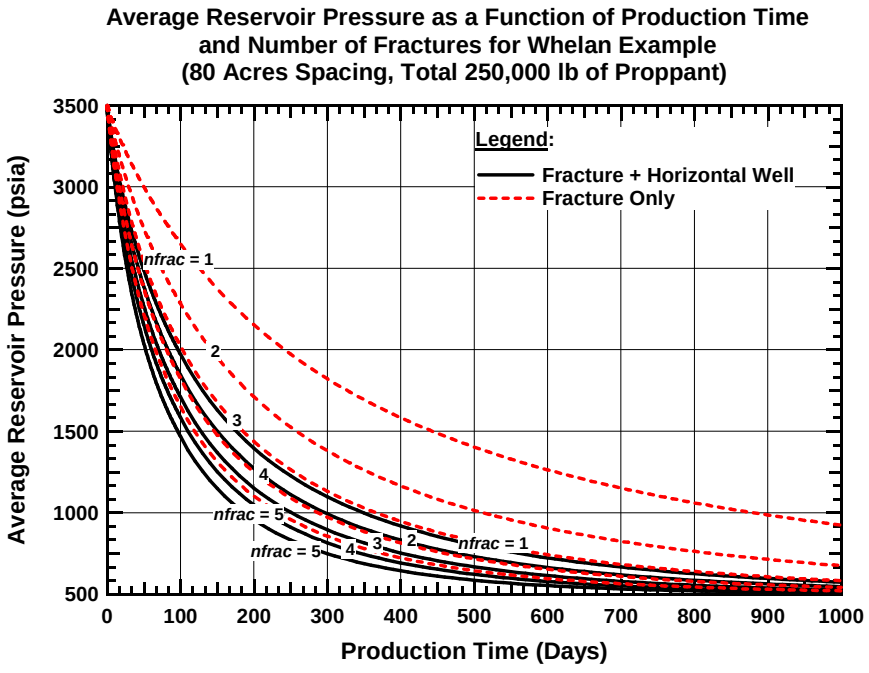

Figure 4.19 — Average Reservoir Pressure as a Function of Production Time, Number of Fractures, and Completion Scheme for Whelan Field (80 Acres Spacing, 250,000 lb Proppant).

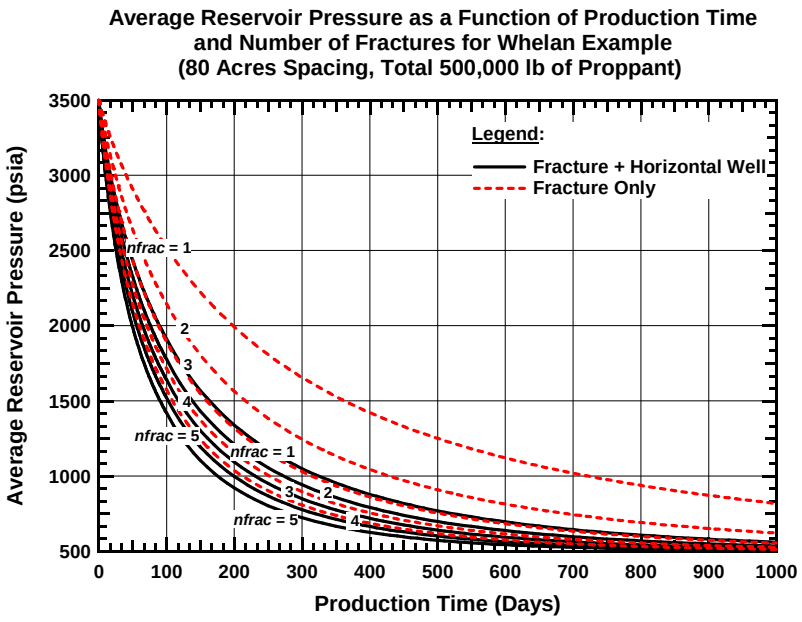

Figure 4.20 — Average Reservoir Pressure as a Function of Production Time, Number of Fractures, and Completion Scheme for Percy Whelan Field (80 Acres Spacing, 500,000 lb Proppant).

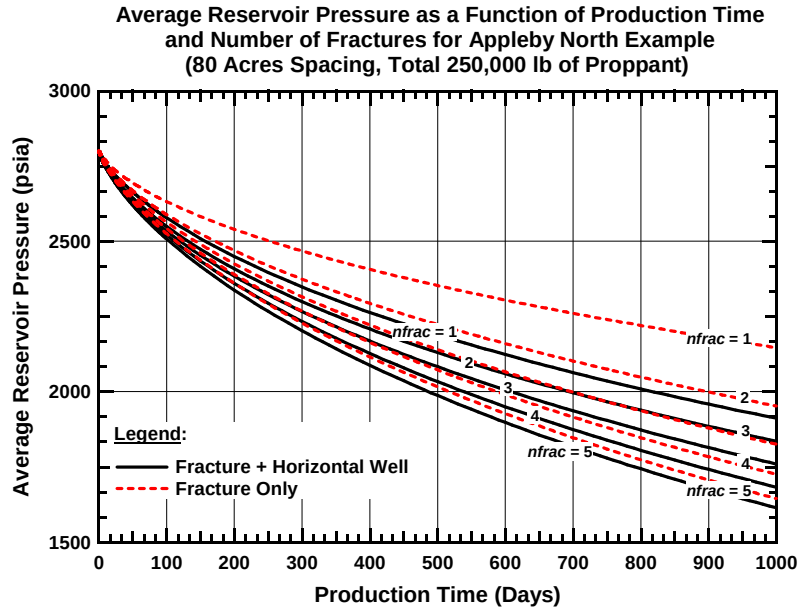

Figure 4.21 — Average Reservoir Pressure as a Function of Production Time, Number of Fractures, and Completion Scheme for Appleby North Field (80 Acres Spacing, 250,000 lb Proppant).

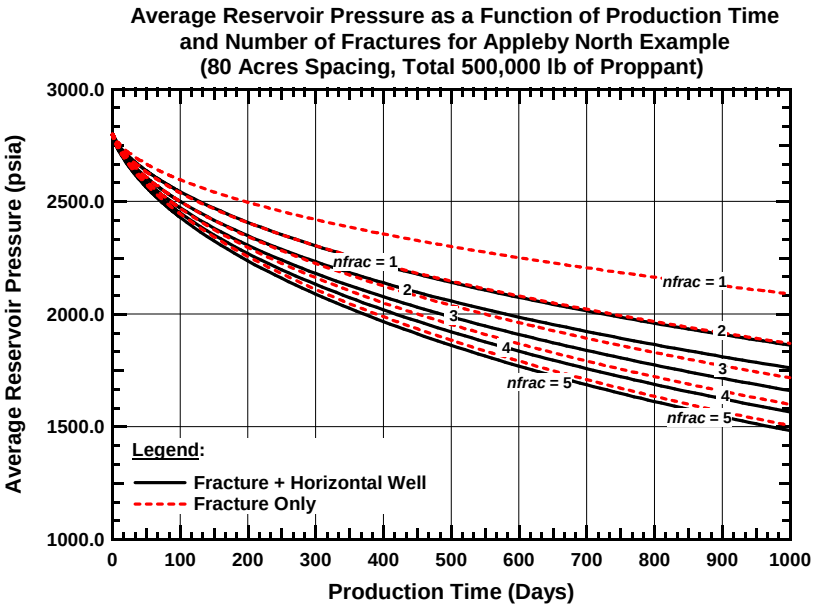

Figure 4.22 — Average Reservoir Pressure as a Function of Production Time, Number of Fractures, and Completion Scheme for Appleby North Field (80 Acres Spacing, 500,000 lb Proppant).

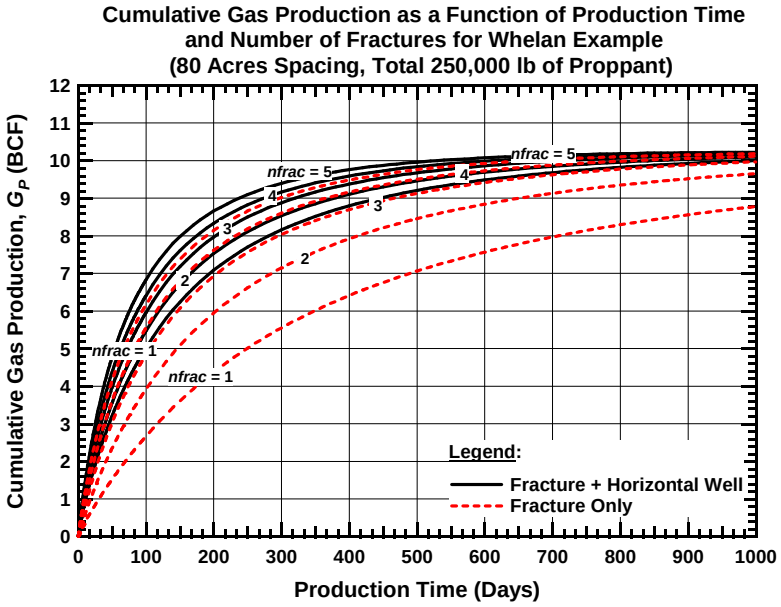

Figure 4.23 — Cumulative Gas Production as a Function of Production Time, Number of Fractures, and Completion Scheme for Whelan Field (80 Acres Spacing, 250,000 lb Proppant).

In contrast to comparison of the computed average reservoir pressure profiles, comparison of the cumulative gas production as a function of time will definitively illustrate "efficient" depletion. That is, the cases with the most rapid depletion (of a fixed resource) will yield the highest return on investment (all factors being equal). In **Figs. 4.23 to 4.28** we present the behavior of the cumulative gas production as a function of production time for all field cases and differing completions (*i.e.*, proppant volumes and well structures).

The most straightforward conclusion we can make is that adding new fractures increases the production and accelerates the production of reserves. We note that the importance of these two issues (production increases and reserve acceleration) varies as the permeability of the reservoir changes. For low permeability reservoirs such as the Appleby North field, additional fracture(s) *may* provide more additional reserves (but this is actually only likely in very low permeability scenarios (<0.001 md) and in cases of geological reservoir heterogeneity (poor vertical and lateral continuity of the reservoir)). In a practical sense, for homogeneous reservoir systems of low to moderate permeability (>0.01 md), we should expect *acceleration* of reserves when we deploy well completions such as these.

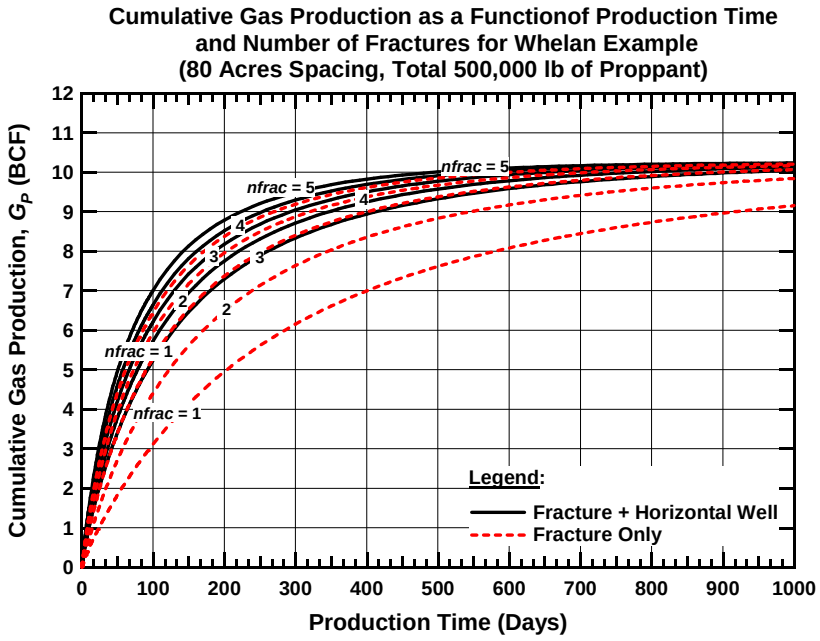

Figure 4.24 — Cumulative Gas Production as a Function of Production Time, Number of Fractures, and Completion Scheme for Whelan Field (80 Acres Spacing, 500,000 lb Proppant).

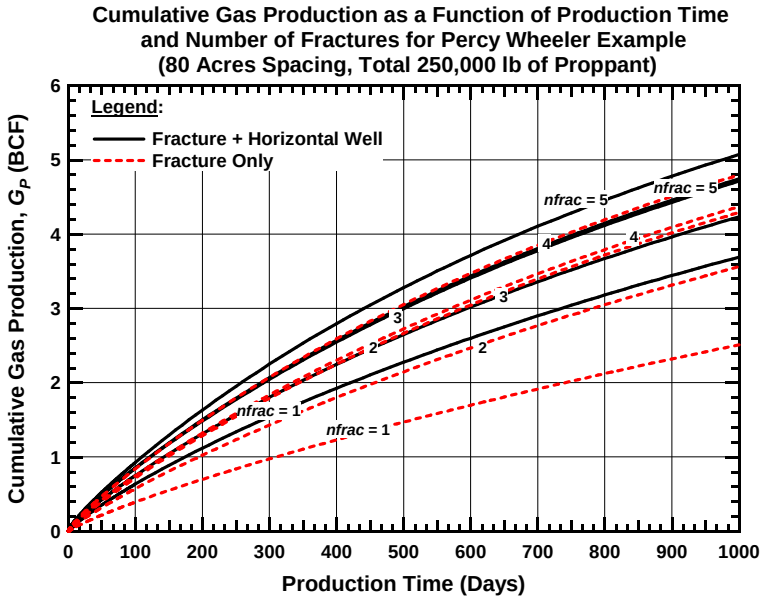

Figure 4.25 — Cumulative Gas Production as a Function of Production Time, Number of Fractures, and Completion Scheme for Percy Wheeler Field (80 Acres Spacing, 250,000 lb Proppant).

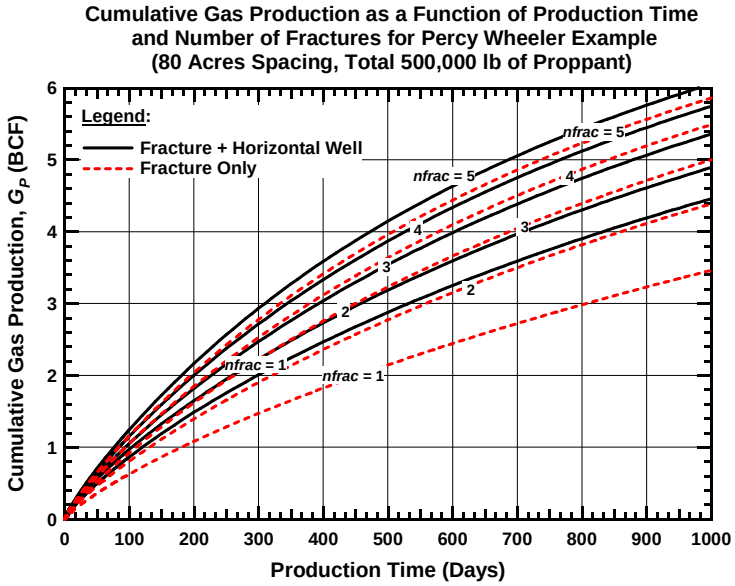

Figure 4.26 — Cumulative Gas Production as a Function of Production Time, Number of Fractures, and Completion Scheme for Percy Wheeler Field (80 Acres Spacing, 500,000 lb Proppant).

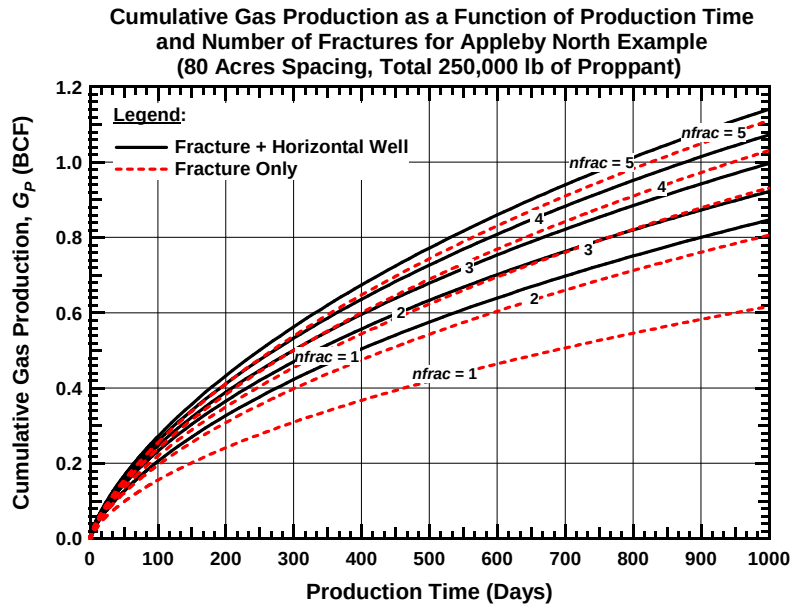

Figure 4.27 — Cumulative Gas Production as a Function of Production Time, Number of Fractures, and Completion Scheme for Appleby North Field (80 Acres Spacing, 250,000 lb Proppant).

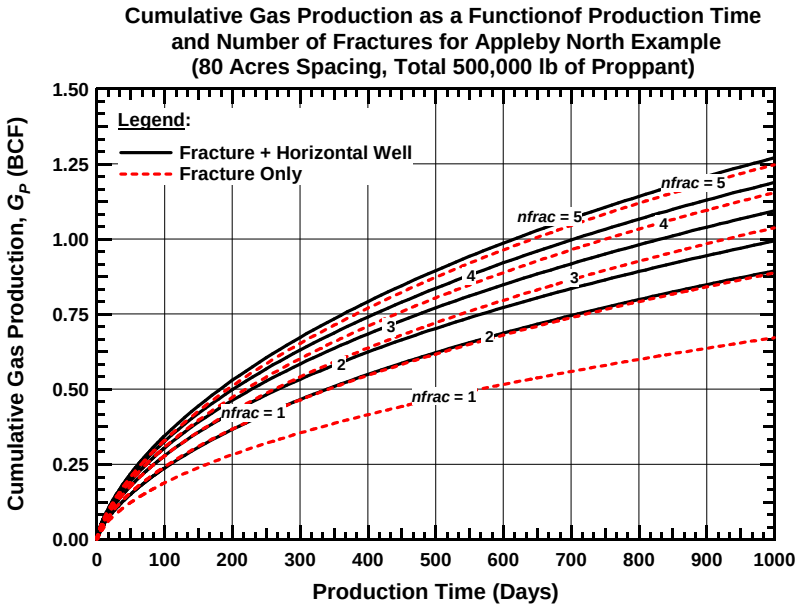

Figure 4.28 — Cumulative Gas Production as a Function of Production Time, Number of Fractures, and Completion Scheme for Appleby North Field (80 Acres Spacing, 500,000 lb Proppant).

It is also a general perception that the advantage of placing additional fractures in the reservoir diminishes as the number of fractures increases. This perception is based on the fact that since the total drainage area is limited, individual fractures will begin to drainage volumes, and produce less over time. This is true for both cases presented in this study — the case where the horizontal well and fractures contribute to flow, and the case where only the fractures contribute to flow. A practical issue regarding multiple fractures is a risk of an adverse event as more and more fractures are added — such as accessing water or damage to the wellbore that limits access to all of the created hydraulic fractures.

For all of the cases we consider, the horizontal well adds more to the production performance than adding another fracture. We note this observation because some may opt to drain a given reservoir partition with only vertically fractured wells, while others may employ horizontal wells with multiple transverse fractures. It is important to recognize that, in a sensitivity study such as this, the contribution of the horizontal well is always relevant, but as Figs. 4.10 to 4.13 illustrate the influence of reservoir anisotropy is extremely important, and may minimize or even negate the effects of the horizontal well.

The use of additional proppant is seen to accelerate the recovery of reserves for all the cases studied, but the level of improvement is dependent on the reservoir permeability and the well/fracture configuration. We generally note positive effects of using more proppant for a larger number of fractures, as more proppant should build more efficient fractures. However; if a given set of fractures can effectively deplete the reservoir, then larger treatments would be unjustifiable in an economic sense.

4.6 Summary

This chapter provides example applications of the DVS method for the prediction of well productivity for various complex well/fracture configurations. Modeling and validation procedures were demonstrated and discussed, and example applications to relevant field cases are given. Our results imply that the most effective well configuration is that of a horizontal well with multiple (transverse) fractures, where as much as proppant and as many fractures as possible are used. Obviously this is an ideal scenario, and we need to establish an optimal well completion for each individual case — which would be the most technically feasible as well as the most economic well completion scheme that yields the highest possible productivity.

The primary objective of this chapter was to demonstrate that the DVS method can be used effectively to design and optimize a well completion from a technical standpoint. We believe that the DVS method has been successfully demonstrated and validated for that purpose, and we recognize that such tools must be used with the relevant economic constraints. Our goal was to provide a tool. We believe that the DVS method can be used to effectively design and model virtually any well completion that can be envisioned.

CHAPTER V

SUMMARY, CONCLUSIONS, AND RECOMMENDATIONS FOR FUTURE WORK

5.1 Summary

The primary purpose of this work is to develop a new method to predict the transient and pseudosteady-state pressure and production behavior of a closed, rectangular reservoir. In particular, to develop an analytical/semi-analytical solution that can be used to model vertical and horizontal wells with or without a variety of hydraulic fractures. Such a solution can be extended to other cases, but the aforementioned cases are the focus of this work.

In this work we performed the following tasks as:

- We developed the method of distributed volumetric sources (DVS) as a solution for the problem of pressure distributions in a closed, rectangular reservoir using a uniform flux source (the simplest case for such problems).
- Using the DVS solution method, we have successfully developed and *validated* the solutions for pressure behavior of simple and complex well/fracture configurations as follows:
  - — Unfractured vertical wells
  - — Horizontal well (uniform-flux and infinite-conductivity)
  - — Hydraulically fractured vertical wells (infinite- and finite-conductivity fractures).
- We have generated the transient and pseudosteady-state productivity index behavior using the pressure response results (using the DVS method) and we validated these results using reservoir simulation and/or existing analytical/semi-analytical models from the production engineering literature.
- We demonstrated the applicability of the new solution method in predicting production behavior for a complex well/fracture configuration — specifically, the case of a horizontal well with multiple transverse fractures, where both the horizontal section and the fractures contribute to production.
- As an application, we applied the DVS method as an optimization/screening tool to obtain the best completion scheme for the development of a field example case (estimated multiple production performance cases for a reservoir with wells produced at constant bottomhole pressures for various completion scenarios).

5.2 Conclusions

We have successfully developed, validated, and demonstrated the DVS method to a practical mechanism for the generation of consistent transient and pseudosteady-state solutions for complex well/fracture systems. The DVS method has been shown to provide reliable results with relatively moderate computational effort.

As a validation, we utilized the DVS approach to create well/reservoir models for simple cases with well-known solutions as well as for a complex well/reservoir configuration case that where a reservoir simulation model was used for validation. The advantage of the DVS method is more obvious for cases with significant complexities — such as permeability anisotropy, partial penetration of the source in any of the principal directions, and/or additional pressure losses stemming from the particular geometry of the flow path inside the sources.

For our particular purposes (production forecasting and optimizing the well completion strategy), we wanted to provide a consistent mechanism to generate the transient and pseudosteady-state productivity indices. In such applications the DVS method has been shown to be extraordinarily flexible in model construction and the DVS method is comparable in terms of computation speeds with most analytical solutions (for simple cases) and the DVS method is competitive with numerical simulation models for complex reservoir cases.

5.3 Recommendations for Future Work

The future work on this topic should focus on the application of the DVS method for more cases of complex well/fracture schemes. In this work we demonstrate a single example case of the application of the DVS method. One of the basic assumptions in development of the DVS solution is the assumption of the reservoir having closed (no flow) boundaries — future efforts should also consider constant pressure and/or mixed boundary conditions.

Also, complex well/fracture completion schemes are typically deployed for the development of economically-marginal gas reservoirs — those in which non-Darcy (*i.e.*, non-laminar) flow effects can considerably affect the production performance of the system. Incorporation of non-Darcy effects should be considered in future research efforts.

Perhaps less important from a research standpoint, but certain important from the application standpoint is the issue of computational efficiency. The DVS method is an analytical/semi-analytical solution approach (the "semi-analytical" label applies to cases such as finite-conductivity wells or fractures which require discretization of the source), and as such the solutions are direct — but this fact does not guarantee speed or efficiency of computations due to the structure and component terms in the DVS solutions. Optimization of DVS solutions in terms of computational speed may be achieved at a cost in accuracy, but in a research initiative such as this, we are far more interested in accuracy than speed. As a suggestion, it is likely that the conversion of the DVS method to a more traditional programming language (all of our work is performed in *Mathematica*) will substantially improve computational times.

NOMENCLATURE

Variables

$\mathbf{A}$	=	matrix of source effects
$\mathbf{b}$	=	drawdown vector
b_f	=	Fracture width, ft
$\mathbf{C}$	=	matrix of pressure drop effects
C_{fD}	=	dimensionless fracture conductivity
c_t	=	total compressibility, psi^{-1}
c_{trad}	=	conversion factor
c_x	=	position of the center of the source in x direction, ft
c_y	=	position of the center of the source in y direction, ft
c_z	=	position of the center of the source in z direction, ft
D_w	=	source domain
$\mathbf{D}$	=	coefficient matrix
d_p	=	proppant diameter, in
f	=	1D solution to the flow equation
G	=	Green's function, initial gas in place, BCF
G_p	=	Cumulative gas production, BCF
H	=	Heaviside unit step function
h	=	Height, ft
J_D	=	dimensionless productivity index
$J_{D,trad}$	=	traditional definition of dimensionless productivity index
K_0	=	Bessel K function of order zero
k	=	permeability, reference permeability, md
k_f	=	fracture permeability
k_x	=	directional permeability in x direction, md
k_y	=	directional permeability in y direction, md
k_z	=	directional permeability in z direction, md
L	=	reference length, ft
$\mathbf{M}$	=	coefficient matrix of material balance equation
m(p)	=	pseudopressure function $2\int_{p_{ref}}^{p} \frac{pdp}{\mu z}$
N_{prop}	=	Proppant number, $\frac{2k_f V_{fracture}}{kV_{reservoir}}$

n	=	number of fracture segments
n_h	=	number segments in horizontal section
n_x	=	number of fracture segments in *x* direction
n_z	=	number of fracture segments in *z* direction
p	=	pressure, psi
$\mathbf{P_D}$	=	Dimensionless pressure vector
p_i	=	initial pressure, psi
p_{wf}	=	well flowing pressure, psi
$\overline{p}_{wD}$	=	Dimensionless wellbore pressure in Laplace domain
$p_{\delta D}$	=	dimensionless pressure due to instantaneous source
PI	=	Productivity index, STB/d/psi
p_{uD}	=	dimensionless pressure due to continuous source
q	=	source strength, production rate
$\overline{q}_{fD}$	=	Dimensionless flow in fracture in Laplace domain
$\mathbf{q}$	=	source strength vector
r_w	=	wellbore radius
s	=	Laplace parameter
S_e	=	Boundary surface domain
t	=	time
t	=	integrating variable
t_D	=	dimensionless time
t_{DA}	=	dimensionless time with regard to reference drainage volume
$t_{DA,trad}$	=	dimensionless time with regard to fracture half-length
t_{Dxf}	=	traditional dimensionless time with regard to drainage area
U	=	Product of 3 unit step functions
u_t	=	derivative of function u with respect to time
u_{xx}	=	second derivative of function u with respect to position
$V_{fracture}$	=	Fracture volume, ft^3
$V_{reservoir}$	=	reservoir volume, ft^3
w_x	=	source width in x direction, ft
w_y	=	source width in y direction, ft
w_z	=	source width in y direction, ft
x_D	=	dimensionless length in x direction, x/x_e
x_e	=	length of the outer box, ft
x_f	=	fracture half length, ft
x_l	=	dimensionless starting position of the source

x_u	=	dimensionless ending position of the source
y_D	=	dimensionless width in y direction, y/y_e
y_e	=	width of the outer box, ft
z	=	Gas compressibility
z_D	=	dimensionless height in z direction, z/z_e
z_e	=	height of the outer box, ft

Greek Symbols

ϕ	=	porosity, fraction
ϕ_p	=	proppant porosity
η	=	diffusivity, $\frac{k}{\phi\mu c_t}$
μ	=	viscosity, cp
ρ_p	=	proppant density

Subscript

f	=	fracture
g	=	gas
gen	=	general
max	=	maximum

REFERENCES

1. Azar-Nejad, F., Tortike, W.S., and Farouq Ali. S.M. 1996. Potential Distribution Around the Sources With Finite Length (Horizontal, Vertical Partially Penetrating Wells and Fractures) Part I: Steady State Fluid Flow. Paper SPE 35270 presented at the Mid-Continent Gas Symposium, Amarillo, Texas, 28–30 April.

2. Azar-Nejad, F., Tortike, W.S., and Farouq Ali. S.M. 1996. Potential Distribution Around the Sources With Finite Length (Horizontal, Vertical Partially Penetrating Wells and Fractures) Part II: Transient Flow. Paper SPE 35269 presented at the Mid-Continent Gas Symposium, Amarillo, Texas, 28–30 April.

3. Azar-Nejad, F, Tortike, W.S., and Farouq Ali S.M. 1996. Performance of Horizontal Wells With Irregular Geometry. Paper SPE 36550 presented at the SPE Annual Technical Conference and Exhibition, Denver, Colorado, 6–9 October.

4. Babu, D.K. and Odeh, A.S. 1989. Productivity of a Horizontal Well. *SPERE* **4** (4): 417–421. SPE-18298-PA.

5. Chen, H.Y. and Asaad, N. 2005. Horizontal-Well Productivity Equations With Both Uniform-Flux and Uniform-Pressure Wellbore Models. Paper SPE 97190 presented at the SPE Annual Technical Conference and Exhibition, Houston, Texas, 9–12 October.

6. Cinco-Ley, H. and Meng, H.-Z. 1988. Pressure Transient Analysis of Wells With Finite Conductivity Vertical Fracture in Double Porosity Reservoirs. Paper SPE 18172 presented at the SPE Annual Technical Conference and Exhibition, Houston, Texas, 2–5 October.

7. Cinco-Ley, H., Samaniego-V. F., and Domínguez, N. 1978. Transient Pressure Behavior of a Well With a Finite-Conductivity Vertical Fracture. *SPEJ* **18** (4): 253–264. SPE-6014-PA.

8. Economides, M.J., Oligney, R.E., and Valkó, P.P. 2002. *Unified Fracture Design*, 23–38. Alvin, Texas: Orsa Press.

9. Goode, P.A. and Kuchuk, F.J. 1991. Inflow Performance of Horizontal Wells. *SPERE* **6** (3): 319–323. SPE-21460-PA.

10. Gringarten, A.C. and Ramey, H.J. Jr. 1973. The Use of Source and Green's Functions in Solving Unsteady-Flow Problems in Reservoirs. *SPEJ* **13** (5): 285–296; *Trans.*, AIME, **255.** SPE-3818-PA.

11. Gringarten, A.C., Ramey, H.J. Jr., and Raghavan, R. 1974. Unsteady-State Pressure Distribution Created by a Well With a Single Infinite-Conductivity Vertical Fracture. *SPEJ* **14** (4): 347–360; *Trans.*, AIME, **257.** SPE-4051-PA.

12. Lee, J, Rollins, J. B., and Spivey, J. P. 2003. *Pressure Transient Testing.* SPE Textbook Series, Richardson, Texas **9**: 313–340

13. Magalhaes, F., Zhu, D., Amini, S., and Valkó, P. P. 2007. Optimization of Fractured Well Performance of Horizontal Gas Wells. Paper SPE 108779 presented at the International Oil Conference and Exhibition, Veracruz, Mexico, 27–30 June.

14. Meyer, B.R. and Jacot, R.H. 2005. Pseudosteady-State Analysis of Finite-Conductivity Vertical Fractures. Paper SPE 95941 presented at the SPE Annual Technical Conference and Exhibition, Dallas, Texas, 9–12 October.

15. Mukherjee, H., and Economides, M. J. 1991. A Parametric Comparison of Horizontal and Vertical Well Performance. *SPEFE* **6** (2): 209–216. SPE-18303-PA.

16. Newman, A.B. 1936. Heating and Cooling Rectangular and Cylindrical Solids. *Ind. and Eng. Chem.* **28** (5): 545–548.

17. Ozkan, E. 1988. Performance of Horizontal Wells, PhD dissertation, U. of Tulsa, Tulsa, Oklahoma.

18. Peaceman, D.W. 1978. Interpretation of Well-Block Pressures in Numerical Reservoir Simulation. *SPEJ* **18** (3): 183–194; *Trans.*, AIME, **265.** SPE-6893-PA.

19. Raghavan, R. 1993. *Well Test Analysis*, Englewood Cliffs, New Jersey, Prentice Hall. 45–68

20. Ramey, H. J. Jr., and Cobb, W. M. 1971. A General Pressure Buildup Theory for a Well in a Closed Drainage Area. *JPT* **23** (12): 1493–1505. SPE-3012-PA.

21. Yildiz, T. and Bassiouni, Z. 1991. Transient Pressure Analysis in Partially-Penetrating Wells. Paper SPE 21551 presented at The International Joint Meeting of the Petroleum Society of CIM and SPE, Calgary, Alberta, Canada, 10–13 June.

APPENDIX A

DEVELOPMENT OF THE SOLUTION

Development of the Model

The model consists of a rectilinear, anisotropic, homogeneous medium with no-flow boundaries with boundaries parallel to the main permeability axes. The source is defined as a rectilinear box in the surrounding box with the same properties of the main reservoir medium. **Fig. A.1** shows the schematic of the model.

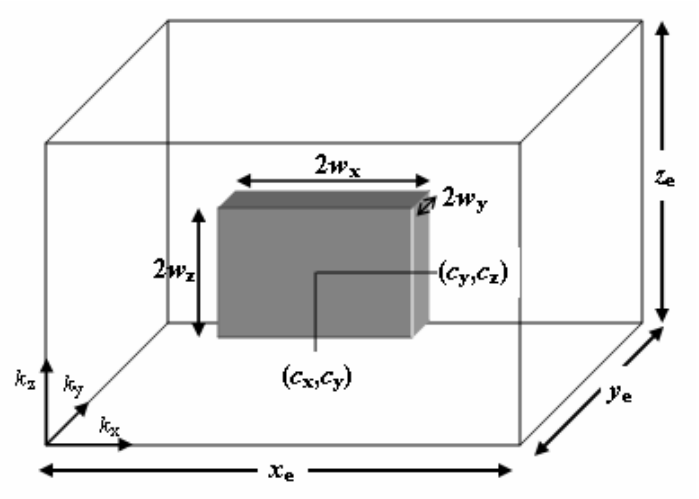

Figure A.1— Schematic of the Model

For an anisotropic, homogeneous reservoir with internal source, the diffusivity equation can be written as:

$$\eta_x \frac{\partial^2 p}{\partial x^2} + \eta_y \frac{\partial^2 p}{\partial y^2} + \eta_z \frac{\partial^2 p}{\partial z^2} + \frac{1}{\phi c_t} Q(x,y,z,t) = \frac{\partial p}{\partial t} \tag{A.1}$$

With the following initial and boundary conditions:

I.C.:

$$p(x,y,z,0) = p_i \tag{A.2}$$

B.C.s:

$$\begin{aligned} \left.\frac{\partial p}{\partial x}\right|_{x=0} &= \left.\frac{\partial p}{\partial x}\right|_{x=x_e} = 0 \\ \left.\frac{\partial p}{\partial y}\right|_{y=0} &= \left.\frac{\partial p}{\partial y}\right|_{y=y_e} = 0 \\ \left.\frac{\partial p}{\partial z}\right|_{z=0} &= \left.\frac{\partial p}{\partial z}\right|_{z=z_e} = 0 \end{aligned} \tag{A.3}$$

Where

$$\eta_i = \frac{k_i}{\phi\mu c_t},\ i = x, y, \text{ and } z \tag{A.4}$$

$Q(x,y,z,t)$ in Eq. A.1 is the source function, which for the instantaneous source can be written as:

$$\begin{aligned} Q(x,y,z,t) = \frac{qB}{8w_x w_y w_z}\delta(t)&[H(x-c_x-w_x)-H(x-c_x+w_x)] \\ &\times[H(y-c_y-w_y)-H(y-c_y+w_y)] \\ &\times[H(z-c_z-w_z)-H(z-c_z+w_z)] \end{aligned} \tag{A.5}$$

$\delta(t)$ represents the Dirac delta function and $H(x)$ represents the Heaviside unit-step function.

To simplify the problem we define dimensionless variables as the followings:

$$\begin{aligned} x_D &= \frac{x}{x_e} \\ y_D &= \frac{y}{y_e} \\ z_D &= \frac{z}{z_e} \end{aligned} \tag{A.6}$$

$$p_D = \frac{kL}{qB\mu}(p_i - p) \tag{A.7}$$

$$t_D = \frac{k}{\phi\mu c_t L^2}t \tag{A.8}$$

It should be noted that the dimensionless pressure and time defined in Eqs. A.7 and A.8 have different definitions than the traditional definitions of the dimensionless pressure and time. *k* and *L* are reference permeability and length with the following definitions:

$$\begin{aligned} k &= (k_x k_y k_z)^{\frac{1}{3}} \\ L &= (x_e y_e z_e)^{\frac{1}{3}} \end{aligned} \tag{A.9}$$

Introducing the dimensionless variables to Eq. A.1 and its initial and boundary conditions we have:

$$(\frac{k_x}{k})(\frac{x_e}{L})^2\frac{\partial^2 p_D}{\partial x_D^2}+(\frac{k_y}{k})(\frac{y_e}{L})^2\frac{\partial^2 p_D}{\partial y_D^2}+(\frac{k_z}{k})(\frac{z_e}{L})^2\frac{\partial^2 p_D}{\partial z_D^2}+\frac{\delta(t_D)U(x_D,y_D,z_D)}{8w_{xD}w_{yD}w_{zD}}=\frac{\partial p_D}{\partial t_D} \quad (A.10)$$

With

I.C.:

$$p_D(x_D,y_D,z_D,0)=0 \quad (A.11)$$

B.C.s:

$$\begin{aligned}\left.\frac{\partial p_D}{\partial x_D}\right|_{x_D=0}&=\left.\frac{\partial p_D}{\partial x_D}\right|_{x_D=1}=0\\ \left.\frac{\partial p_D}{\partial y_D}\right|_{y_D=0}&=\left.\frac{\partial p_D}{\partial y_D}\right|_{y_D=1}=0\\ \left.\frac{\partial p_D}{\partial z_D}\right|_{z_D=0}&=\left.\frac{\partial p_D}{\partial z_D}\right|_{z_D=1}=0\end{aligned} \quad (A.12)$$

$U(x_D,y_D,z_D)$ represents the product of three unit step functions in the three coordinate axes as:

$$\begin{aligned}U(x_D,y_D,z_D)=&[H(x_D-c_{xD}-w_{xD})-H(x_D-c_{xD}+w_{xD})][H(y_D-c_{yD}-w_{yD})\\&-H(y_D-c_{yD}+w_{yD})][H(z_D-c_{zD}-w_{zD})-H(z_D-c_{zD}+w_{zD})]\end{aligned} \quad (A.13)$$

$$c_{iD}=\frac{c_i}{i_e},\ i=x,y,\text{ and }z \quad (A.14)$$

$$w_{iD}=\frac{w_i}{i_e},\ i=x,y,\text{ and }z \quad (A.15)$$

Solution of the Problem

According to our definition of the instantaneous source function and benefiting from the properties of the Dirac delta function, we can assume that the source function is only effective at the time (t_D= 0) and there is no continuous effect of source after this time. Based on this assumption we can transfer the source function from the partial differential equation (Eq. A.10) to the initial condition. The two equations are essentially equivalent. The new equation with its new initial condition (boundary conditions are still the same as described in Eq. A.12) can be written as:

$$(\frac{k_x}{k})(\frac{x_e}{L})^2\frac{\partial^2 p_D}{\partial x_D^2}+(\frac{k_y}{k})(\frac{y_e}{L})^2\frac{\partial^2 p_D}{\partial y_D^2}+(\frac{k_z}{k})(\frac{z_e}{L})^2\frac{\partial^2 p_D}{\partial z_D^2}=\frac{\partial p_D}{\partial t_D} \quad (A.16)$$

I.C.:

$$p_D(x_D,y_D,z_D,0)=\frac{U(x_D,y_D,z_D)}{8w_{xD}w_{yD}w_{zD}} \quad (A.17)$$

This condition describe the system at time (t_D= 0), where a unit-strength change is introduced uniformly over the source volume. This change raises the dimensionless pressure of the source to the value equal to

$\frac{1}{8w_{xD}w_{yD}w_{zD}}$, whereas the rest of the system is still in its initial pressure. This situation is formulated in Eq. A.17.

Regarding to the homogeneity of the main PDE and its initial and boundary conditions, we applied the method of separation of variables to solve the problem. In this method we assume that the solution in 3D can be described as the product of three 1D solutions in different axes.

$$p_D(x_D,y_D,z_D,t_D) = X(x_D,t_D)Y(y_D,t_D)Z(z_D,t_D) \tag{A.18}$$

Introducing this assumption to Eq. A.16 and A.12 we will have 3 separate simple PDEs as the followings:

$$\begin{aligned} &(\frac{k_i}{k})(\frac{i_e}{L})^2\frac{\partial^2 I}{\partial i_D^2} = \frac{\partial I}{\partial t_D} \\ &\left.\frac{\partial I}{\partial i_D}\right|_{i_D=0} = \left.\frac{\partial I}{\partial i_D}\right|_{i_D=1} = 0 \end{aligned} \quad , i = x, y, \text{ and } z,\ I = X, Y, \text{ and } Z \tag{A.19}$$

Eq. A.19 has a solution in the form of an infinite series as:

$$I(i_D,t_D) = \sum_{n=0}^{\infty} a_{in}\cos(n\pi i_D)\exp(-n^2\pi^2\frac{k_i}{k}(\frac{i_e}{L})^2 t_D) \text{ , } i = x, y, \text{ and } z,\ I = X, Y, \text{ and } Z \tag{A.20}$$

In order to obtain the series coefficients (a_{in}) we have to use the initial condition. It can be seen in Eq. A.17 that the initial condition function is the product of three separate functions of x, y, and z as the following:

$$\begin{aligned} p_D(x_D,y_D,z_D,0) = &\frac{[H(x_D - c_{xD} - w_{xD}) - H(x_D - c_{xD} + w_{xD})]}{2w_{xD}} \\ &\times\frac{[H(y_D - c_{yD} - w_{yD}) - H(y_D - c_{yD} + w_{yD})]}{2w_{yD}} \\ &\times\frac{[H(z_D - c_{zD} - w_{zD}) - H(z_D - c_{zD} + w_{zD})]}{2w_{zD}} \end{aligned} \tag{A.21}$$

This leads us to use the following initial condition for a 1D solution as:

$$I(i_D,t_D) = a_{i0} + \sum_{n=1}^{\infty} a_{in}\cos(n\pi i_D) = \frac{[H(i_D - c_{iD} - w_{iD}) - H(i_D - c_{iD} + w_{iD})]}{2w_{iD}} \tag{A.22}$$

Using the orthogonality property of the cosine function the values of a_{in}s are calculated as:

$$a_{in} = \begin{cases} 1 & ,n = 0 \\ \frac{[\sin(n\pi(i_D - c_{iD} + w_{iD}) - \sin(n\pi(i_D - c_{iD} + w_{iD})]}{n\pi w_{iD}} & ,n \neq 0 \end{cases} \quad , i = x, y, \text{ and } z \tag{A.23}$$

We can define a new dimensionless time for each direction as:

$$t_{Di} = \frac{k_i}{k}\left(\frac{i_e}{L}\right)^2 t_D \text{ , } i = x, y, \text{ and } z \tag{A.24}$$

The final form of 1D solution can be described as:

$$I(i_D, t_{Di}) = 1 + \sum_{n=1}^{\infty} \frac{[\sin(n\pi(i_D - c_{iD} + w_{iD}) - \sin(n\pi(i_D - c_{iD} + w_{iD})]}{n\pi w_{iD}} \cos(n\pi i_D) \times \exp(-n^2\pi^2 t_{Di}) \tag{A.25}$$

Apart from the solution in the form of time series, we can describe the solution in 1D as the following forms:

- Solution in the form of Jacobian Elliptic Theta function:

$$I(i_D, t_{Di}) = \frac{1}{2(i_{Du} - i_{Dl})} \int_{i_{Dl}}^{i_{Du}} \vartheta 3\left(\frac{i_D - \xi}{2}, t_{Di}\right) + \vartheta 3\left(\frac{i_D + \xi}{2}, t_{Di}\right) d\xi \tag{A.26}$$

- Solution in Laplace domain

$$I(i_D, s) = \frac{1}{2s(s-1)(i_{Du} - i_{Dl})} s^{\frac{i_D + i_{Du} + i_{Dl}}{2}} [\left(s + s^{i_D}\right)\left(s^{\frac{i_{Du}}{2}} - s^{\frac{i_{Dl}}{2}} + s^{\frac{2i_{Du} + i_{Dl}}{2}} - s^{\frac{2i_{Dl} + i_{Du}}{2}}\right) + (s-1)\left(s^{\frac{i_{Du}}{2}}\left(s^{\frac{i_D}{2}} - s^{\frac{i_{Dl}}{2}}\right)^2 H(i_{Dl} - i_D) - s^{\frac{i_{Dl}}{2}}\left(s^{\frac{i_{Du}}{2}} - s^{\frac{i_D}{2}}\right)^2\right) H(i_{Du} - i_D)] \tag{A.27}$$

In Eqs. A.26 and A.27 i_{Dl} and i_{Du} are defined as the following:

$$i_{Dl} = \frac{c_i - w_i}{i_e}, \quad i_{Du} = \frac{c_i + w_i}{i_e} \text{ , } i = x, y, \text{ and } z, I = X, Y, \text{ and } Z \tag{A.28}$$

Each of these representations has advantages and disadvantages. For instance, the Laplace transform solution is in closed form, but needs numerical inversion. The Theta function form needs numerical integration. The time series form, used in this work, is easy to calculate for moderate and large times, but converges slowly for short times. A numerically efficient formulation uses an additional "trick":

The infinite sum is replaced by a finite sum

$$I(i_D, t_{Di}) = 1 + 2n_{del} \sum_{n=1, n_{del}}^{n_{\max}} \frac{[\sin(n\pi(i_D - c_{iD} + w_{iD}) - \sin(n\pi(i_D - c_{iD} + w_{iD})]}{n\pi w_{iD}} \cos(n\pi i_D) \times \exp(-n^2\pi^2 t_{Di}) \tag{A.29}$$

Where

$$n_{\max} = 1 + \text{Ceiling}\left[\frac{5.58}{\sqrt{t}}\right] \tag{A.30}$$

and

$$n_{del} = 1 + 2 \times \text{Floor}\left[\frac{n_{\max}}{10{,}000}\right] \tag{A.31}$$

With this modification the 1D solution is calculated with maximum a couple of thousand terms, and the result is very accurate according to the corroboration done both with multi-precision inversion of the Laplace transform form and numerical integration of the Theta function form.

And the final solution for dimensionless pressure is:

$$p_{\delta D}(x_D, y_D, z_D, t_D) = X(x_D, t_{Dx}) Y(y_D, t_{Dy}) Z(z_D, t_{Dz}) \tag{A.32}$$

It should be noted that the use of symbol $(p_{\delta D})$ is to emphasize on the fact that the solution for dimensionless pressure is derived for the case where we have an instantaneous source. Solution to a continuous source can be derived by integration of the instantaneous source solution over the time.

$$p_{uD} = \int_0^{t_D} p_{\delta D}(t_D^{'}).dt_D^{'} \tag{A.33}$$

Integration of Eq. A.33 is carried out numerically. Starting from a very early time (in this work $t_D = 10^{-12}$), we assume the value of pressure is equal to the value of pressure derivative. Integration is then taking place from the starting point over the time.

It should be noted again that the dimensionless pressure and time used for this calculation differs from what is defined traditionally. The dimensionless time with respect to the drainage area is related to our dimensionless time through the relation:

$$\begin{aligned} c_{trad} &= \frac{z_e \sqrt{k_x k_x}}{L k} \\ t_{DA,trad} &= c_{trad}\, t_D \end{aligned} \tag{A.34}$$

The dimensionless pressure, traditionally used in the petroleum industry is related to our p_{uD} function according to the relation:

$$p_{uD,trad} = 2\pi c_{trad}\, p_{uD} \tag{A.35}$$

In field units, the pressure drawdown is correlated to dimensionless pressure as:

$$p_i - p_{wf} = \frac{z_e\sqrt{k_x k_y}}{141.2qB\mu} p_{uD,trad} \tag{A.36}$$

and the time as

$$t = \frac{\phi c_t \mu (x_e y_e)}{0.0002637\sqrt{k_x k_y}} t_{DA,trad} \tag{A.37}$$

where k is in md, μ in cp, B in resBBL/STB, x_e,y_e,z_e,c_x,c_y,c_z,w_x,w_y and w_z in ft, q in STB/D, p_{wf} and p_i in psi, t in hr, c_t in 1/psi, and φ is dimensionless.

APPENDIX B

DIMENSIONLESS PRODUCTIVITY INDEX FROM PRESSURE DATA

In production engineering, the productivity index is defined as the ability of the reservoir to produce hydrocarbon per unit pressure drop in the reservoir (volume/time/pressure).

$$J = \frac{q}{(p_{avg} - p_{wf})} \tag{B.1}$$

In which

q = Flow Rate

p_{avg} = Average Reservoir Pressure

p_{wf} = Well Flowing Pressure

Introducing the Dimensionless parameters as the followings the expression for the Dimensionless productivity index would be obtained.

$$p_{D,trad} = \frac{2\pi kh}{qB\mu}(p_i - p) \tag{B.2}$$

$$J_D = \frac{\mu B}{2\pi kh} J\ . \tag{B.3}$$

With:

P_i = Initial Reservoir Pressure

k = Reservoir Permeability

h = Reservoir Thickness

B = Formation Volume Factor

μ = Fluid Viscosity

Combining Eqs. B.1 through B.3 we have:

$$J_D = \frac{1}{p_{D,trad} - p_{D,avg,trad}} \tag{B.4}$$

Assuming a constant compressibility during depletion we can write:

$$c_t = -\frac{1}{V}\frac{\partial p}{\partial V} \tag{B.5}$$

$$V = \phi Ah \tag{B.6}$$

$$\frac{\partial p}{\partial V} = \frac{1}{\phi A h c_t} = cte \tag{B.7}$$

$$\Delta p = p_{avg} - p_i = \frac{\Delta V}{\phi A h c_t} = \frac{N_p B}{\phi A h c_t} = \frac{qBt}{\phi A h c_t} \text{ (Constant flow rate production)} \tag{B.8}$$

Using the definition for dimensionless pressure and applying it on Eq. B.8 we have:

$$p_{D,avg,trad} = 2\pi \frac{kt}{\phi \mu c_t A} = 2\pi t_{DA} \tag{B.9}$$

Where;

$$t_{DA} = \frac{kt}{\phi \mu c_t A} \text{ (Dimensionless time defined based on drainage area)} \tag{B.10}$$

Combination of Eqs. B.9 and B.4 would lead us to an expression correlating the dimensionless productivity index as a function of dimensionless pressure and dimensionless time (Eq. B.11)

$$J_D = \frac{1}{p_{D,trad} - 2\pi t_{DA}} \tag{B.11}$$

Or based on the new dimensionless variables defined in Appendix A

$$J_D = \frac{1}{2\pi c_{trad} (p_{uD} - t_D)} \tag{B.12}$$

The dimensionless productivity index is time dependent in the transient flow regime and constant in the pseudo-steady state.

In field units, the productivity index is expressed as

$$PI = \frac{z_e \sqrt{k_x k_y}}{141.2 B \mu} J_{D,trad} \tag{B.13}$$

Where k is in md, μ in cp, B in resBBL/STB, q in STB/D, p_{wf} and p_i in psi, t in hr, c_t in 1/psi, φ is dimensionless and PI is in (STB/D/psi).

APPENDIX C

DETAILED RESULTS OF CALCULATION FOR MAXIMUM DIMENSIONLESS PRODUCTIVITY INDEX OF THE EXAMPLE CASE, PROPPANT NUMBER (N_{Prop}) = 0.001

In this appendix we provide details of calculation results and complete set of graphs describing the production behavior of example problem in chapter IV when 1,000 lb of proppant (N_{Prop} =0.001) is used for stimulation. All the fracture sizes have been described in ft.

Table C.1 — Table of Mathematically Feasible Fracture Sizes for Example Case in Chapter IV (N_{Prop} =0.001)

N_{frac}	w_x	w_y	w_z	n_{frac}	w_x	w_y	w_z
1	4.4	0.005	50.0	2	660.00	0.03	0.03
1	332.2	0.005	0.7	2	0.36	0.03	50.00
1	660.0	0.005	0.3	2	330.18	0.03	0.05
1	2.2	0.010	50.0	2	660.00	0.03	0.03
1	331.1	0.010	0.3	2	0.31	0.04	50.00
1	660.0	0.010	0.2	2	330.16	0.04	0.05
1	1.5	0.015	50.0	2	660.00	0.04	0.02
1	330.7	0.015	0.2	2	0.27	0.04	50.00
1	660.0	0.015	0.1	2	330.14	0.040	0.041
1	1.1	0.020	50.0	2	660.00	0.040	0.021
1	330.5	0.020	0.2	2	0.24	0.045	50.000
1	660.0	0.020	0.1	2	330.12	0.045	0.037
1	0.9	0.025	50.0	2	660.00	0.045	0.018
1	330.4	0.025	0.1	2	0.22	0.050	50.000
1	660.0	0.025	0.1	2	330.11	0.050	0.033
1	0.7	0.030	50.0	2	660.00	0.050	0.017
1	330.4	0.030	0.1	3	1.45	0.005	50.000
1	660.0	0.030	0.1	3	330.73	0.005	0.220
1	0.6	0.035	50.0	3	660.00	0.005	0.110
1	330.3	0.035	0.1	3	0.73	0.010	50.000
1	660.0	0.035	0.0	3	330.36	0.010	0.110
1	0.5	0.040	50.0	3	660.00	0.010	0.055
1	330.3	0.040	0.1	3	0.48	0.015	50.000
1	660.0	0.040	0.0	3	330.24	0.015	0.073
1	0.5	0.045	50.0	3	660.00	0.015	0.037
1	330.2	0.045	0.1	3	0.36	0.020	50.000
1	660.0	0.045	0.0	3	330.18	0.020	0.055
1	0.4	0.050	50.0	3	660.00	0.020	0.028
1	330.2	0.050	0.1	3	0.29	0.025	50.000
1	660.0	0.050	0.0	3	330.15	0.025	0.044
2	2.2	0.005	50.0	3	660.00	0.025	0.022
2	331.1	0.005	0.3	3	0.24	0.030	50.000
2	660.0	0.005	0.2	3	330.12	0.030	0.037
2	1.1	0.010	50.0	3	660.00	0.030	0.018
2	330.5	0.010	0.2	3	0.207	0.035	50.000
2	660.0	0.010	0.1	3	330.104	0.035	0.031
2	0.7	0.015	50.0	3	660.000	0.035	0.016
2	330.4	0.015	0.1	3	0.182	0.040	50.000
2	660.0	0.015	0.1	3	330.091	0.040	0.027
2	0.54	0.02	50.00	3	660.000	0.040	0.014
2	330.27	0.02	0.08	3	0.161	0.045	50.000
2	660.00	0.02	0.04	3	330.081	0.045	0.024
2	0.44	0.03	50.00	3	660.000	0.045	0.012
2	330.22	0.03	0.07	3	0.145	0.050	50.000

Table C.1— Continued

n_{frac}	w_x	w_y	w_z	n_{frac}	w_x	w_y	w_z
3	330.073	0.050	0.022	4	660.000	0.050	0.008
3	660.000	0.050	0.011	5	0.871	0.005	50.000
4	1.089	0.005	50.000	5	330.436	0.005	0.132
4	330.545	0.005	0.165	5	660.000	0.005	0.066
4	660.000	0.005	0.083	5	0.436	0.010	50.000
4	0.545	0.010	50.000	5	330.218	0.010	0.066
4	330.272	0.010	0.082	5	660.000	0.010	0.033
4	660.000	0.010	0.041	5	0.290	0.015	50.000
4	0.363	0.015	50.000	5	330.145	0.015	0.044
4	330.182	0.015	0.055	5	660.000	0.015	0.022
4	660.000	0.015	0.028	5	0.218	0.020	50.000
4	0.272	0.020	50.000	5	330.109	0.020	0.033
4	330.136	0.020	0.041	5	660.000	0.020	0.017
4	660.000	0.020	0.021	5	0.174	0.025	50.000
4	0.218	0.025	50.000	5	330.087	0.025	0.026
4	330.109	0.025	0.033	5	660.000	0.025	0.013
4	660.000	0.025	0.017	5	0.145	0.030	50.000
4	0.182	0.030	50.000	5	330.073	0.030	0.022
4	330.091	0.030	0.027	5	660.000	0.030	0.011
4	660.000	0.030	0.014	5	0.124	0.035	50.000
4	0.156	0.035	50.000	5	330.062	0.035	0.019
4	330.078	0.035	0.024	5	660.000	0.035	0.009
4	660.000	0.035	0.012	5	0.109	0.040	50.000
4	0.136	0.040	50.000	5	330.054	0.040	0.016
4	330.068	0.040	0.021	5	660.000	0.040	0.008
4	660.000	0.040	0.010	5	0.097	0.045	50.000
4	0.121	0.045	50.000	5	330.048	0.045	0.015
4	330.061	0.045	0.018	5	660.000	0.045	0.007
4	660.000	0.045	0.009	5	0.087	0.050	50.000
4	0.109	0.050	50.000	5	330.044	0.050	0.013
4	330.054	0.050	0.016	5	660.000	0.050	0.007

Table C.2 — Locus of Maxima for Example Case in Chapter IV as a Function of Number of Fractures and Permeability Anisotropy (N_{Prop} =0.001)

n_{frac}	w_x	w_y	w_z	k_v/k_h	$J_{D,\,pss,\,max}$, 1 fracture	$J_{D,\,pss,\,max}$, Total	Fracture Contribution
1	660.00	0.050	0.03	1.000	1.2953	1.2953	0.1229
2	660.00	0.050	0.02	1.000	0.7010	1.4020	0.1913
3	660.00	0.050	0.01	1.000	0.5154	1.5462	0.2676
4	660.00	0.050	0.01	1.000	0.4319	1.7278	0.3339
5	660.00	0.050	0.01	1.000	0.3846	1.9231	0.3900
1	660.00	0.050	0.03	0.100	0.6971	0.6971	0.1389
2	660.00	0.043	0.02	0.100	0.3794	0.7588	0.2211
3	660.00	0.050	0.01	0.100	0.2789	0.8368	0.2981
4	660.00	0.050	0.01	0.100	0.2311	0.9246	0.3619
5	660.00	0.043	0.01	0.100	0.2030	1.0151	0.4148
1	0.79	0.028	50.00	0.010	0.3225	0.3225	0.2722
2	0.54	0.020	50.00	0.010	0.1802	0.3605	0.3523
3	0.58	0.013	50.00	0.010	0.1314	0.3941	0.4094
4	0.44	0.013	50.00	0.010	0.1069	0.4277	0.4535
5	0.35	0.013	50.00	0.010	0.0920	0.4601	0.4887
1	0.79	0.028	50.00	0.001	0.1649	0.1649	0.5397
2	0.54	0.020	50.00	0.001	0.1051	0.2101	0.6191
3	0.36	0.020	50.00	0.001	0.0820	0.2461	0.6715
4	0.44	0.013	50.00	0.001	0.0697	0.2788	0.7079
5	0.35	0.013	50.00	0.001	0.0621	0.3106	0.7354

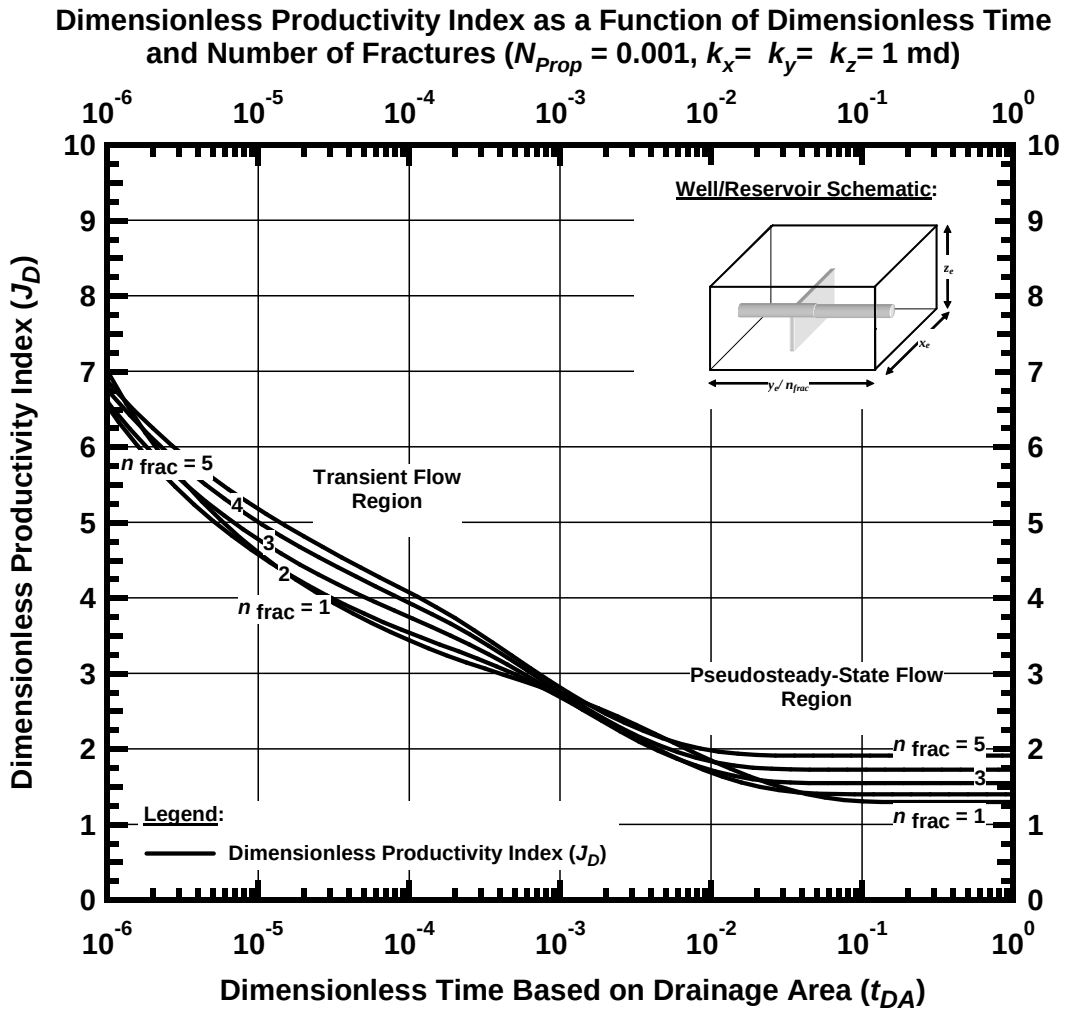

Figure C.1 — Dimensionless Productivity Index as a Function of Dimensionless Time and Number of Fractures for Example Case (N_{Prop} = 0.001, $k_x = k_y = k_z$ = 1 md)

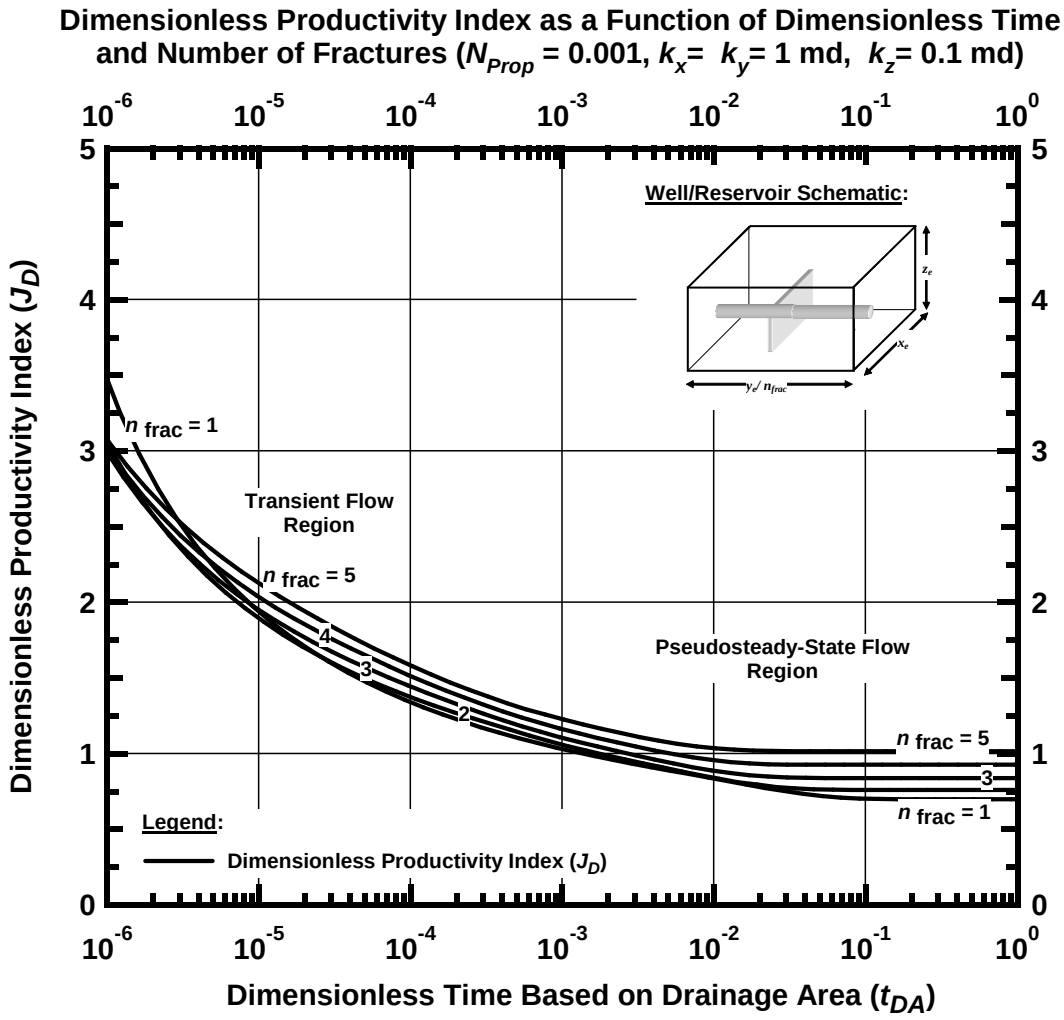

Figure C.2 — Dimensionless Productivity Index as a Function of Dimensionless Time and Number of Fractures for Example Case (N_{Prop} = 0.001, k_x = k_y = 1 md, k_z = 0.1 md)

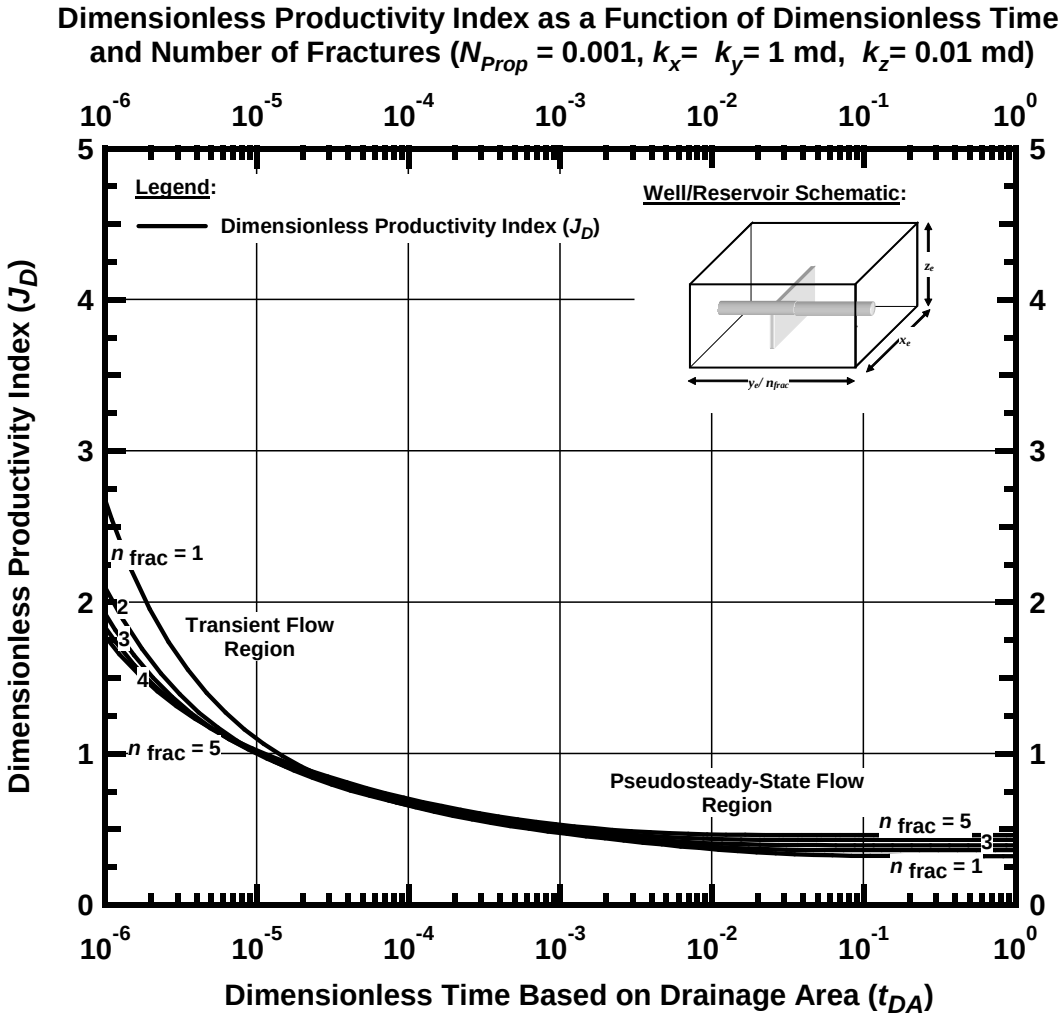

Figure C.3 — Dimensionless Productivity Index as a Function of Dimensionless Time and Number of Fractures for Example Case (N_{Prop} = 0.001, k_x = k_y = 1 md, k_z = 0.01 md)

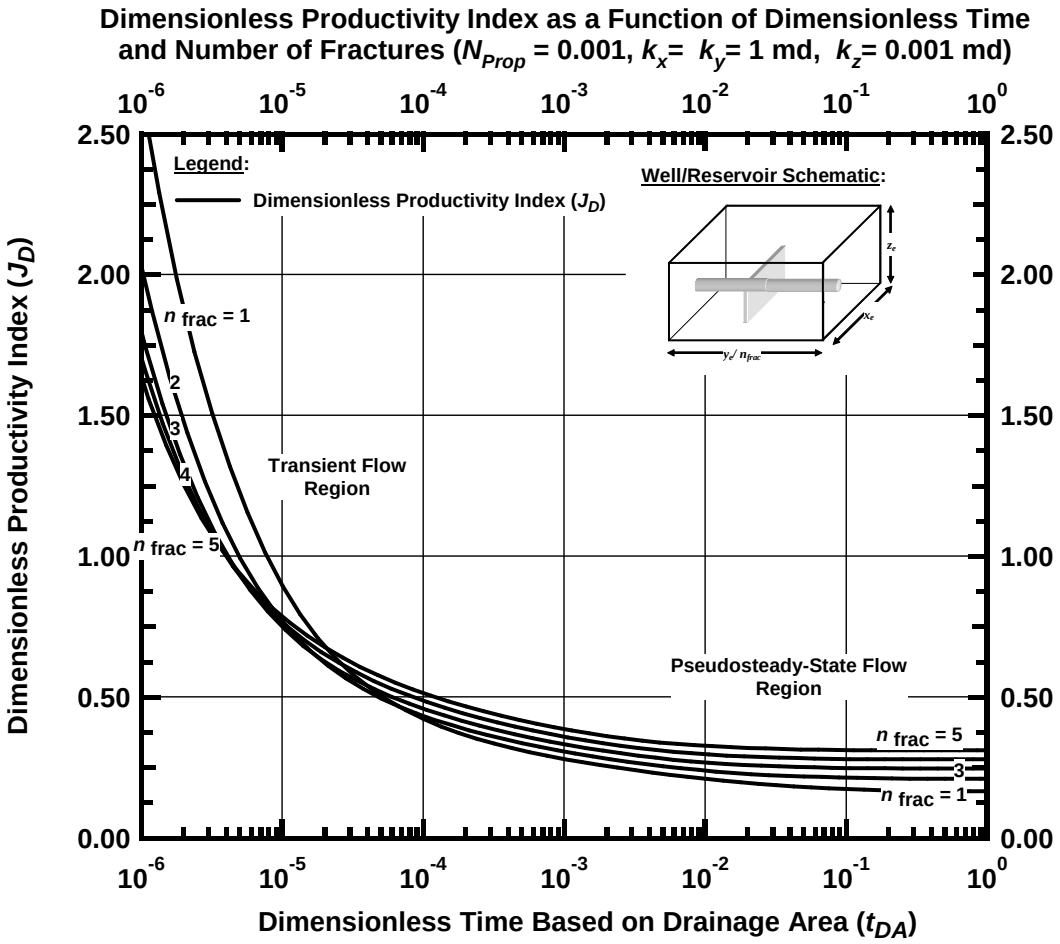

Figure C.4 — Dimensionless Productivity Index as a Function of Dimensionless Time and Number of Fractures for Example Case (N_{Prop} = 0.001, k_x = k_y = 1 md, k_z = 0.001 md)

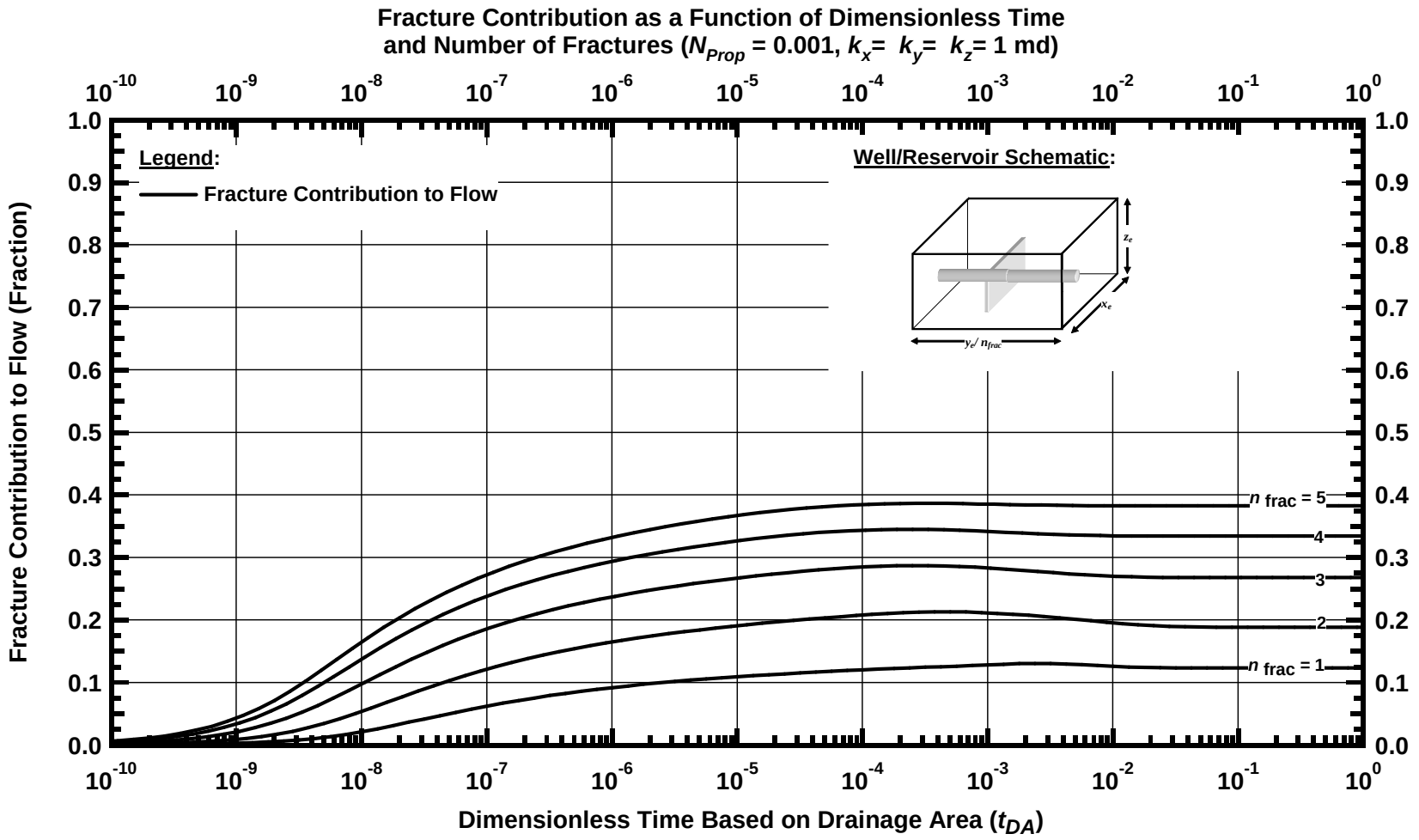

Figure C.5 — Fracture Contribution to Flow as a Function of Dimensionless Time and Number of Fractures for Example Case (N_{Prop} = 0.001, $k_x = k_y = k_z$ = 1 md)

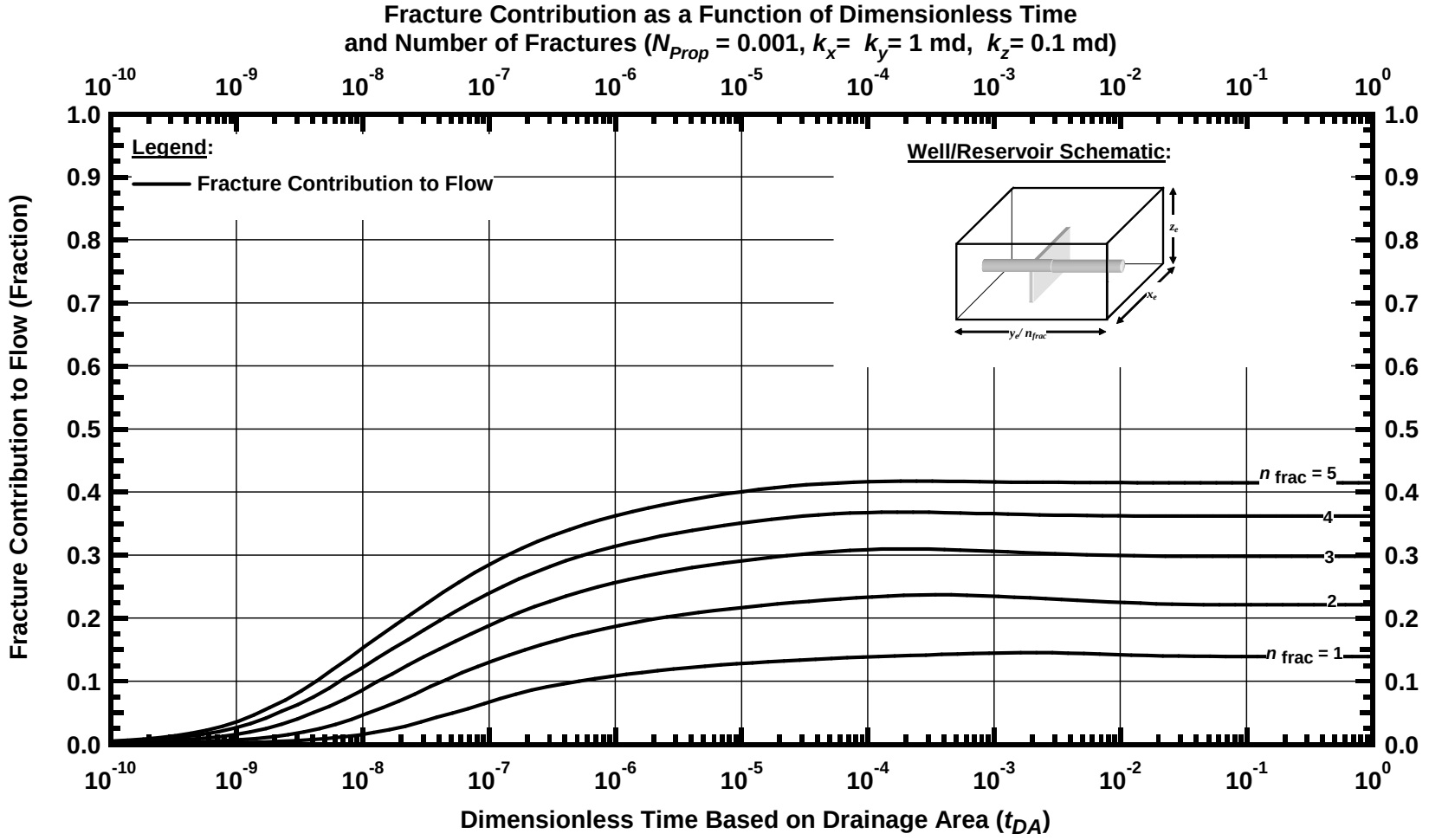

Figure C.6 — Fracture Contribution to Flow as a Function of Dimensionless Time and Number of Fractures for Example Case (N_{Prop} = 0.001, k_x = k_y = 1 md, k_z = 0.1 md)

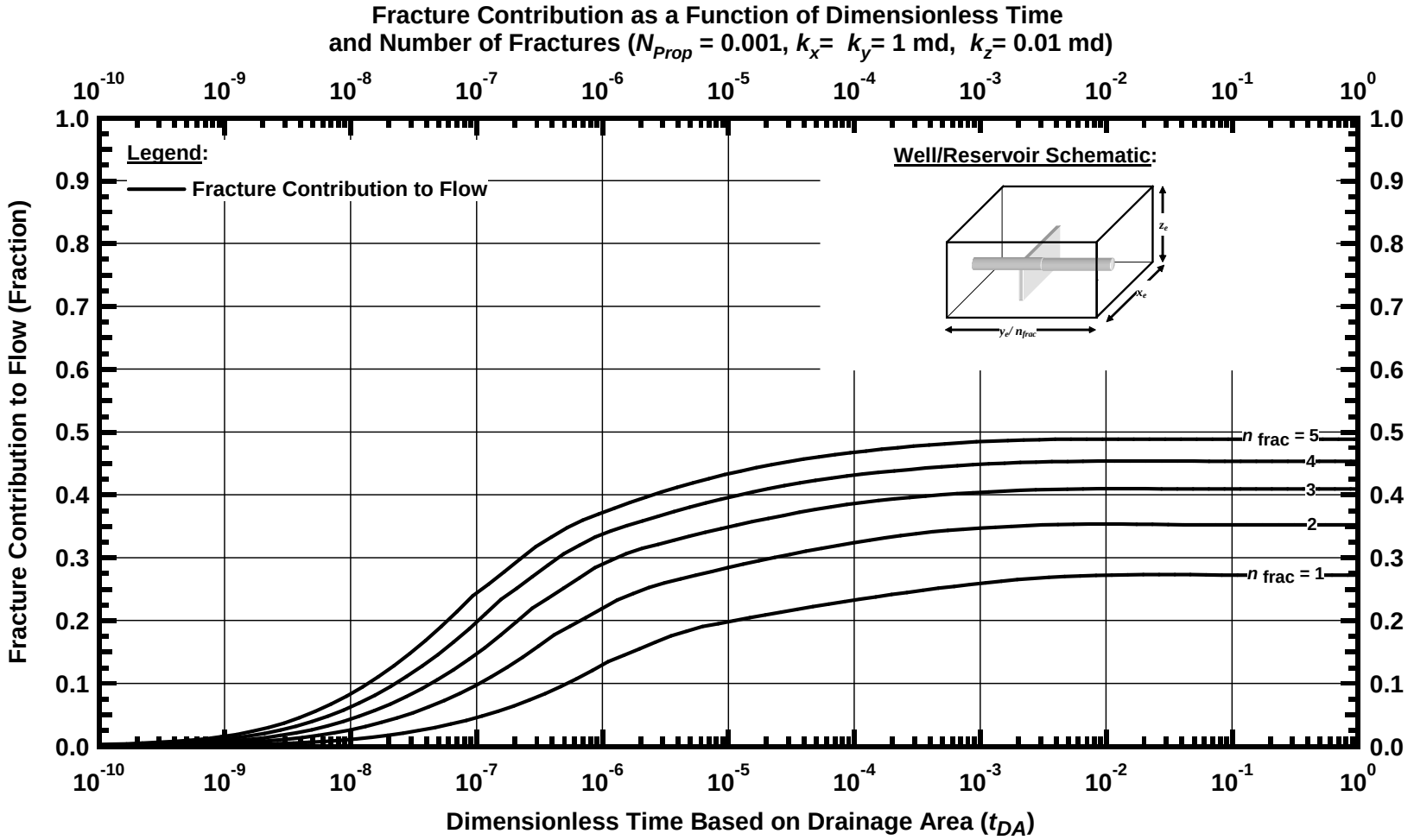

Figure C.7 — Fracture Contribution to Flow as a Function of Dimensionless Time and Number of Fractures for Example Case (N_{Prop} = 0.001, k_x = k_y = 1 md, k_z = 0.01 md)

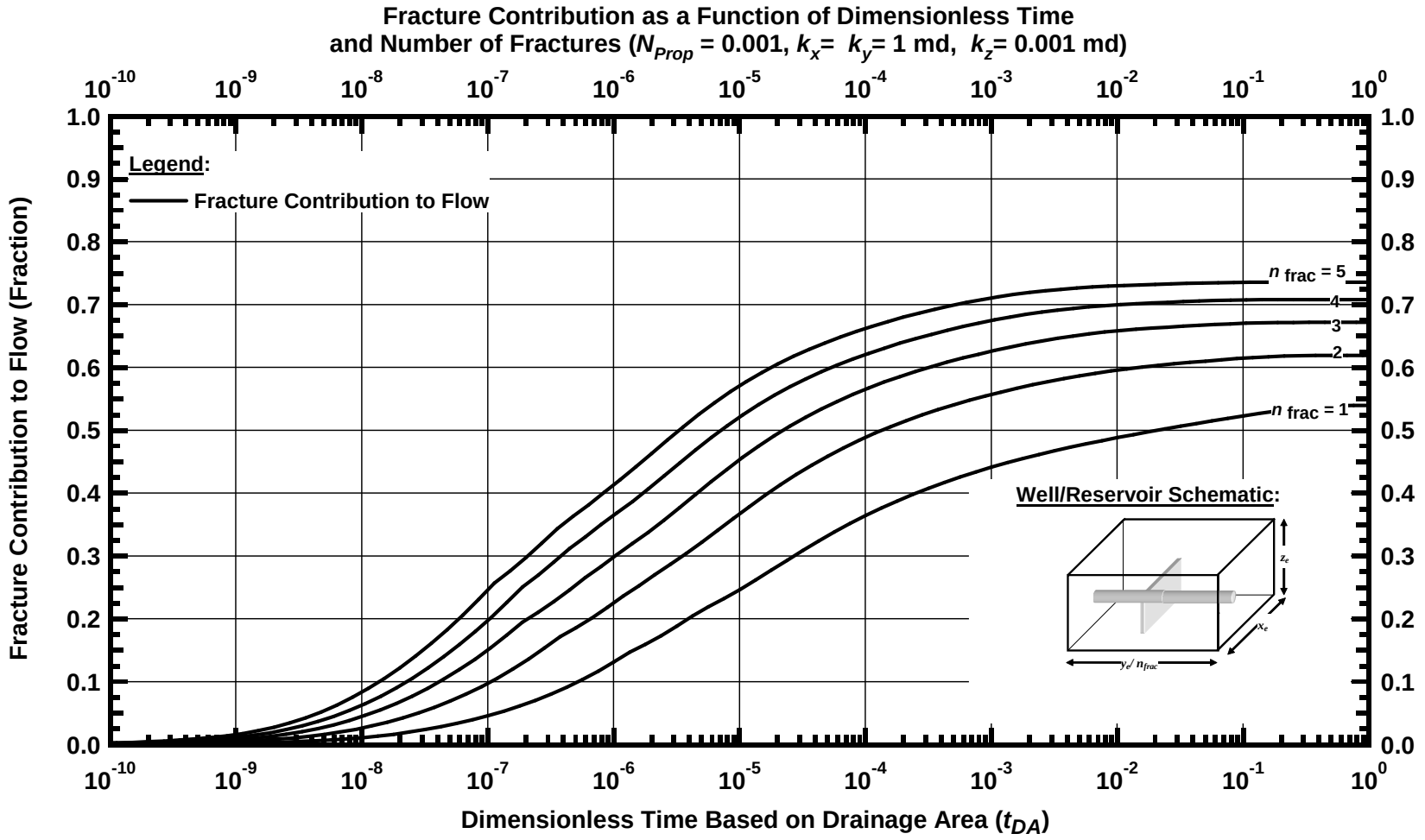

Figure C.8 — Fracture Contribution to Flow as a Function of Dimensionless Time and Number of Fractures for Example Case (N_{Prop} = 0.001, k_x = k_y = 1 md, k_z = 0.001 md)

APPENDIX D

DETAILED RESULTS OF CALCULATION FOR MAXIMUM DIMENSIONLESS PRODUCTIVITY INDEX OF THE EXAMPLE CASE, PROPPANT NUMBER (N_{Prop}) = 0.01

In this appendix we provide details of calculation results and complete set of graphs describing the production behavior of example problem in chapter IV when 10,000 lb of proppant (N_{Prop} =0.01) is used for stimulation. All the fracture sizes have been described in ft.

Table D.1 — Table of Mathematically Feasible Fracture Sizes for Example Case in Chapter IV (N_{Prop} =0.01)

n_{frac}	w_x	w_y	w_z	n_{frac}	w_x	w_y	w_z
1	660.0	0.000	50.0	2	4.36	0.03	50.00
1	43.6	0.005	50.0	2	332.18	0.03	0.66
1	351.8	0.005	6.2	2	660.00	0.03	0.33
1	660.0	0.005	3.3	2	3.63	0.03	50.00
1	21.8	0.010	50.0	2	331.82	0.03	0.55
1	340.9	0.010	3.2	2	660.00	0.03	0.28
1	660.0	0.010	1.7	2	3.11	0.04	50.00
1	14.5	0.015	50.0	2	331.56	0.04	0.47
1	337.3	0.015	2.2	2	660.00	0.035	0.236
1	660.0	0.015	1.1	2	2.72	0.040	50.000
1	10.9	0.020	50.0	2	331.36	0.040	0.411
1	335.4	0.020	1.6	2	660.00	0.040	0.206
1	660.0	0.020	0.8	2	2.42	0.045	50.000
1	8.7	0.025	50.0	2	331.21	0.045	0.365
1	334.4	0.025	1.3	2	660.00	0.045	0.183
1	660.0	0.025	0.7	2	2.18	0.050	50.000
1	7.3	0.030	50.0	2	331.09	0.050	0.329
1	333.6	0.030	1.1	2	660.00	0.050	0.165
1	660.0	0.030	0.6	3	660.00	0.000	50.000
1	6.2	0.035	50.0	3	14.52	0.005	50.000
1	333.1	0.035	0.9	3	337.26	0.005	2.153
1	660.0	0.035	0.5	3	660.00	0.005	1.100
1	5.4	0.040	50.0	3	7.26	0.010	50.000
1	332.7	0.040	0.8	3	333.63	0.010	1.088
1	660.0	0.040	0.4	3	660.00	0.010	0.550
1	4.8	0.045	50.0	3	4.84	0.015	50.000
1	332.4	0.045	0.7	3	332.42	0.015	0.728
1	660.0	0.045	0.4	3	660.00	0.015	0.367
1	4.4	0.050	50.0	3	3.63	0.020	50.000
1	332.2	0.050	0.7	3	331.82	0.020	0.547
1	660.0	0.050	0.3	3	660.00	0.020	0.275
2	660.0	0.000	50.0	3	2.90	0.025	50.000
2	21.8	0.005	50.0	3	331.45	0.025	0.438
2	340.9	0.005	3.2	3	660.00	0.025	0.220
2	660.0	0.005	1.7	3	2.420	0.030	50.000
2	10.9	0.010	50.0	3	331.210	0.030	0.365
2	335.4	0.010	1.6	3	660.000	0.030	0.183
2	660.0	0.010	0.8	3	2.074	0.035	50.000
2	7.3	0.015	50.0	3	331.037	0.035	0.313
2	333.63	0.02	1.09	3	660.000	0.035	0.157
2	660.00	0.02	0.55	3	1.815	0.040	50.000
2	5.45	0.02	50.00	3	330.908	0.040	0.274
2	332.72	0.02	0.82	3	660.000	0.040	0.138
2	660.00	0.02	0.41	3	1.613	0.045	50.000

Table D.1 — Continued

n_{frac}	w_x	w_y	w_z	n_{frac}	w_x	w_y	w_z
3	330.807	0.045	0.244	4	330.545	0.050	0.165
3	660.000	0.045	0.122	4	660.000	0.050	0.083
3	1.452	0.050	50.000	5	660.000	0.000	50.000
3	330.726	0.050	0.220	5	8.712	0.005	50.000
3	660.000	0.050	0.110	5	334.356	0.005	1.303
4	660.000	0.000	50.000	5	660.000	0.005	0.660
4	10.890	0.005	50.000	5	4.356	0.010	50.000
4	335.445	0.005	1.623	5	332.178	0.010	0.656
4	660.000	0.005	0.825	5	660.000	0.010	0.330
4	5.445	0.010	50.000	5	2.904	0.015	50.000
4	332.723	0.010	0.818	5	331.452	0.015	0.438
4	660.000	0.010	0.413	5	660.000	0.015	0.220
4	3.630	0.015	50.000	5	2.178	0.020	50.000
4	331.815	0.015	0.547	5	331.089	0.020	0.329
4	660.000	0.015	0.275	5	660.000	0.020	0.165
4	2.723	0.020	50.000	5	1.742	0.025	50.000
4	331.361	0.020	0.411	5	330.871	0.025	0.263
4	660.000	0.020	0.206	5	660.000	0.025	0.132
4	2.178	0.025	50.000	5	1.452	0.030	50.000
4	331.089	0.025	0.329	5	330.726	0.030	0.220
4	660.000	0.025	0.165	5	660.000	0.030	0.110
4	1.815	0.030	50.000	5	1.245	0.035	50.000
4	330.908	0.030	0.274	5	330.622	0.035	0.188
4	660.000	0.030	0.138	5	660.000	0.035	0.094
4	1.556	0.035	50.000	5	1.089	0.040	50.000
4	330.778	0.035	0.235	5	330.545	0.040	0.165
4	660.000	0.035	0.118	5	660.000	0.040	0.083
4	1.361	0.040	50.000	5	0.968	0.045	50.000
4	330.681	0.040	0.206	5	330.484	0.045	0.146
4	660.000	0.040	0.103	5	660.000	0.045	0.073
4	1.210	0.045	50.000	5	0.871	0.050	50.000
4	330.605	0.045	0.183	5	330.436	0.050	0.132
4	660.000	0.045	0.092	5	660.000	0.050	0.066
4	1.089	0.050	50.000				

Table D.2 — Locus of Maxima for Example Case in Chapter IV as a Function of Number of Fractures and Permeability Anisotropy (N_{Prop} =0.01)

n_{frac}	w_x	w_y	w_z	k_v/k_h	$J_{D,\,pss,\,max}$, 1 fracture	$J_{D,\,pss,\,max}$, Total	Fracture Contribution
1	660.00	0.050	0.33	1.000	1.3090	1.3090	0.1347
2	660.00	0.050	0.17	1.000	0.7090	1.4181	0.2076
3	660.00	0.050	0.11	1.000	0.5233	1.5700	0.2891
4	660.00	0.050	0.08	1.000	0.4405	1.7620	0.3596
5	660.00	0.050	0.07	1.000	0.3935	1.9676	0.4176
1	10.89	0.020	50.00	0.100	0.7363	0.7363	0.2027
2	3.11	0.035	50.00	0.100	0.4028	0.8055	0.2950
3	1.71	0.043	50.00	0.100	0.2961	0.8882	0.3677
4	1.28	0.043	50.00	0.100	0.2440	0.9758	0.4220
5	660.00	0.043	0.08	0.100	0.2134	1.0670	0.4585
1	10.89	0.020	50.00	0.010	0.3999	0.3999	0.4244
2	3.96	0.028	50.00	0.010	0.2531	0.5062	0.5618
3	2.64	0.028	50.00	0.010	0.2015	0.6045	0.6407
4	1.56	0.035	50.00	0.010	0.1739	0.6955	0.6901
5	1.24	0.035	50.00	0.010	0.1558	0.7791	0.7242
1	10.89	0.020	50.00	0.001	0.2561	0.2561	0.6937
2	3.96	0.028	50.00	0.001	0.1914	0.3829	0.7887
3	2.64	0.028	50.00	0.001	0.1632	0.4897	0.8360
4	1.56	0.035	50.00	0.001	0.1460	0.5841	0.8629
5	1.24	0.035	50.00	0.001	0.1338	0.6689	0.8805

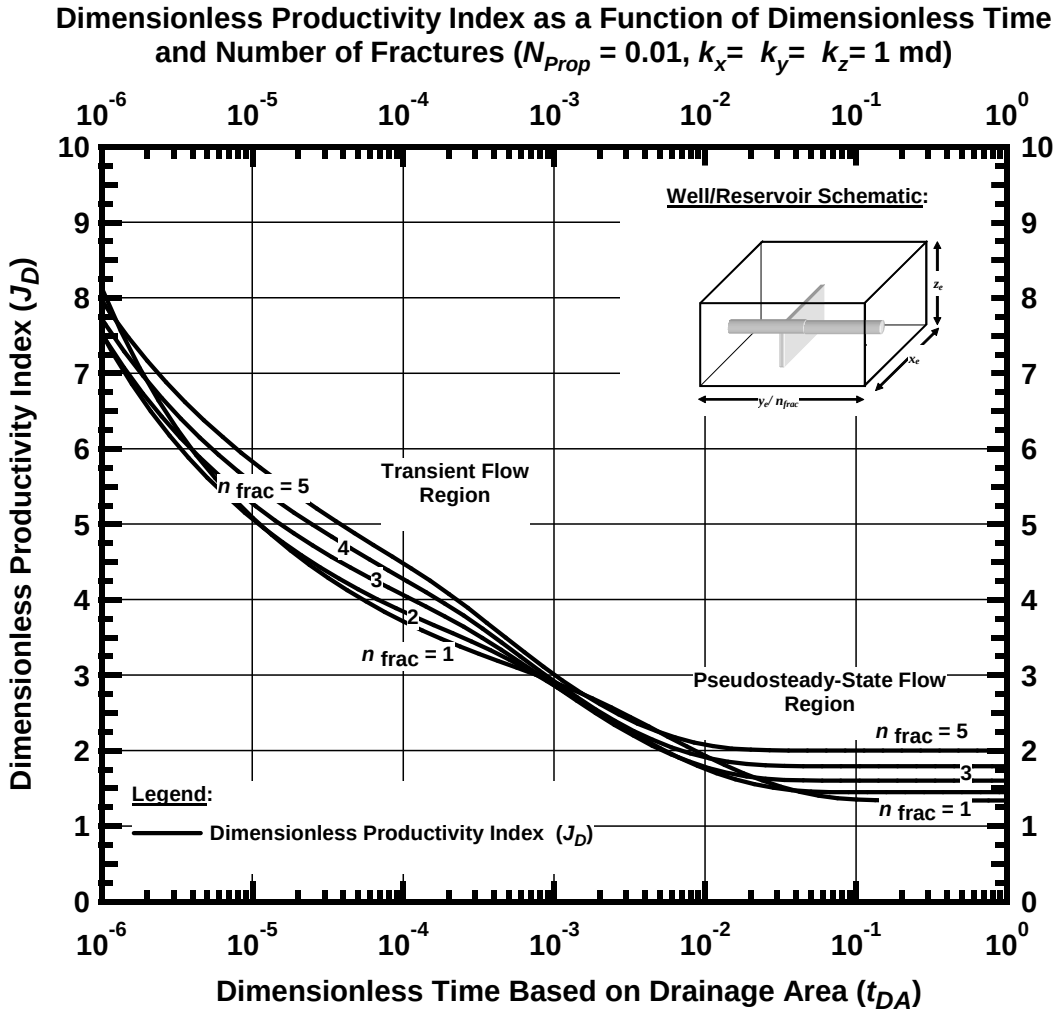

Figure D.1 — Dimensionless Productivity Index as a Function of Dimensionless Time and Number of Fractures for Example Case (N_{Prop} = 0.01, $k_x = k_y = k_z$ = 1 md)

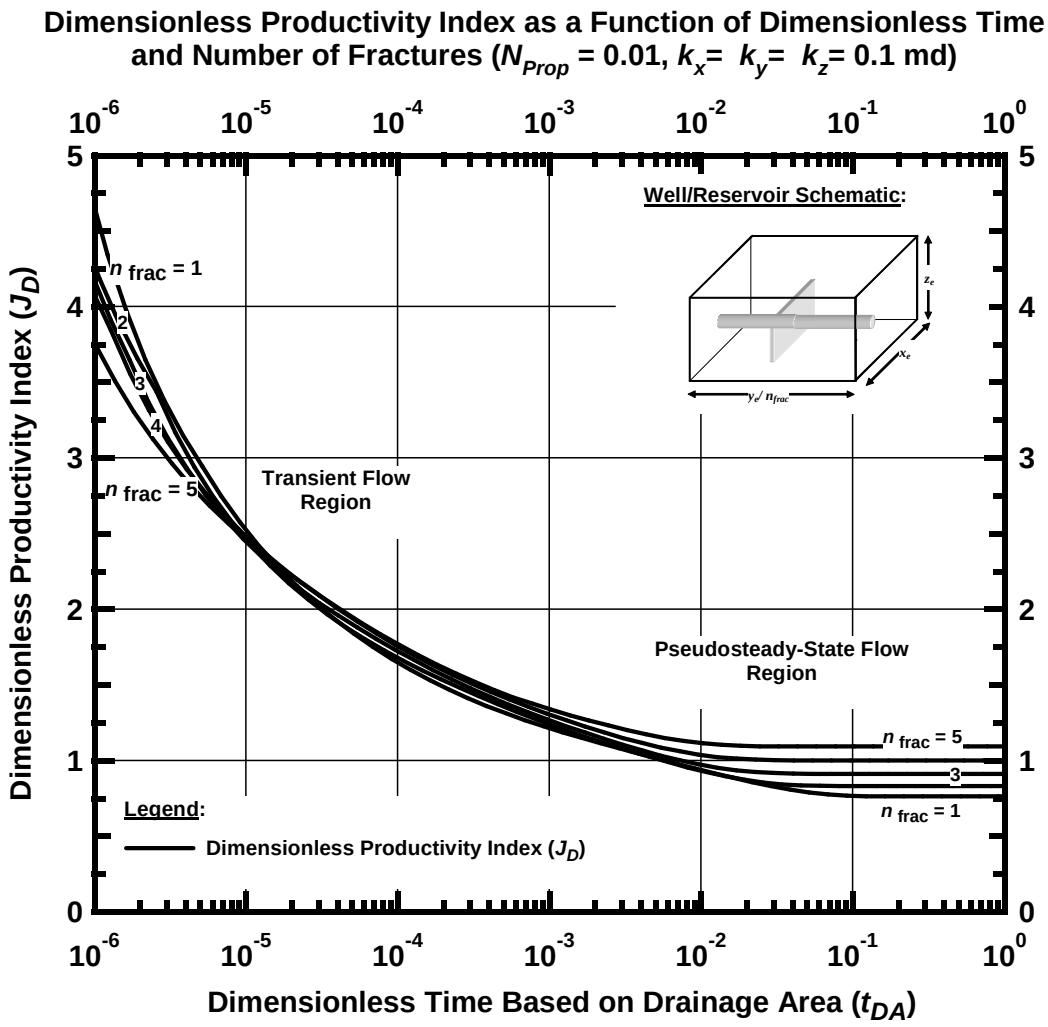

Figure D.2 — Dimensionless Productivity Index as a Function of Dimensionless Time and Number of Fractures for Example Case (N_{Prop} = 0.01, k_x = k_y = 1 md, k_z = 0.1 md)

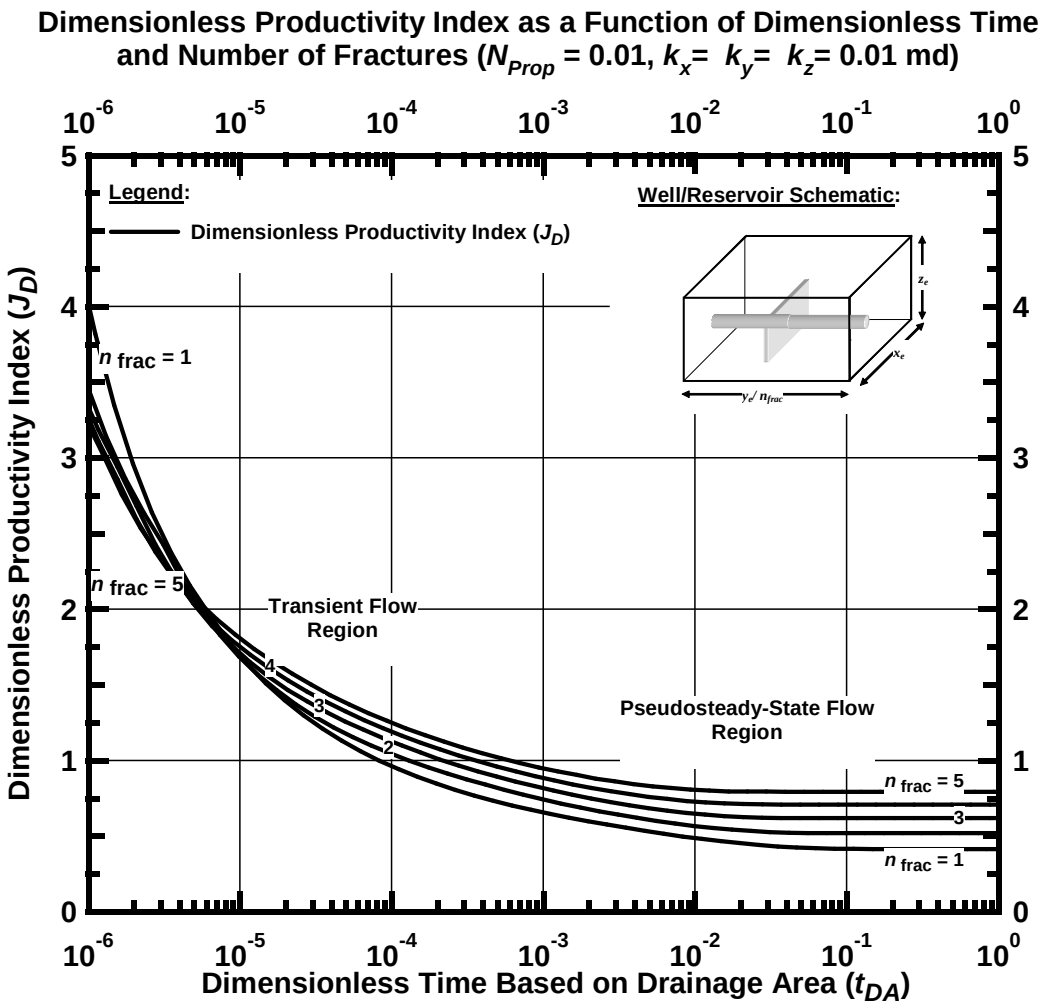

Figure D.3 — Dimensionless Productivity Index as a Function of Dimensionless Time and Number of Fractures for Example Case (N_{Prop} = 0.01, k_x = k_y = 1 md, k_z = 0.01 md)

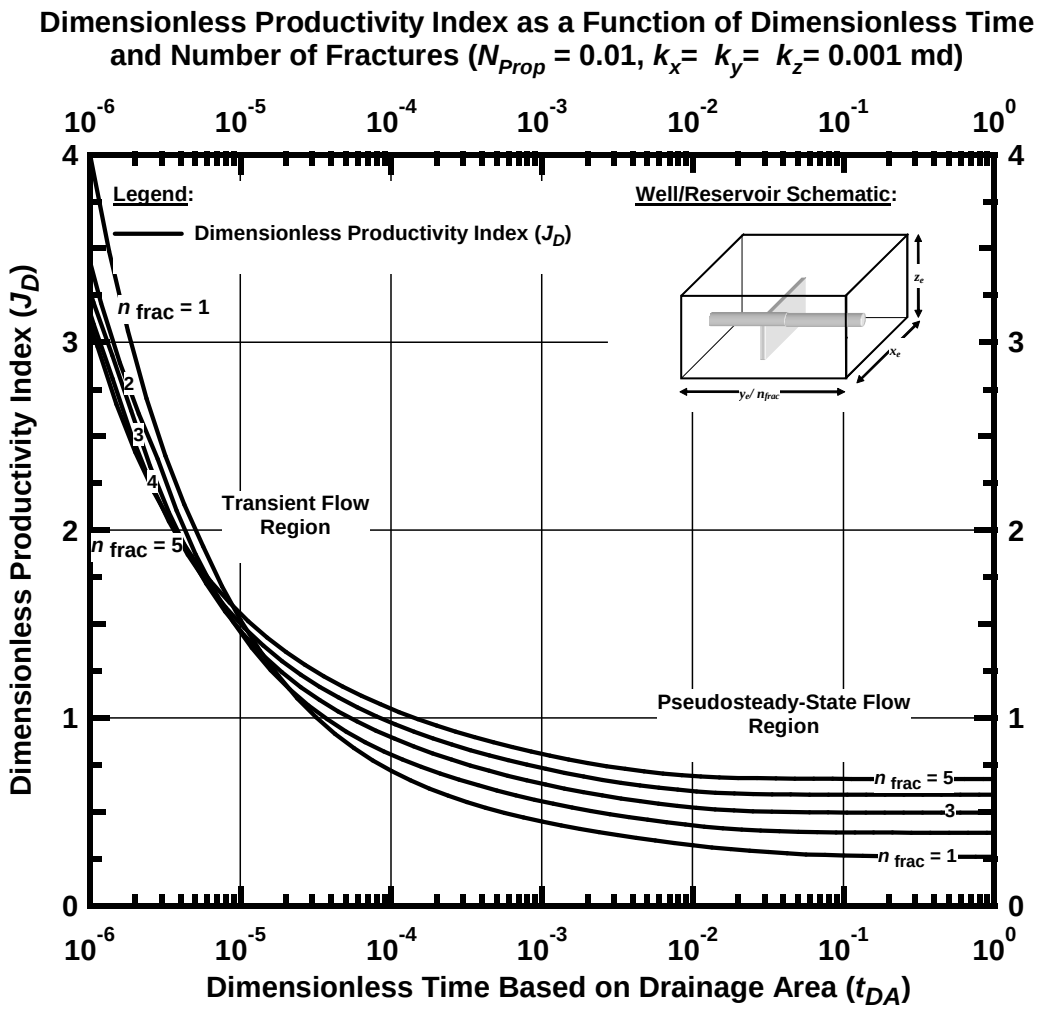

Figure D.4 — Dimensionless Productivity Index as a Function of Dimensionless Time and Number of Fractures for Example Case (N_{Prop} = 0.01, k_x = k_y = 1 md, k_z = 0.001 md)

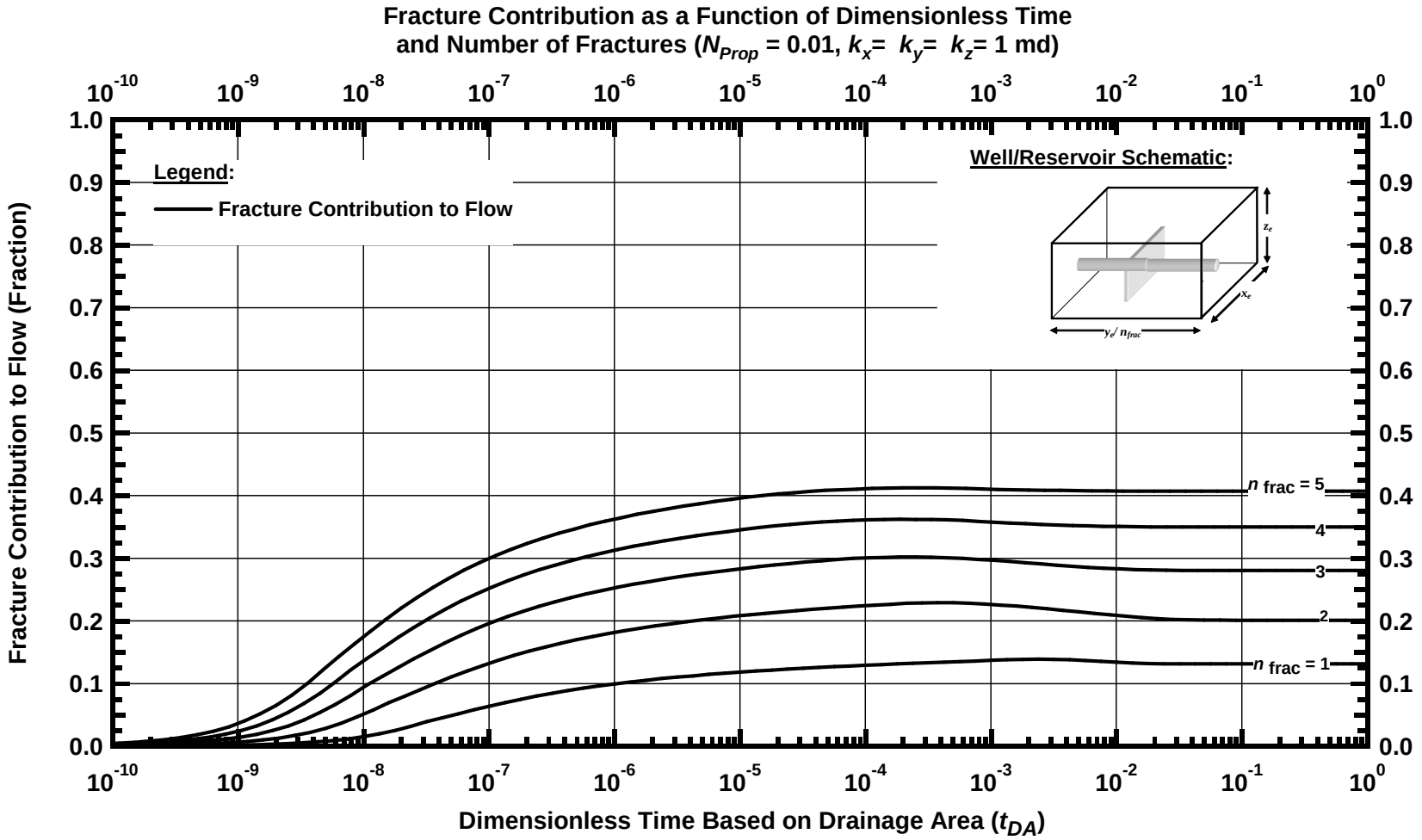

Figure D.5 — Fracture Contribution to Flow as a Function of Dimensionless Time and Number of Fractures for Example Case (N_{Prop} = 0.01, $k_x = k_y = k_z$ = 1 md)

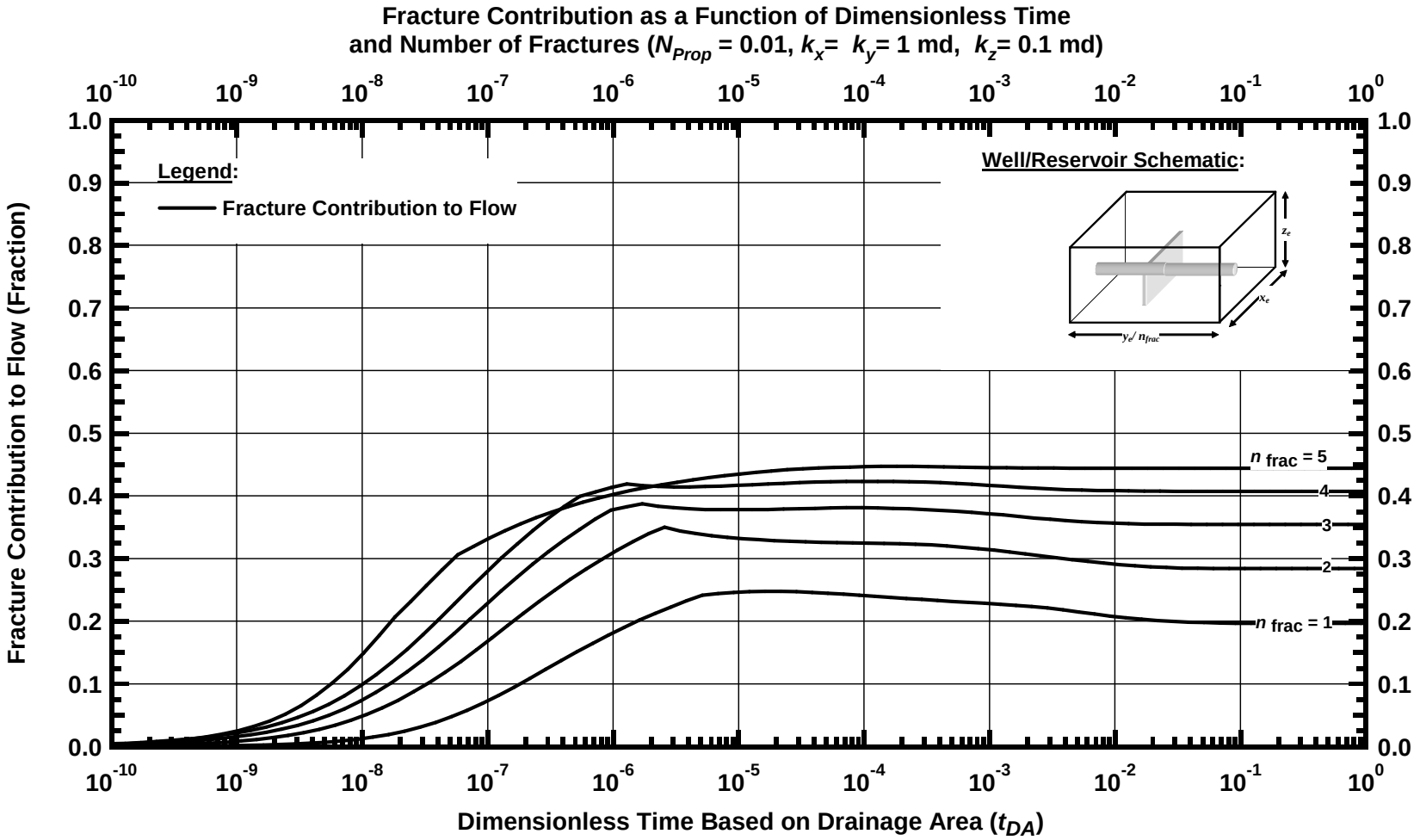

Figure D.6 — Fracture Contribution to Flow as a Function of Dimensionless Time and Number of Fractures for Example Case (N_{Prop} = 0.01, k_x = k_y = 1 md, k_z = 0.1 md)

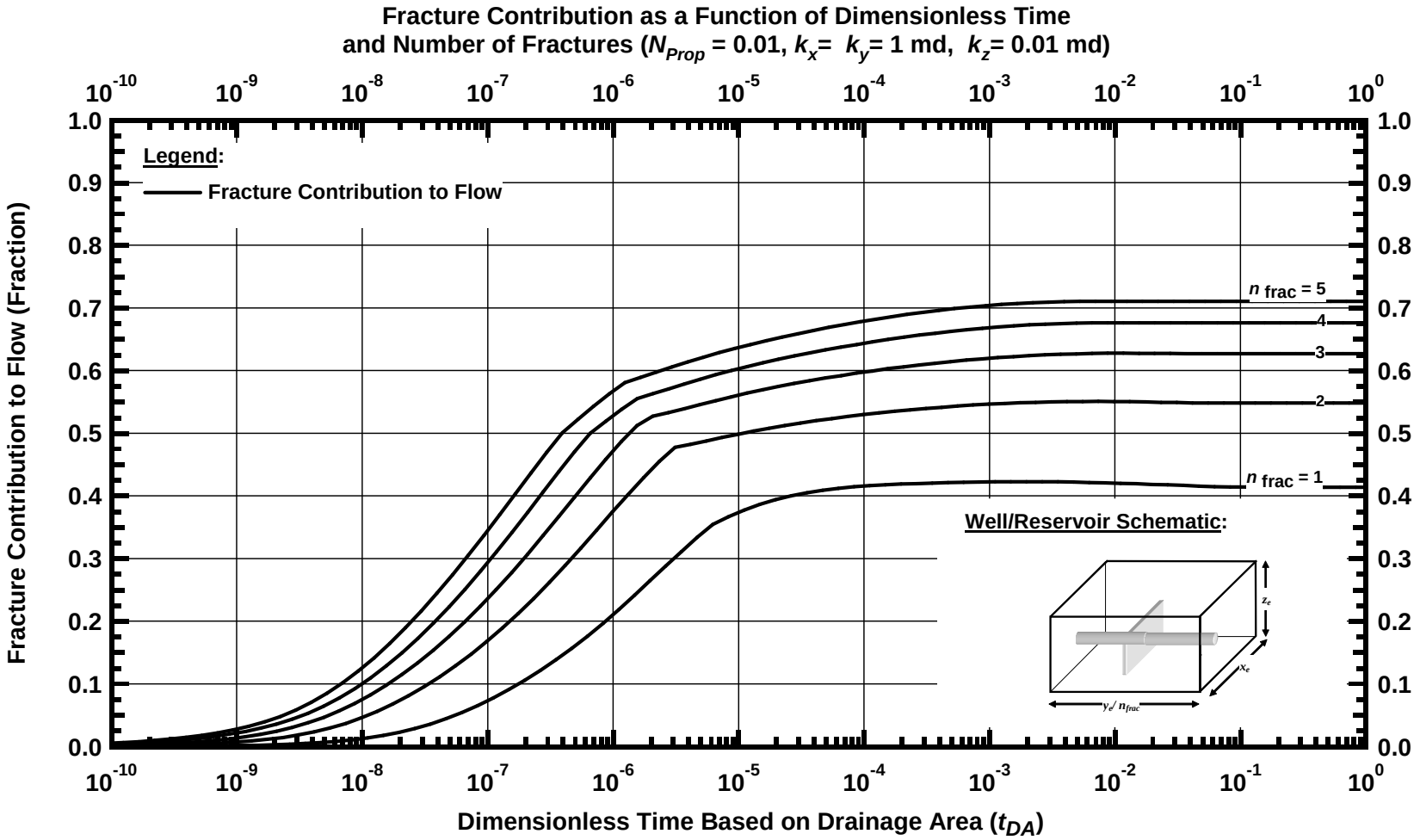

Figure D.7 — Fracture Contribution to Flow as a Function of Dimensionless Time and Number of Fractures for Example Case (N_{Prop} = 0.01, k_x = k_y = 1 md, k_z = 0.01 md)

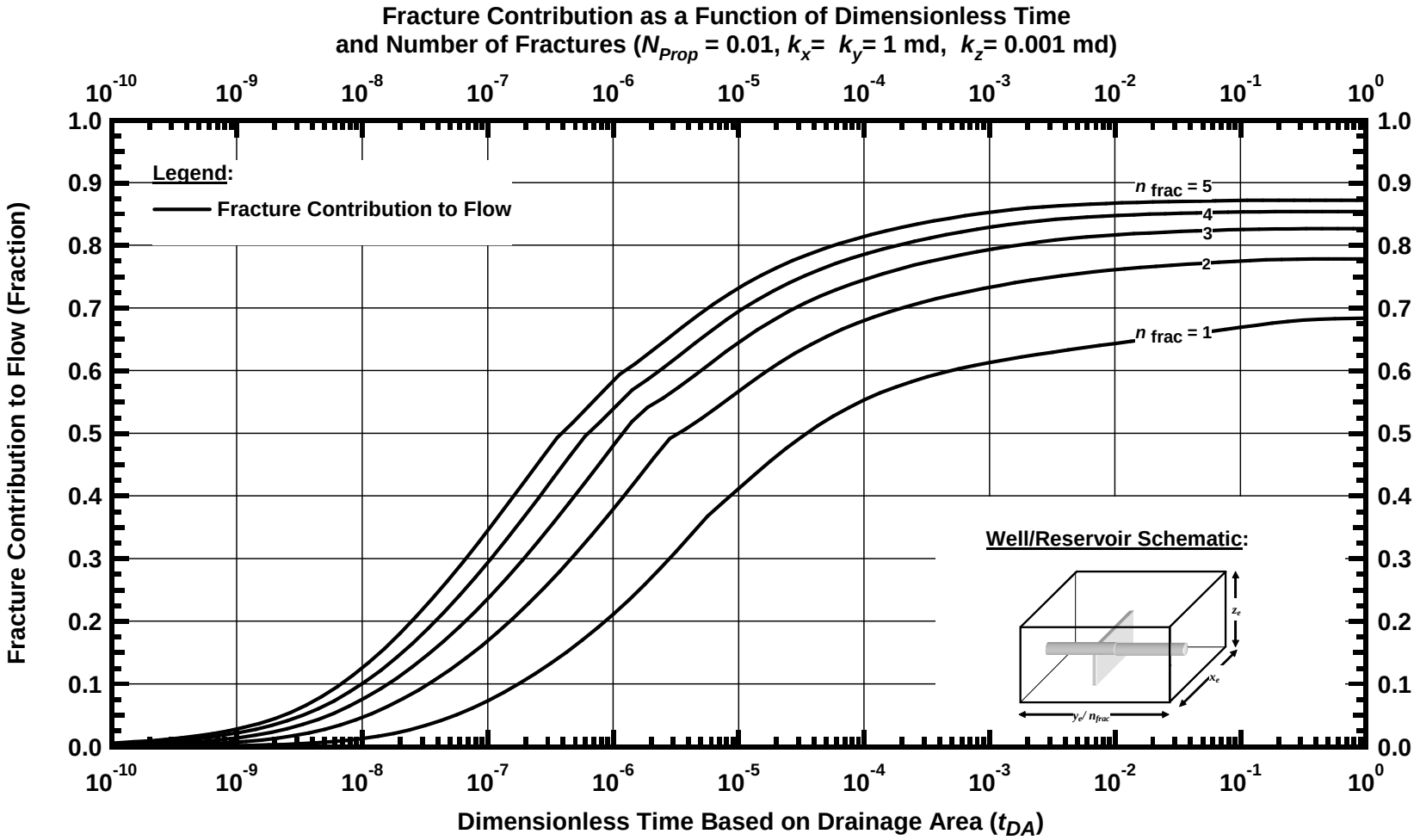

Figure D.8 — Fracture Contribution to Flow as a Function of Dimensionless Time and Number of Fractures for Example Case (N_{Prop} = 0.01, k_x = k_y = 1 md, k_z = 0.001 md)

APPENDIX E

DETAILED RESULTS OF CALCULATION FOR MAXIMUM DIMENSIONLESS PRODUCTIVITY INDEX OF THE EXAMPLE CASE, PROPPANT NUMBER (N_{Prop}) = 0.1

In this appendix we provide details of calculation results and complete set of graphs describing the production behavior of example problem in chapter IV when 100,000 lb of proppant (N_{Prop} =0.1) is used for stimulation. All the fracture sizes have been described in ft.

Table E.1 — Table of Mathematically Feasible Fracture Sizes for Example Case in Chapter IV (N_{Prop} =0.1)

n_{frac}	w_x	w_y	w_z	n_{frac}	w_x	w_y	w_z
1	660.0	0.003	50.0	2	43.56	0.03	50.00
1	435.6	0.005	50.0	2	351.78	0.03	6.19
1	547.8	0.005	39.8	2	660.00	0.03	3.30
1	660.0	0.005	33.0	2	36.30	0.03	50.00
1	217.8	0.010	50.0	2	348.15	0.03	5.21
1	438.9	0.010	24.8	2	660.00	0.03	2.75
1	660.0	0.010	16.5	2	31.11	0.04	50.00
1	145.2	0.015	50.0	2	345.56	0.04	4.50
1	402.6	0.015	18.0	2	660.00	0.035	2.357
1	660.0	0.015	11.0	2	27.23	0.040	50.000
1	108.9	0.020	50.0	2	343.61	0.040	3.962
1	384.5	0.020	14.2	2	660.00	0.040	2.063
1	660.0	0.020	8.3	2	24.20	0.045	50.000
1	87.1	0.025	50.0	2	342.10	0.045	3.537
1	373.6	0.025	11.7	2	660.00	0.045	1.833
1	660.0	0.025	6.6	2	21.78	0.050	50.000
1	72.6	0.030	50.0	2	340.89	0.050	3.195
1	366.3	0.030	9.9	2	660.00	0.050	1.650
1	660.0	0.030	5.5	3	660.00	0.001	50.000
1	62.2	0.035	50.0	3	145.20	0.005	50.000
1	361.1	0.035	8.6	3	402.60	0.005	18.033
1	660.0	0.035	4.7	3	660.00	0.005	11.000
1	54.5	0.040	50.0	3	72.60	0.010	50.000
1	357.2	0.040	7.6	3	366.30	0.010	9.910
1	660.0	0.040	4.1	3	660.00	0.010	5.500
1	48.4	0.045	50.0	3	48.40	0.015	50.000
1	354.2	0.045	6.8	3	354.20	0.015	6.832
1	660.0	0.045	3.7	3	660.00	0.015	3.667
1	43.6	0.050	50.0	3	36.30	0.020	50.000
1	351.8	0.050	6.2	3	348.15	0.020	5.213
1	660.0	0.050	3.3	3	660.00	0.020	2.750
2	660.0	0.002	50.0	3	29.04	0.025	50.000
2	217.8	0.005	50.0	3	344.52	0.025	4.215
2	438.9	0.005	24.8	3	660.00	0.025	2.200
2	660.0	0.005	16.5	3	24.200	0.030	50.000
2	108.9	0.010	50.0	3	342.100	0.030	3.537
2	384.5	0.010	14.2	3	660.000	0.030	1.833
2	660.0	0.010	8.3	3	20.743	0.035	50.000
2	72.6	0.015	50.0	3	340.371	0.035	3.047
2	366.30	0.02	9.91	3	660.000	0.035	1.571
2	660.00	0.02	5.50	3	18.150	0.040	50.000
2	54.45	0.02	50.00	3	339.075	0.040	2.676
2	357.23	0.02	7.62	3	660.000	0.040	1.375
2	660.00	0.02	4.13	3	16.133	0.045	50.000

Table E.1 — Continued

n_{frac}	w_x	w_y	w_z	n_{frac}	w_x	w_y	w_z
3	338.067	0.045	2.386	4	335.445	0.050	1.623
3	660.000	0.045	1.222	4	660.000	0.050	0.825
3	14.520	0.050	50.000	5	660.000	0.001	50.000
3	337.260	0.050	2.153	5	87.120	0.005	50.000
3	660.000	0.050	1.100	5	373.560	0.005	11.661
4	660.000	0.001	50.000	5	660.000	0.005	6.600
4	108.900	0.005	50.000	5	43.560	0.010	50.000
4	384.450	0.005	14.163	5	351.780	0.010	6.191
4	660.000	0.005	8.250	5	660.000	0.010	3.300
4	54.450	0.010	50.000	5	29.040	0.015	50.000
4	357.225	0.010	7.621	5	344.520	0.015	4.215
4	660.000	0.010	4.125	5	660.000	0.015	2.200
4	36.300	0.015	50.000	5	21.780	0.020	50.000
4	348.150	0.015	5.213	5	340.890	0.020	3.195
4	660.000	0.015	2.750	5	660.000	0.020	1.650
4	27.225	0.020	50.000	5	17.424	0.025	50.000
4	343.613	0.020	3.962	5	338.712	0.025	2.572
4	660.000	0.020	2.063	5	660.000	0.025	1.320
4	21.780	0.025	50.000	5	14.520	0.030	50.000
4	340.890	0.025	3.195	5	337.260	0.030	2.153
4	660.000	0.025	1.650	5	660.000	0.030	1.100
4	18.150	0.030	50.000	5	12.446	0.035	50.000
4	339.075	0.030	2.676	5	336.223	0.035	1.851
4	660.000	0.030	1.375	5	660.000	0.035	0.943
4	15.557	0.035	50.000	5	10.890	0.040	50.000
4	337.779	0.035	2.303	5	335.445	0.040	1.623
4	660.000	0.035	1.179	5	660.000	0.040	0.825
4	13.613	0.040	50.000	5	9.680	0.045	50.000
4	336.806	0.040	2.021	5	334.840	0.045	1.445
4	660.000	0.040	1.031	5	660.000	0.045	0.733
4	12.100	0.045	50.000	5	8.712	0.050	50.000
4	336.050	0.045	1.800	5	334.356	0.050	1.303
4	660.000	0.045	0.917	5	660.000	0.050	0.660
4	10.890	0.050	50.000				

Table E.2— Locus of Maxima for Example Case in Chapter IV as a Function of Number of Fractures and Permeability Anisotropy (N_{Prop} =0.1)

n_{frac}	w_x	w_y	w_z	k_v/k_h	$J_{D,\,pss,\,max}$, 1 fracture	$J_{D,\,pss,\,max}$, Total	Fracture Contribution
1	660.00	0.050	3.30	1.000	1.3845	1.3845	0.1845
2	660.00	0.050	1.65	1.000	0.7429	1.4858	0.2571
3	660.00	0.050	1.10	1.000	0.5478	1.6435	0.3366
4	660.00	0.050	0.83	1.000	0.4608	1.8431	0.4034
5	660.00	0.050	0.66	1.000	0.4117	2.0583	0.4588
1	79.20	0.028	50.00	0.100	0.8297	0.8297	0.3178
2	39.60	0.028	50.00	0.100	0.4672	0.9344	0.4424
3	36.30	0.020	50.00	0.100	0.3577	1.0732	0.5333
4	27.23	0.020	50.00	0.100	0.3059	1.2236	0.5990
5	21.78	0.020	50.00	0.100	0.2750	1.3750	0.6469
1	79.20	0.028	50.00	0.010	0.5162	0.5162	0.5681
2	39.60	0.028	50.00	0.010	0.3431	0.6862	0.7010
3	36.30	0.020	50.00	0.010	0.2852	0.8556	0.7688
4	27.23	0.020	50.00	0.010	0.2559	1.0238	0.8116
5	21.78	0.020	50.00	0.010	0.2373	1.1866	0.8400
1	79.20	0.028	50.00	0.001	0.3852	0.3852	0.7948
2	39.60	0.028	50.00	0.001	0.2939	0.5877	0.8673
3	26.40	0.028	50.00	0.001	0.2571	0.7714	0.9017
4	27.23	0.020	50.00	0.001	0.2367	0.9470	0.9203
5	21.78	0.020	50.00	0.001	0.2230	1.1150	0.9331

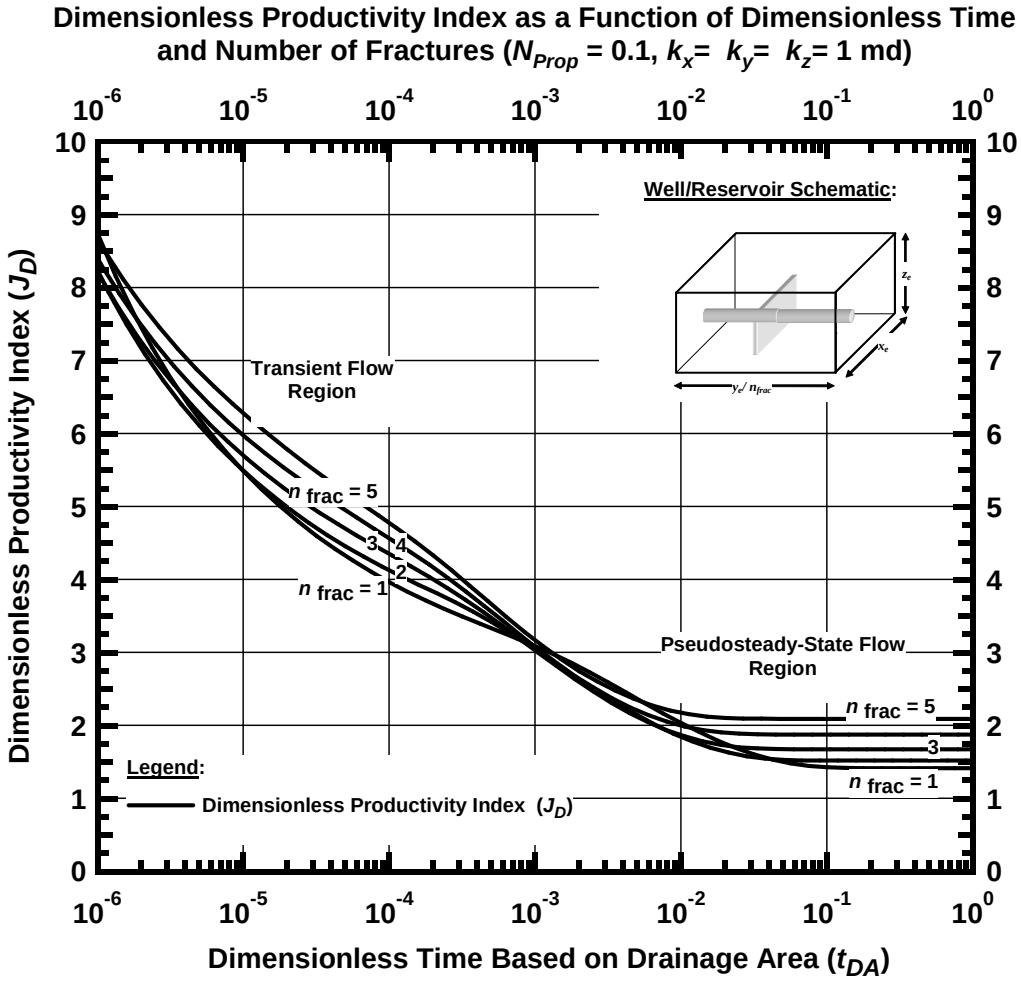

Figure E.1 — Dimensionless Productivity Index as a Function of Dimensionless Time and Number of Fractures for Example Case (N_{Prop} = 0.1, k_x = k_y = k_z = 1 md)

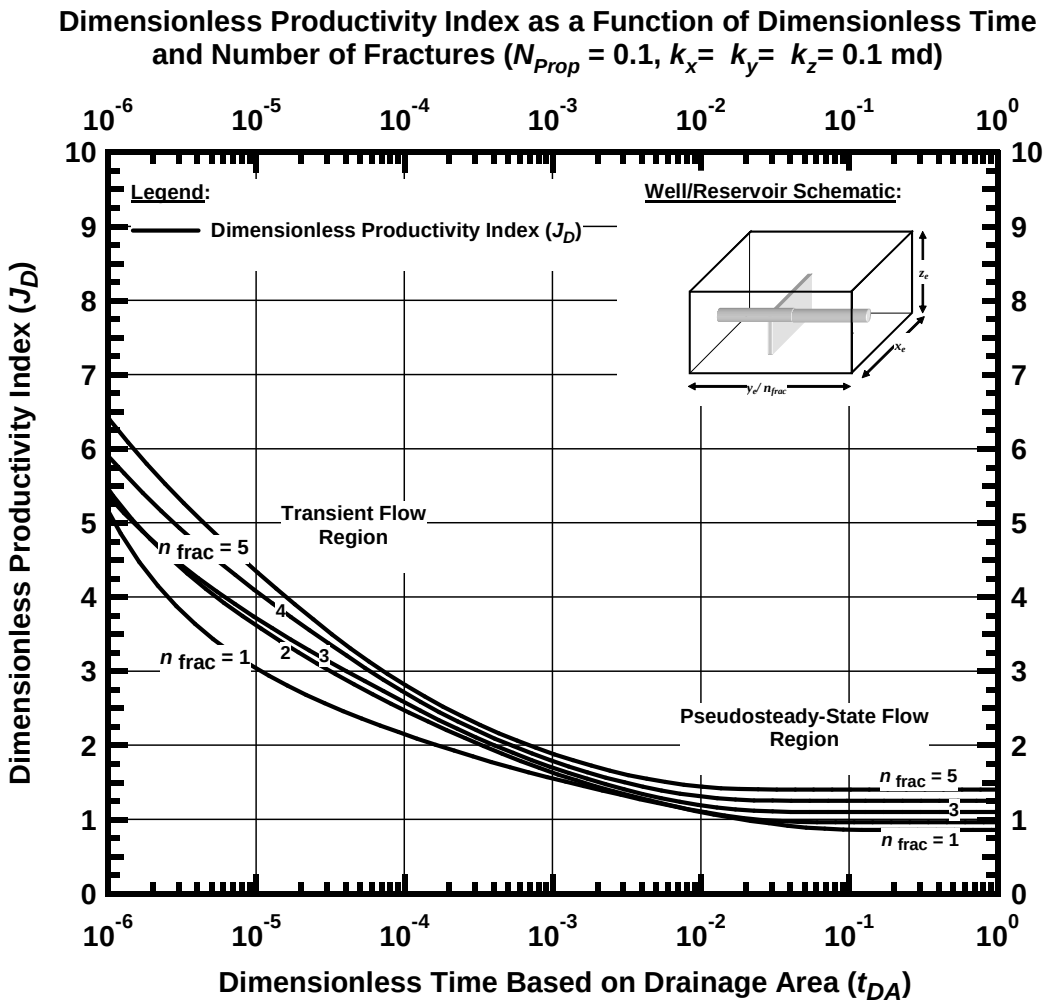

Figure E.2 — Dimensionless Productivity Index as a Function of Dimensionless Time and Number of Fractures for Example Case (N_{Prop} = 0.1, k_x = k_y = 1 md, k_z = 0.1 md)

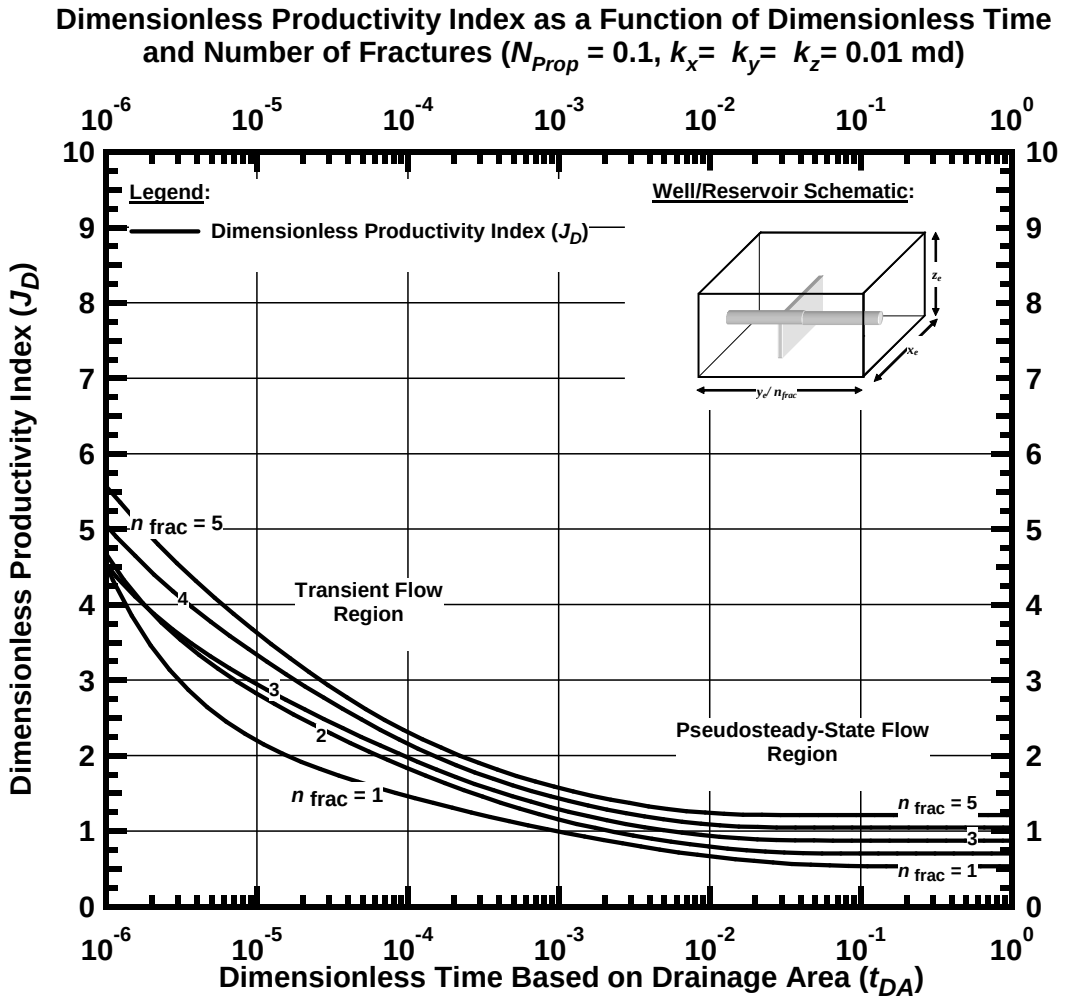

Figure E.3 — Dimensionless Productivity Index as a Function of Dimensionless Time and Number of Fractures for Example Case (N_{Prop} = 0.1, k_x = k_y = 1 md, k_z = 0.01 md)

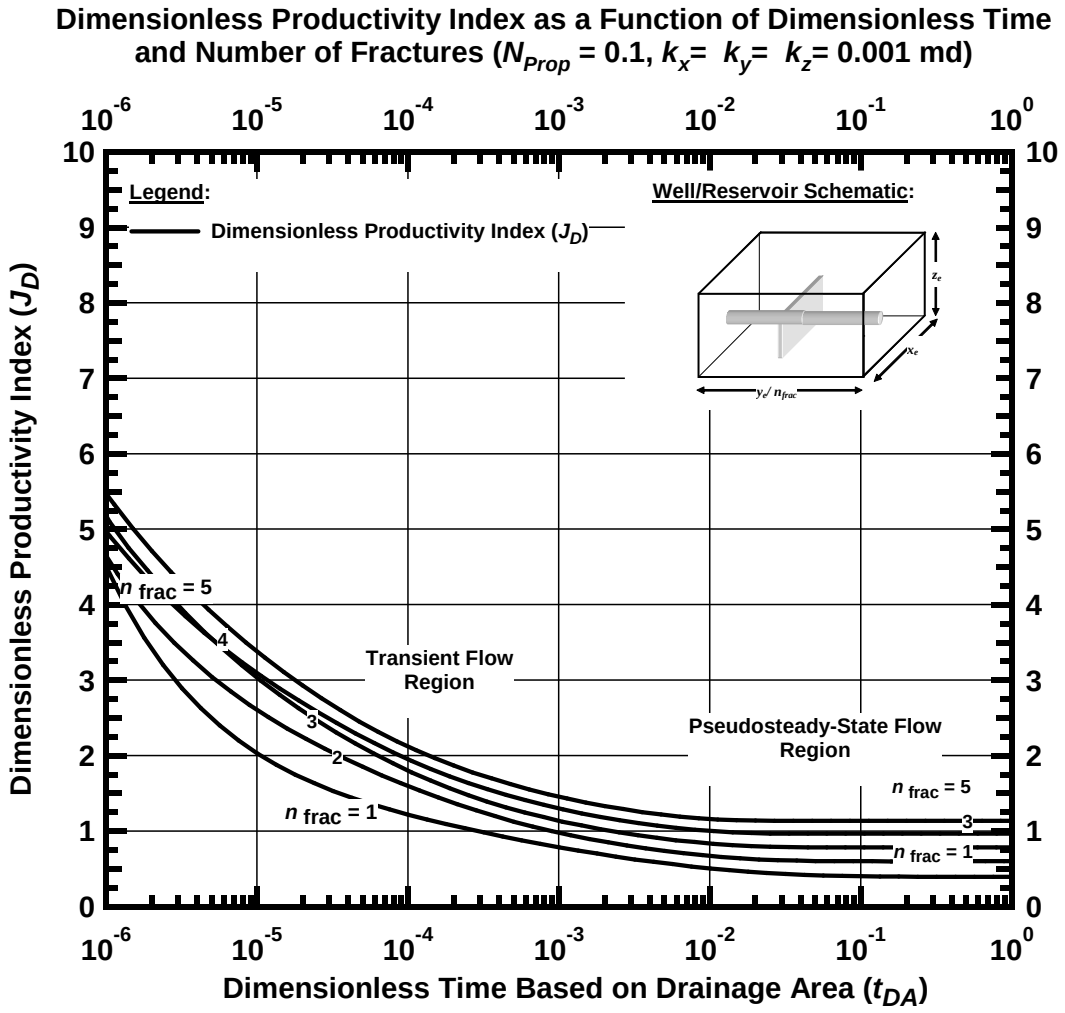

Figure E.4 — Dimensionless Productivity Index as a Function of Dimensionless Time and Number of Fractures for Example Case (N_{Prop} = 0.1, k_x = k_y = 1 md, k_z = 0.001 md)

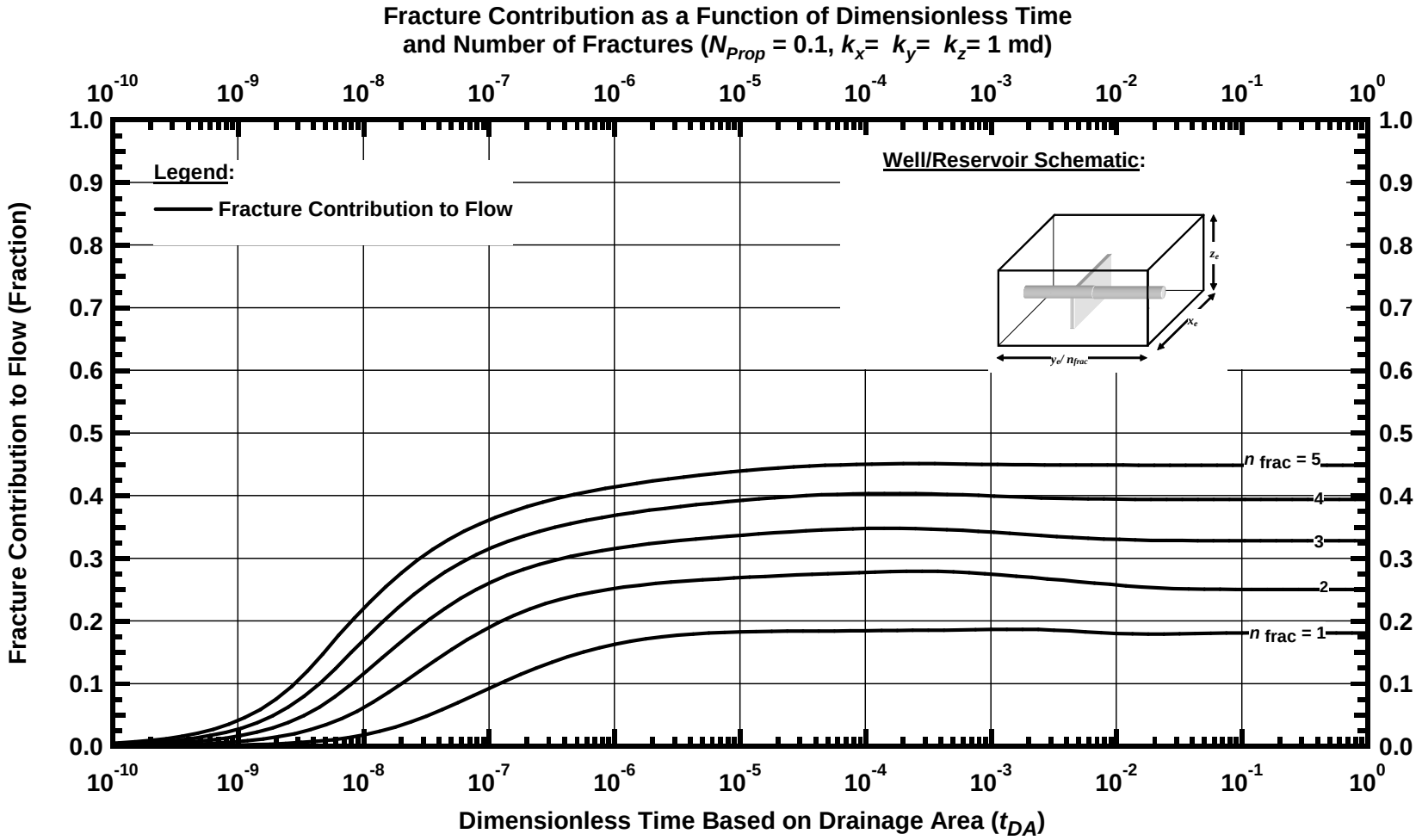

Figure E.5 — Fracture Contribution to Flow as a Function of Dimensionless Time and Number of Fractures for Example Case (N_{Prop} = 0.1, k_x = k_y = k_z = 1 md)

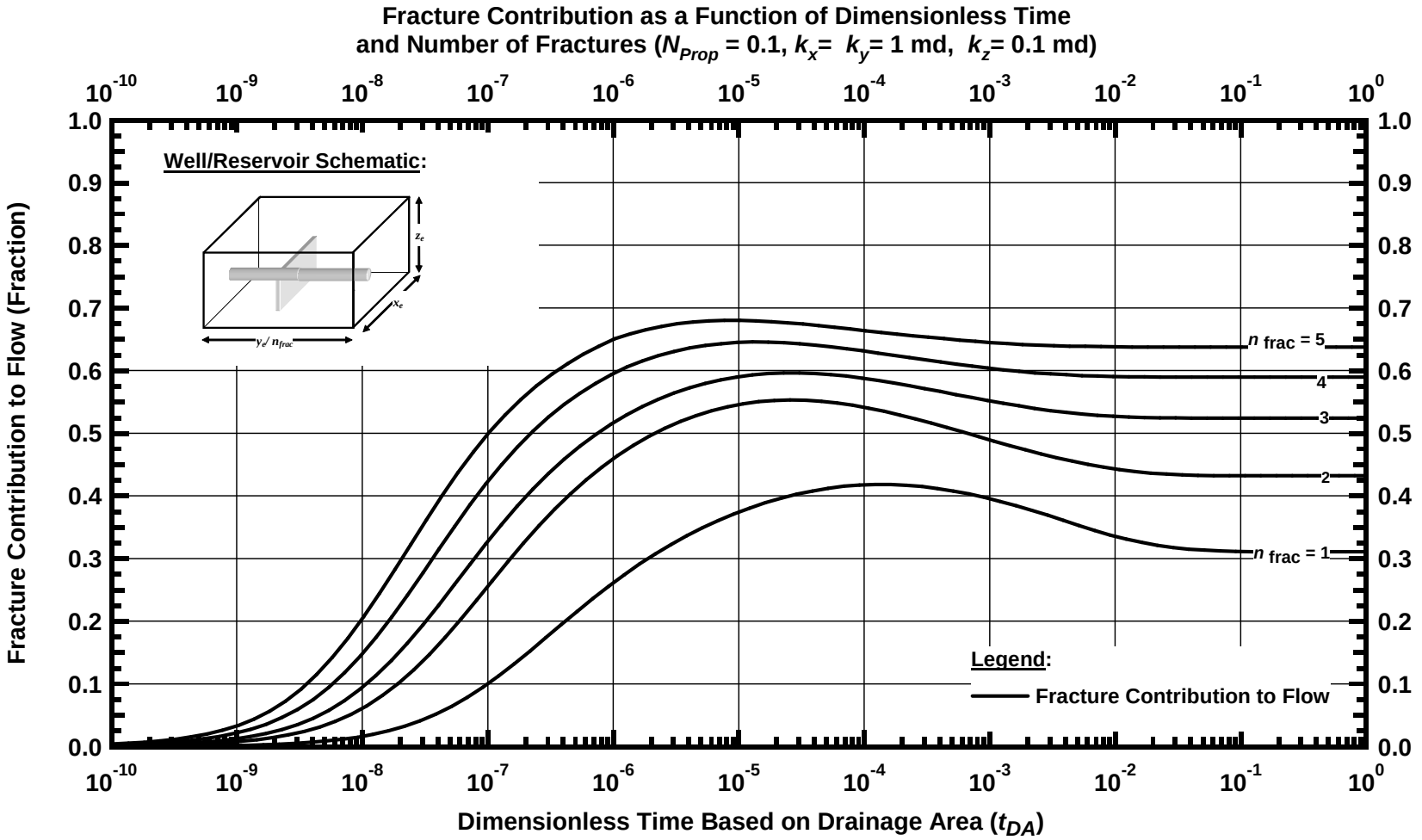

Figure E.6 — Fracture Contribution to Flow as a Function of Dimensionless Time and Number of Fractures for Example Case (N_{Prop} = 0.1, k_x = k_y = 1 md, k_z = 0.1 md)

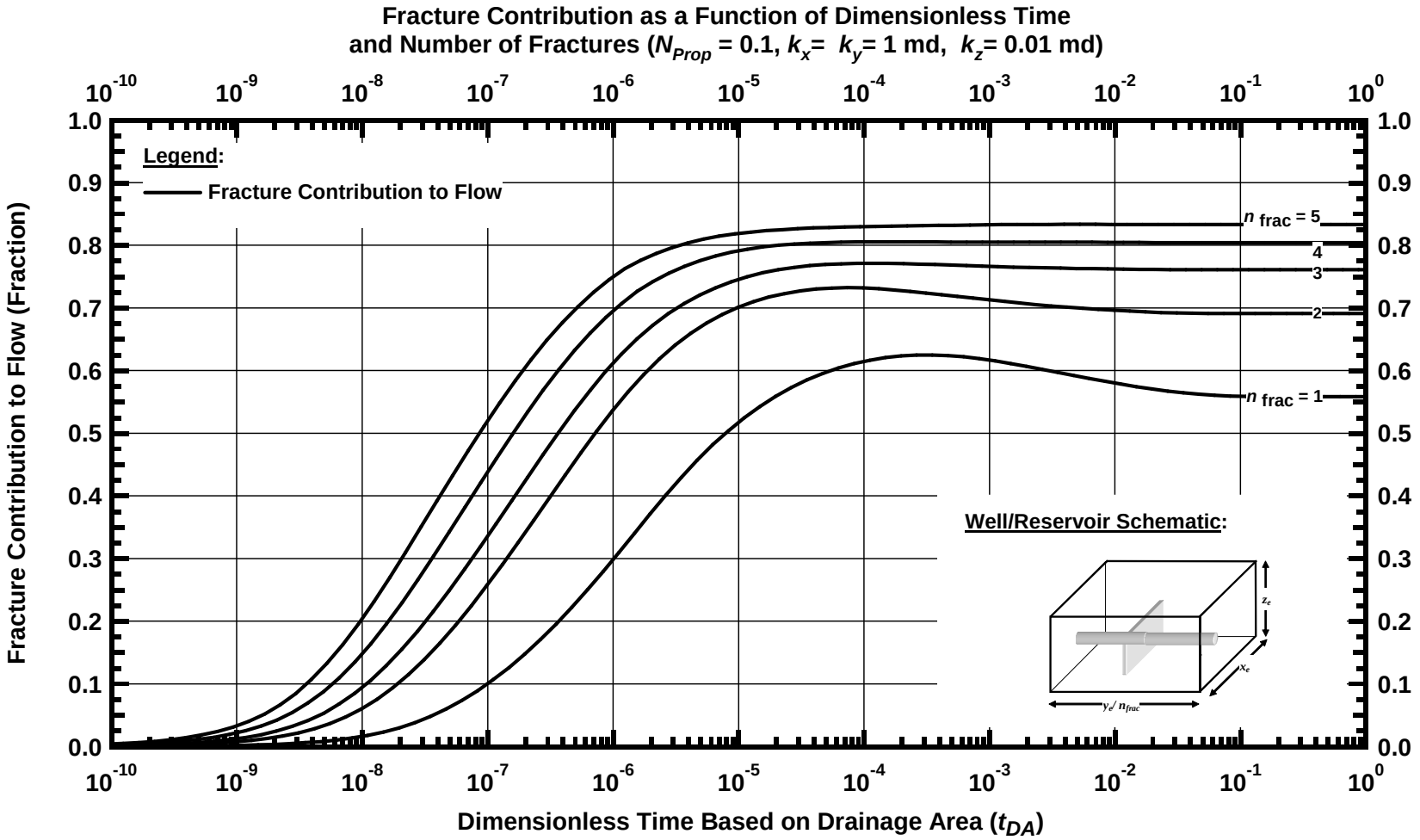

Figure E.7 — Fracture Contribution to Flow as a Function of Dimensionless Time and Number of Fractures for Example Case (N_{Prop} = 0.1, k_x = k_y = 1 md, k_z = 0.01 md)

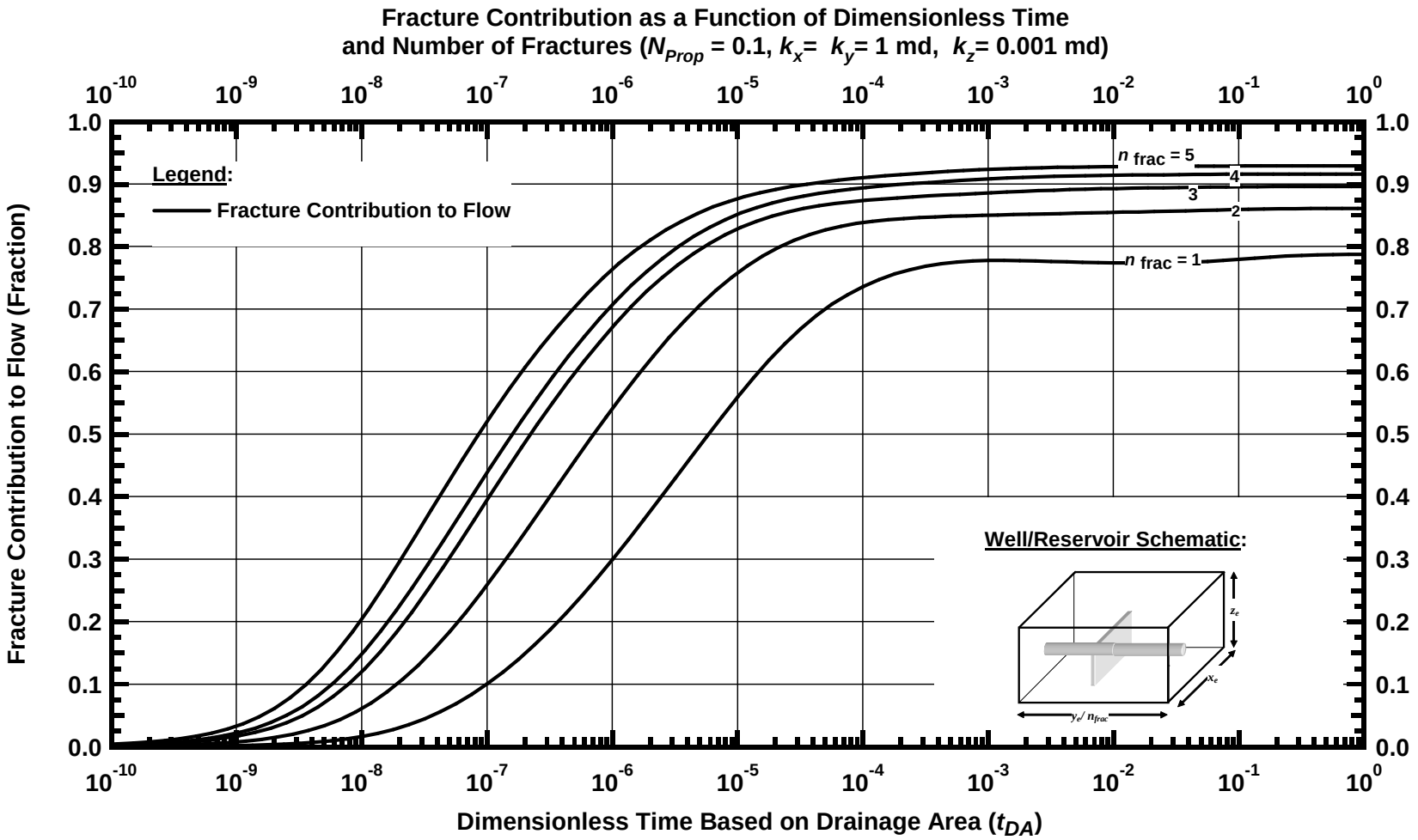

Figure E.8 — Fracture Contribution to Flow as a Function of Dimensionless Time and Number of Fractures for Example Case (N_{Prop} = 0.1, k_x = k_y = 1 md, k_z = 0.001 md).

APPENDIX F

DETAILED RESULTS OF CALCULATION FOR MAXIMUM DIMENSIONLESS PRODUCTIVITY INDEX OF THE EXAMPLE CASE, PROPPANT NUMBER (N_{Prop}) = 1.0

In this appendix we provide details of calculation results and complete set of graphs describing the production behavior of example problem in chapter IV when 1,000,000 lb of proppant (N_{Prop} = 1.0) is used for stimulation. All the fracture sizes have been described in ft.

Table F.1 — Table of Mathematically Feasible Fracture Sizes for Example Case in Chapter IV (N_{Prop} = 1.0)

n_{frac}	w_x	w_y	w_z	n_{frac}	w_x	w_y	w_z
1	660.0	0.033	50.0	3	660.0	0.025	22.0
1	622.3	0.035	50.0	3	242.0	0.030	50.0
1	641.1	0.035	48.5	3	451.0	0.030	26.8
1	660.0	0.035	47.1	3	660.0	0.030	18.3
1	544.5	0.040	50.0	3	207.4	0.035	50.0
1	602.3	0.040	45.2	3	433.7	0.035	23.9
1	660.0	0.040	41.3	3	660.0	0.035	15.7
1	484.0	0.045	50.0	3	181.5	0.040	50.0
1	572.0	0.045	42.3	3	420.8	0.040	21.6
1	660.0	0.045	36.7	3	660.0	0.040	13.8
1	435.6	0.050	50.0	3	161.3	0.045	50.0
1	547.8	0.050	39.8	3	410.7	0.045	19.6
1	660.0	0.050	33.0	3	660.0	0.045	12.2
2	660.0	0.017	50.0	3	145.2	0.050	50.0
2	544.5	0.020	50.0	3	402.6	0.050	18.0
2	602.3	0.020	45.2	3	660.0	0.050	11.0
2	660.0	0.020	41.3	4	660.0	0.008	50.0
2	435.6	0.025	50.0	4	544.5	0.010	50.0
2	547.8	0.025	39.8	4	602.3	0.010	45.2
2	660.0	0.025	33.0	4	660.0	0.010	41.3
2	363.0	0.030	50.0	4	363.0	0.015	50.0
2	511.5	0.030	35.5	4	511.5	0.015	35.5
2	660.0	0.030	27.5	4	660.0	0.015	27.5
2	311.1	0.035	50.0	4	272.3	0.020	50.0
2	485.6	0.035	32.0	4	466.1	0.020	29.2
2	660.0	0.035	23.6	4	660.0	0.020	20.6
2	272.3	0.040	50.0	4	217.8	0.025	50.0
2	466.1	0.040	29.2	4	438.9	0.025	24.8
2	660.0	0.040	20.6	4	660.0	0.025	16.5
2	242.0	0.045	50.0	4	181.5	0.030	50.0
2	451.0	0.045	26.8	4	420.8	0.030	21.6
2	660.0	0.045	18.3	4	660.0	0.030	13.8
2	217.8	0.050	50.0	4	155.6	0.035	50.0
2	438.9	0.050	24.8	4	407.8	0.035	19.1
2	660.0	0.050	16.5	4	660.0	0.035	11.8
3	660.0	0.011	50.0	4	136.1	0.040	50.0
3	484.0	0.015	50.0	4	398.1	0.040	17.1
3	572.0	0.015	42.3	4	660.0	0.040	10.3
3	660.0	0.015	36.7	4	121.0	0.045	50.0
3	363.0	0.020	50.0	4	390.5	0.045	15.5
3	511.5	0.020	35.5	4	660.0	0.045	9.2
3	660.0	0.020	27.5	4	108.9	0.050	50.0
3	290.4	0.025	50.0	4	384.5	0.050	14.2
3	475.2	0.025	30.6	4	660.0	0.050	8.3

Table F.1 — Continued

n_{frac}	w_x	w_y	w_z
5	660.0	0.007	50.0
5	435.6	0.010	50.0
5	547.8	0.010	39.8
5	660.0	0.010	33.0
5	290.4	0.015	50.0
5	475.2	0.015	30.6
5	660.0	0.015	22.0
5	217.8	0.020	50.0
5	438.9	0.020	24.8
5	660.0	0.020	16.5
5	174.2	0.025	50.0
5	417.1	0.025	20.9
5	660.0	0.025	13.2
5	145.2	0.030	50.0
5	402.6	0.030	18.0
5	660.0	0.030	11.0
5	124.5	0.035	50.0
5	392.2	0.035	15.9
5	660.0	0.035	9.4
5	108.9	0.040	50.0
5	384.5	0.040	14.2
5	660.0	0.040	8.3
5	96.8	0.045	50.0
5	378.4	0.045	12.8
5	660.0	0.045	7.3
5	87.1	0.050	50.0
5	373.6	0.050	11.7
5	660.0	0.050	6.6

Table F.2 — Locus of Maxima for Example Case in Chapter IV as a Function of Number of Fractures and Permeability Anisotropy (N_{Prop} = 1.0)

n_{frac}	w_x	w_y	w_z	k_v/k_h	$J_{D,\,pss,\,max}$, 1 fracture	$J_{D,\,pss,\,max}$, Total	Fracture Contribution
1	547.80	0.050	39.76	1.000	1.7435	1.7435	0.3242
2	438.90	0.050	24.81	1.000	0.9374	1.8748	0.4239
3	402.60	0.050	18.03	1.000	0.6989	2.0968	0.5065
4	384.45	0.050	14.16	1.000	0.5886	2.3544	0.5645
5	373.56	0.050	11.66	1.000	0.5229	2.6144	0.6072
1	547.80	0.050	39.76	0.100	1.1816	1.1816	0.4971
2	438.90	0.050	24.81	0.100	0.6882	1.3764	0.6286
3	207.43	0.035	50.00	0.100	0.5304	1.5912	0.7197
4	155.57	0.035	50.00	0.100	0.4605	1.8420	0.7758
5	124.46	0.035	50.00	0.100	0.4178	2.0890	0.8126
1	435.60	0.050	50.00	0.010	0.8423	0.8423	0.7268
2	217.80	0.050	50.00	0.010	0.5705	1.1410	0.8374
3	170.82	0.043	50.00	0.010	0.4758	1.4275	0.8820
4	155.57	0.035	50.00	0.010	0.4258	1.7032	0.9042
5	124.46	0.035	50.00	0.010	0.3939	1.9696	0.9216
1	435.60	0.050	50.00	0.001	0.7070	0.7070	0.8810
2	217.80	0.050	50.00	0.001	0.5324	1.0648	0.9320
3	170.82	0.043	50.00	0.001	0.4570	1.3711	0.9513
4	155.57	0.035	50.00	0.001	0.4137	1.6547	0.9607
5	124.46	0.035	50.00	0.001	0.3859	1.9294	0.9680

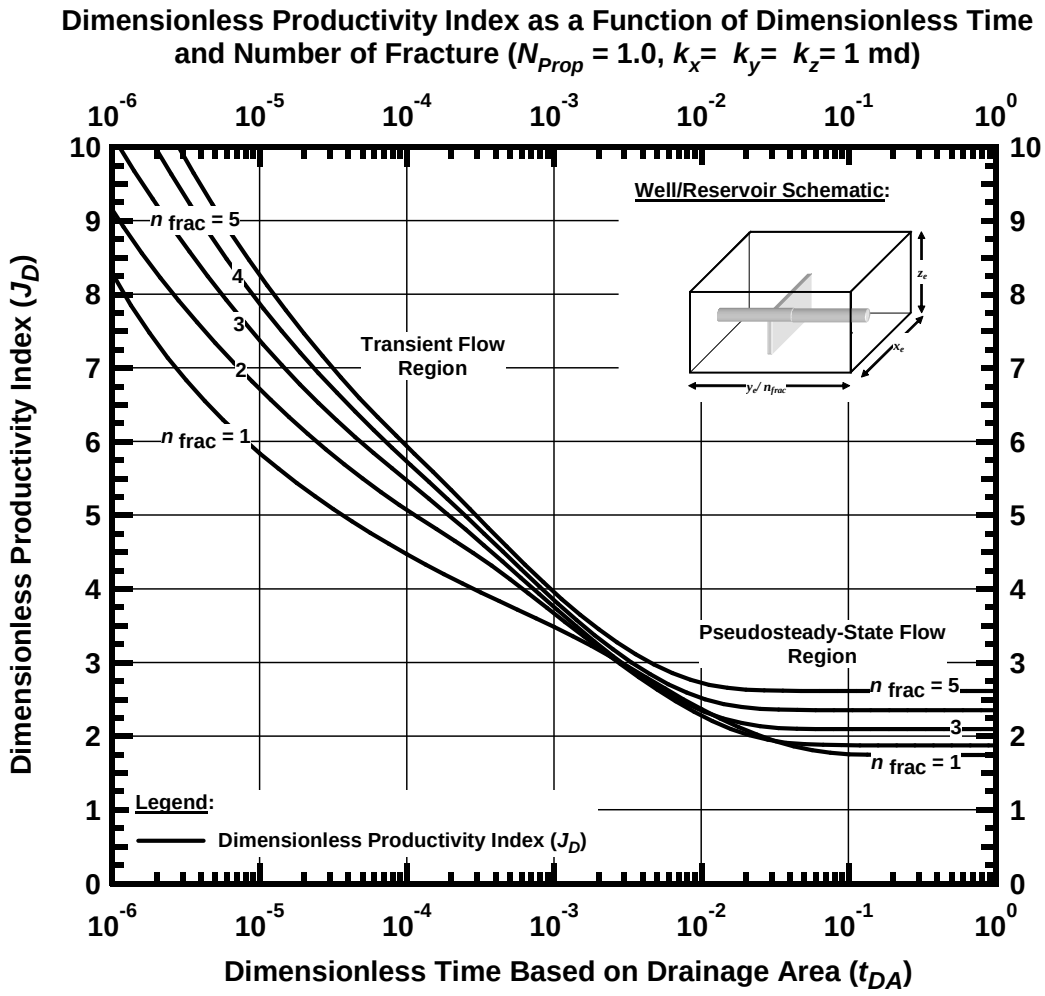

Figure F.1 — Dimensionless Productivity Index as a Function of Dimensionless Time and Number of Fractures for Example Case (N_{Prop} = 1.0, $k_x = k_y = k_z$ = 1 md)

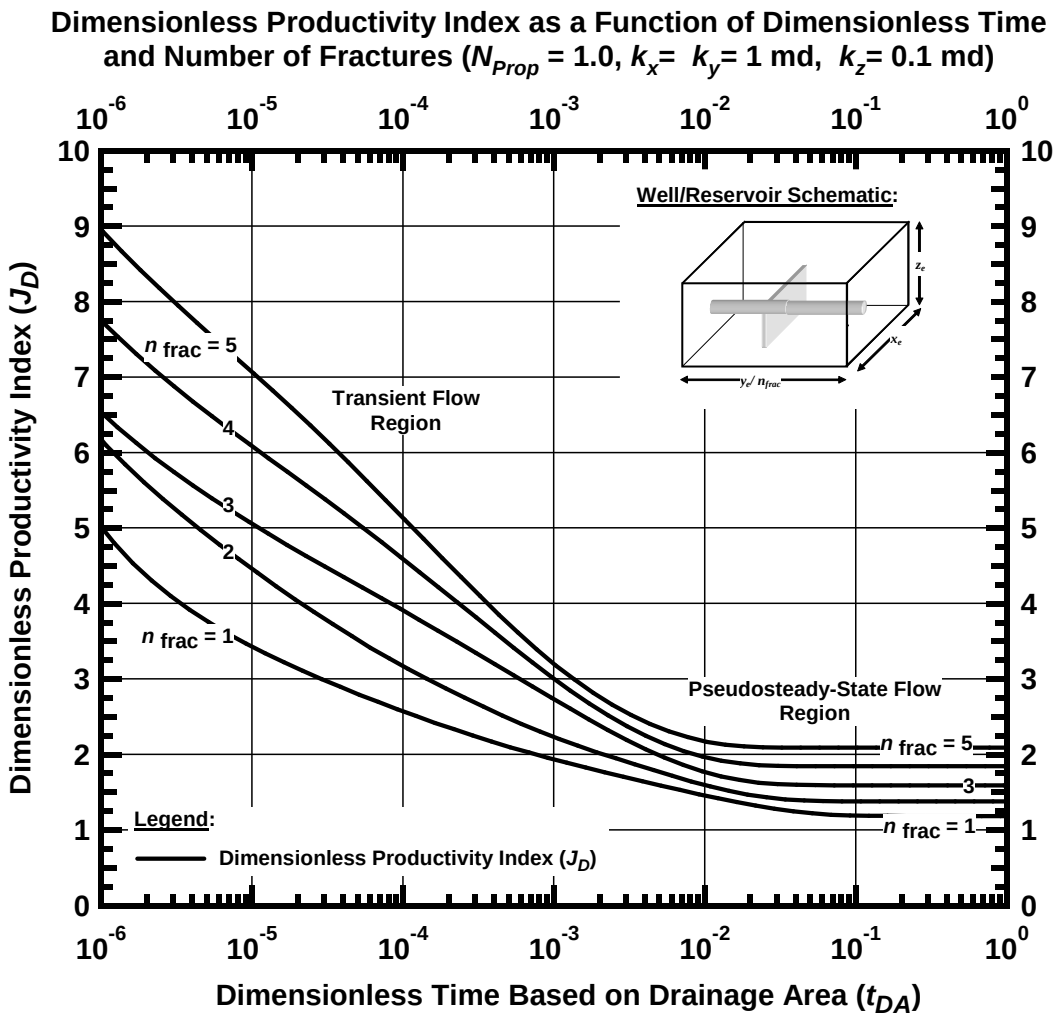

Figure F.2 — Dimensionless Productivity Index as a Function of Dimensionless Time and Number of Fractures for Example Case (N_{Prop} = 1.0, k_x = k_y = 1 md, k_z = 0.1 md)

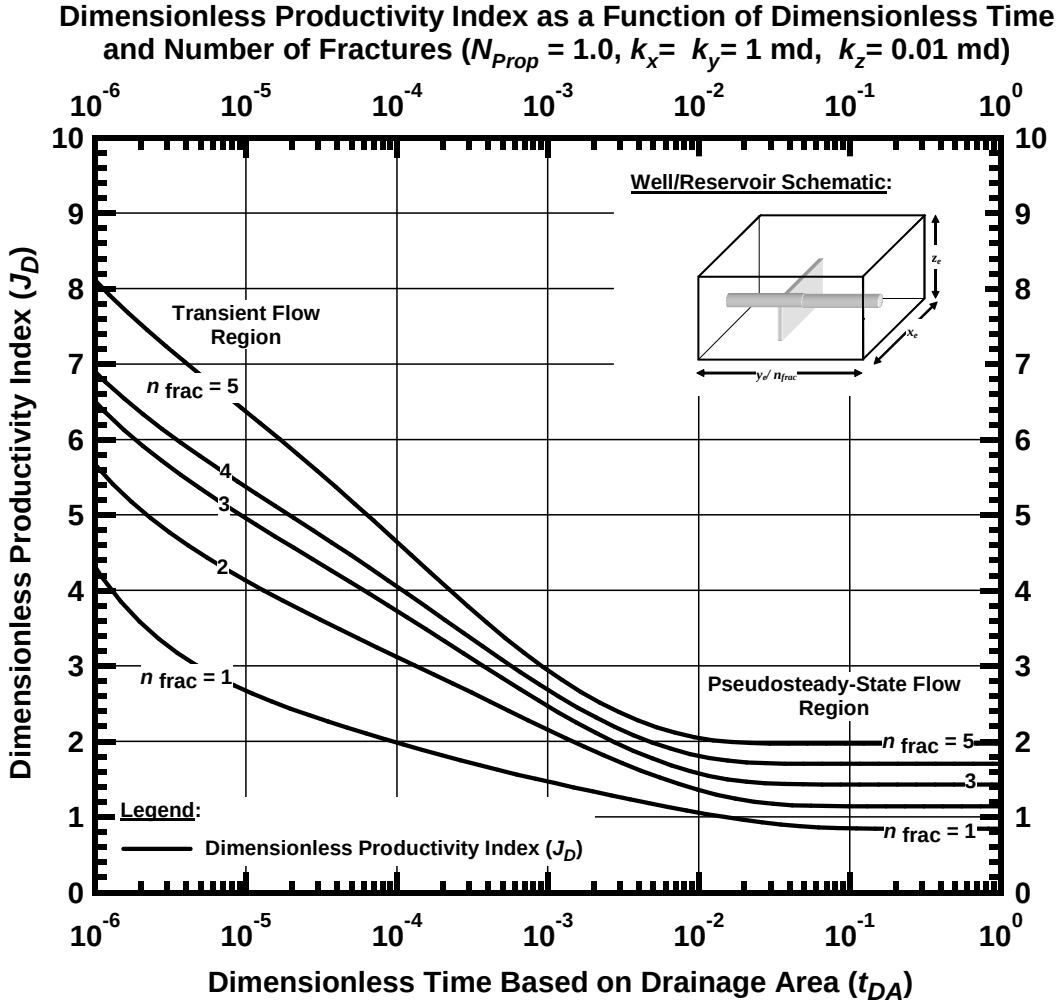

Figure F.3 — Dimensionless Productivity Index as a Function of Dimensionless Time and Number of Fractures for Example Case (N_{Prop} = 1.0, k_x = k_y = 1 md, k_z = 0.01 md)

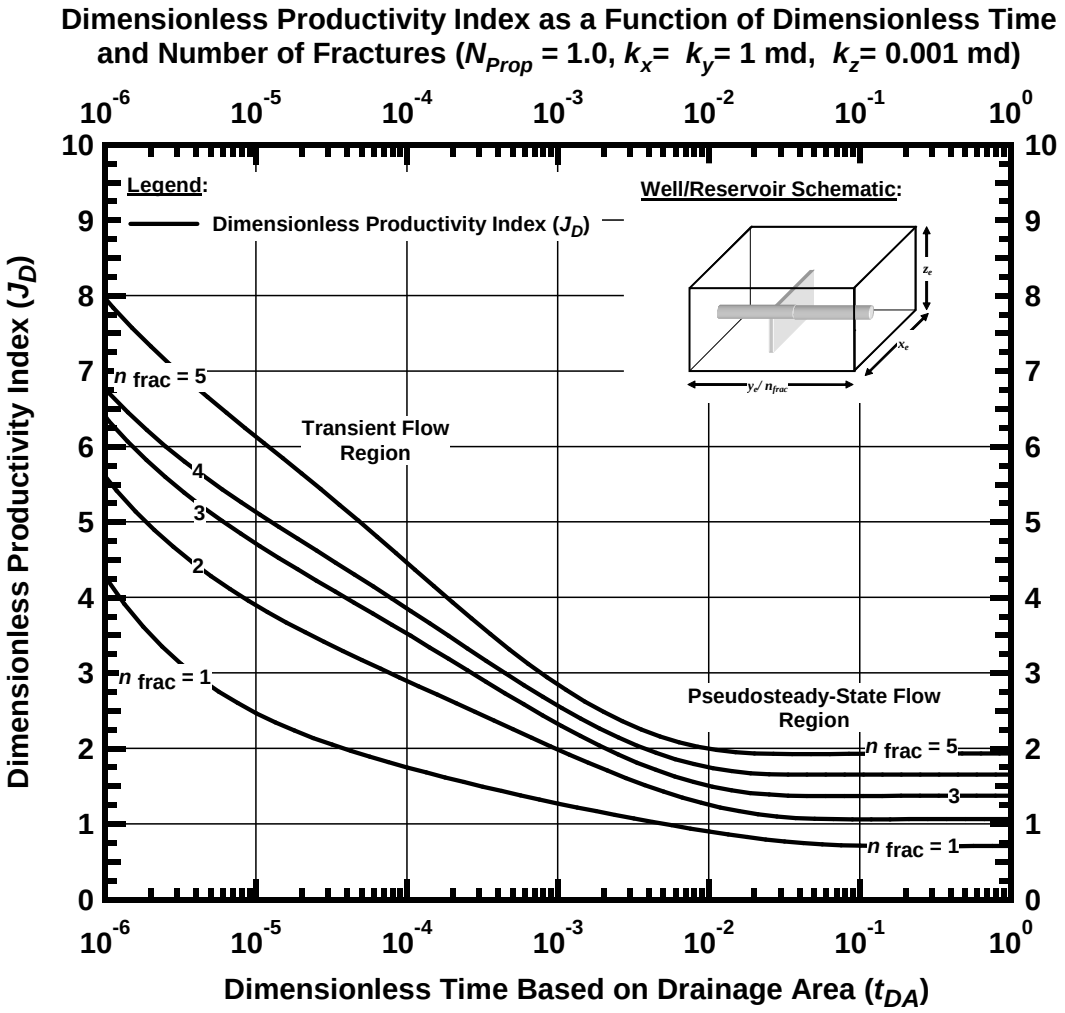

Figure F.4 — Dimensionless Productivity Index as a Function of Dimensionless Time and Number of Fractures for Example Case (N_{Prop} = 1.0, k_x = k_y = 1 md, k_z = 0.001 md)

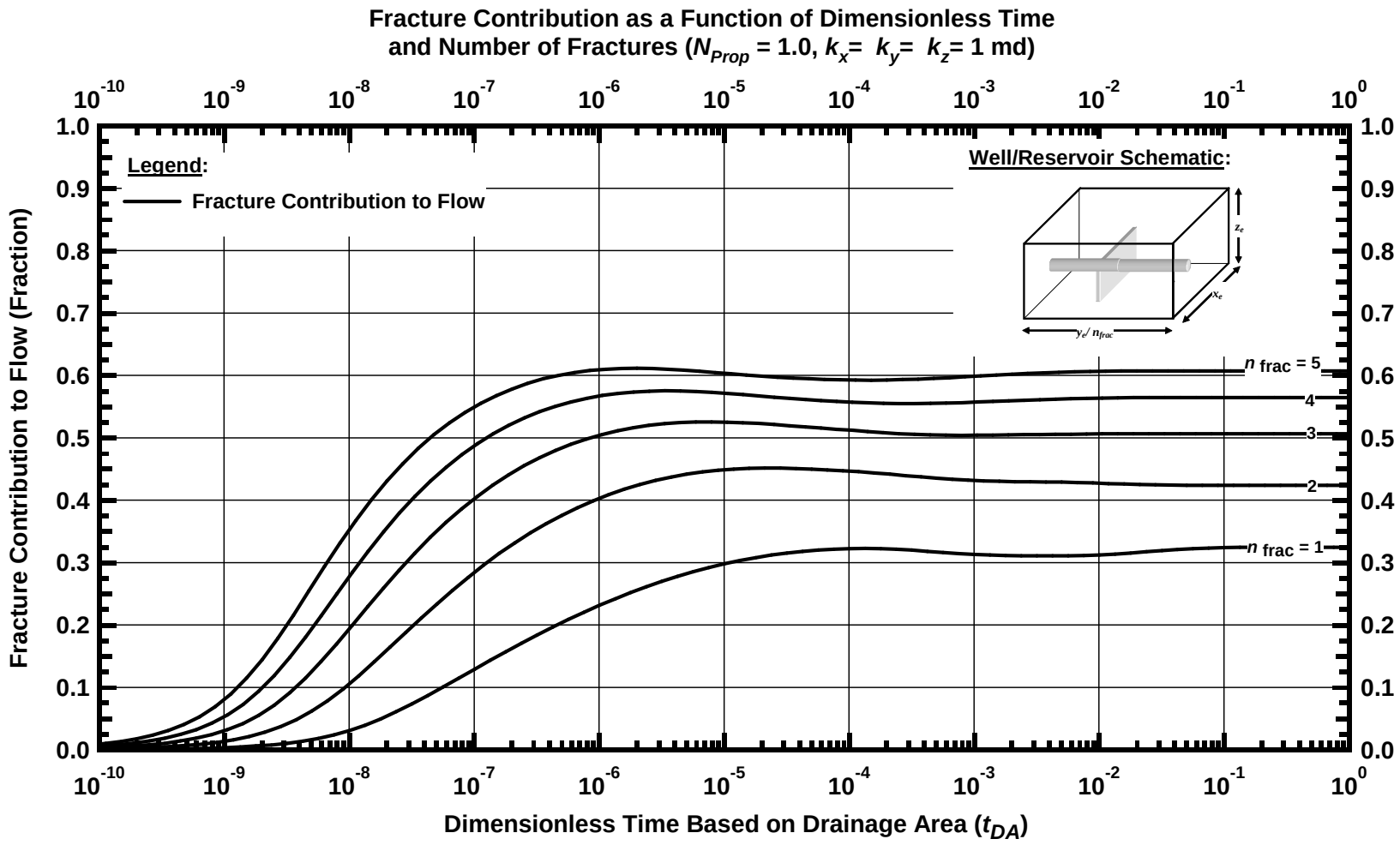

Figure F.5 — Fracture Contribution to Flow as a Function of Dimensionless Time and Number of Fractures for Example Case (N_{Prop} = 1.0, $k_x = k_y = k_z$ = 1 md)

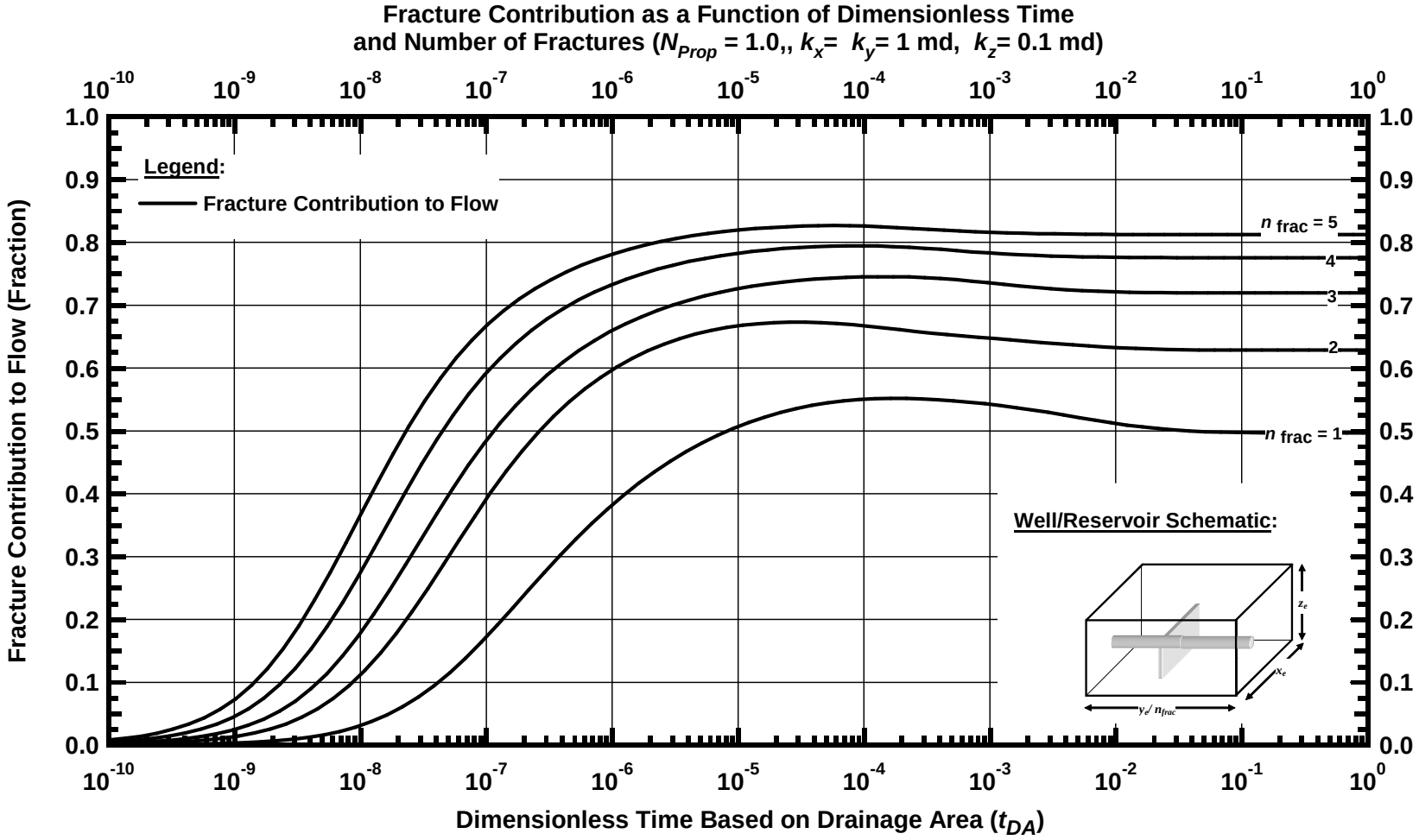

Figure F.6 — Fracture Contribution to Flow as a Function of Dimensionless Time and Number of Fractures for Example Case (N_{Prop} = 1.0, k_x = k_y = 1 md, k_z = 0.1 md)

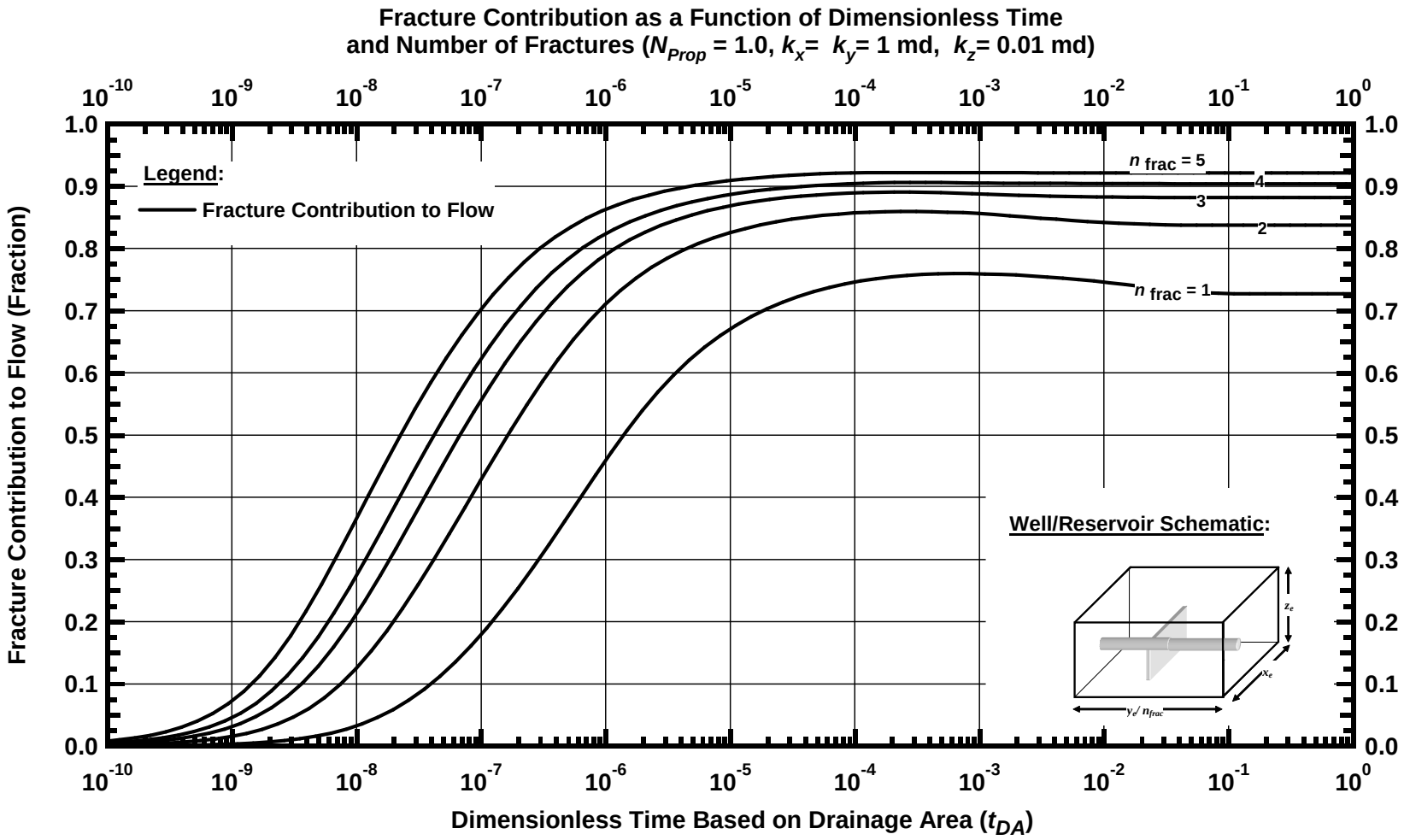

Figure F.7 — Fracture Contribution to Flow as a Function of Dimensionless Time and Number of Fractures for Example Case (N_{Prop} = 1.0, k_x = k_y = 1 md, k_z = 0.01 md)

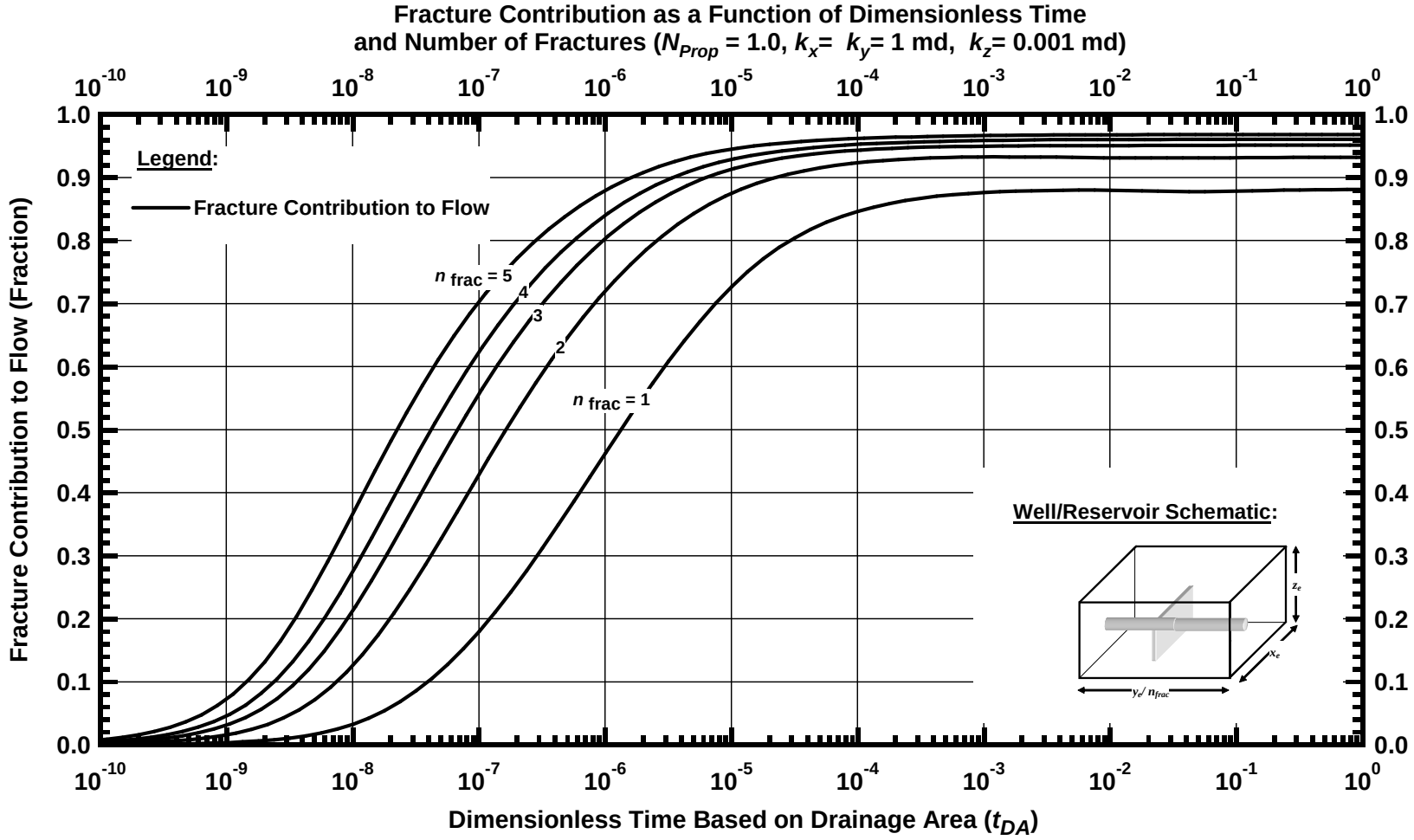

Figure F.8 — Fracture Contribution to Flow as a Function of Dimensionless Time and Number of Fractures for Example Case (N_{Prop} = 1.0, k_x = k_y = 1 md, k_z = 0.001 md)

APPENDIX G

COMPLETE RESULTS OF FIELD APPLICATION WHELAN GAS FIELD

The material balance equation for dry gas volumetric reservoirs has been integrated to the results of DVS calculation to obtain the production performance behavior of Whelan gas field in East Texas, USA. This Appendix provides figures of the estimation of gas production rate, average reservoir pressure, and cumulative gas production of this field for an 80-acre spacing, development plan as a function of the completion scheme— Fracture and horizontal section produce together and production only from fractures—, number of transverse fractures, and the amount of propant (250,000 and 500,000 lb). **Table G.1** Provides the reservoir and fluid properties used for the calculations

Table G.1 — Reservoir and Fluid Properties for Whelan Field Example

	Whelan
Net Pay (ft)	200
Hor. Permeability (md)	0.9
Porosity (%)	8.8
Initial Pressure (psia)	3500
Reservoir Temperature(°F)	220
Gas Gravity	0.63
Gas in Place(BCF)	11.907

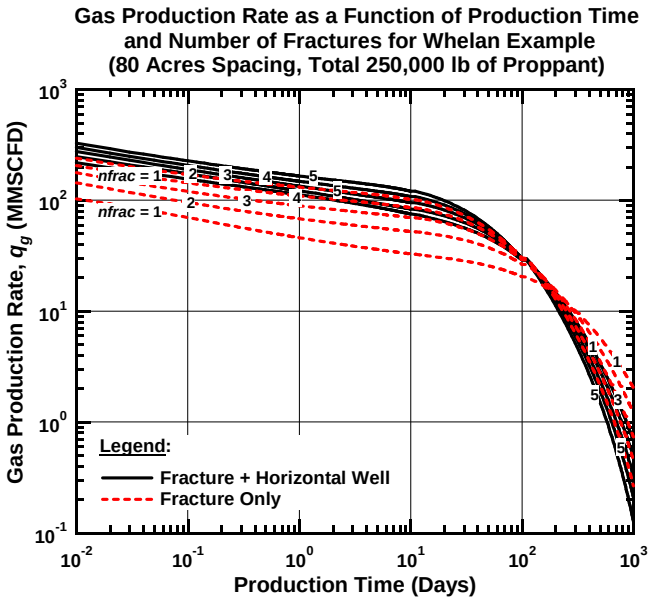

Figure G.1 — Gas Production Rate as a Function of Production Time, Number of Fractures, and Completion Scheme for Whelan Field (80 Acres Spacing, 250,000 lb

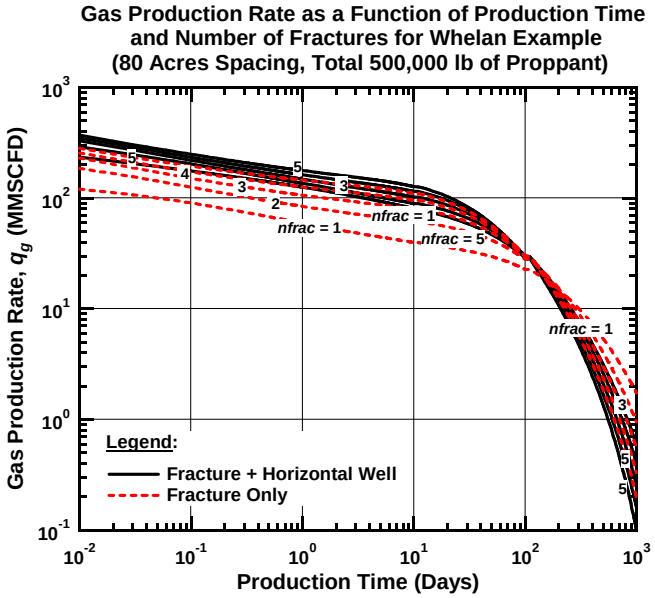

Figure G.2 — Gas Production Rate as a Function of Production Time, Number of Fractures, and Completion Scheme for Whelan Field (80 Acres Spacing, 500,000 lb

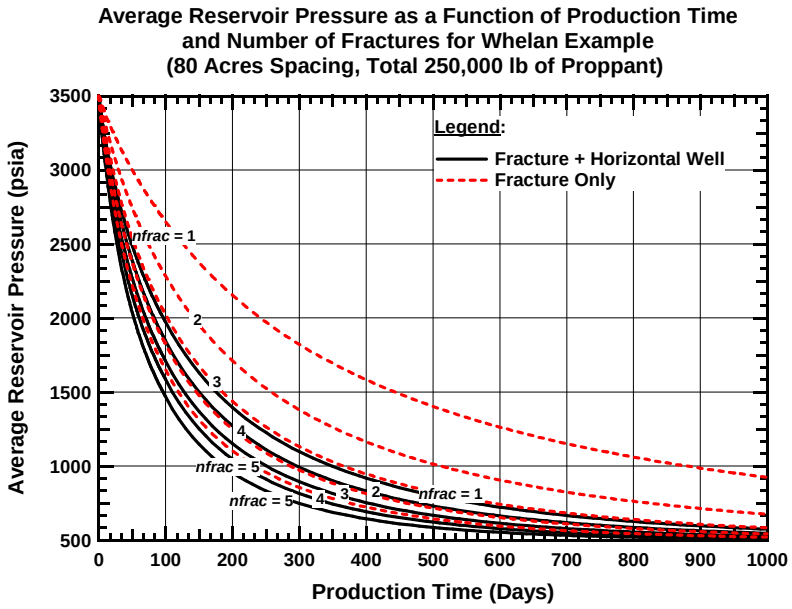

Figure G.3 — Average Reservoir Pressure as a Function of Production Time, Number of Fractures, and Completion Scheme for Whelan Field (80 Acres Spacing, 250,000 lb Proppant)

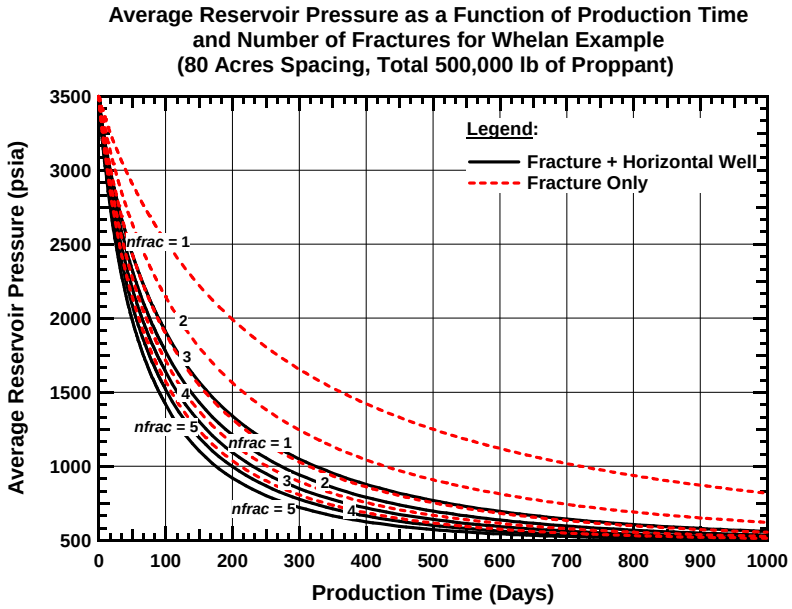

Figure G.4 — Average Reservoir Pressure as a Function of Production Time, Number of Fractures, and Completion Scheme for Whelan Field (80 Acres Spacing, 500,000 lb Proppant)

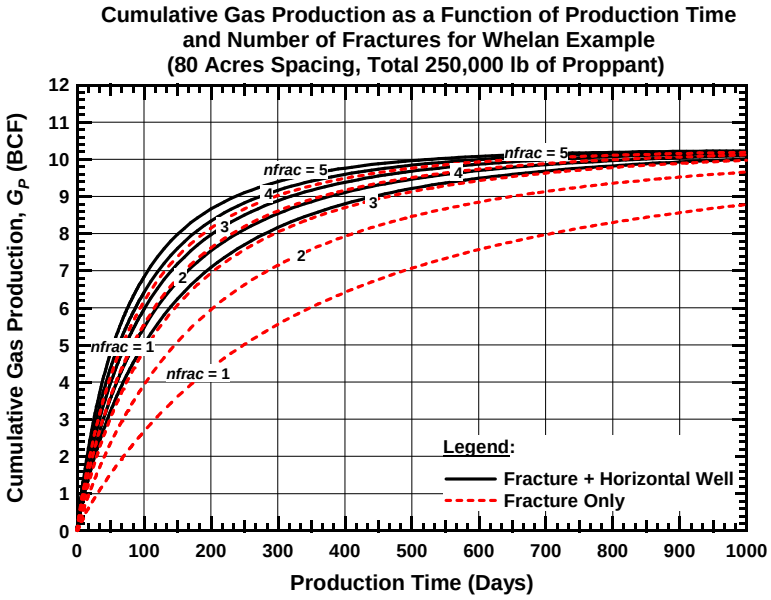

Figure G.5 — Cumulative Gas Production as a Function of Production Time, Number of Fractures, and Completion Scheme for Whelan Field (80 Acres Spacing, 250,000 lb Proppant)

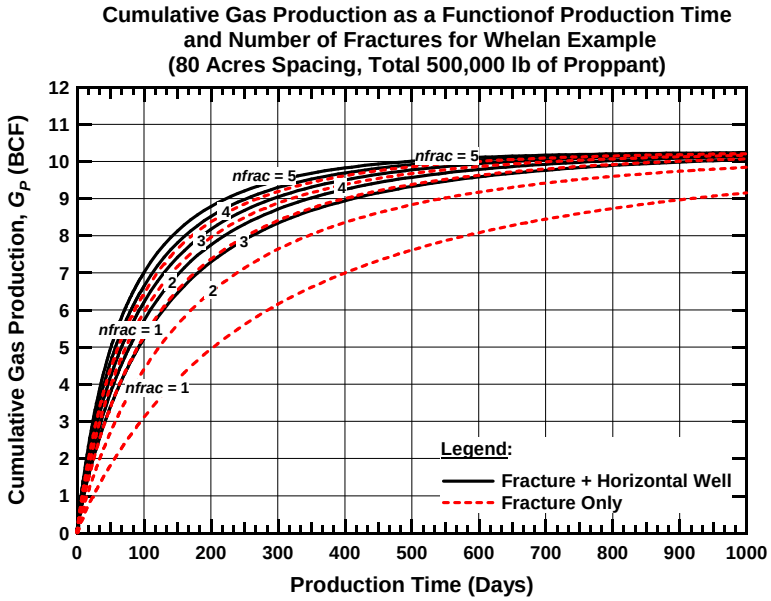

Figure G.6 — Cumulative Gas Production as a Function of Production Time, Number of Fractures, and Completion Scheme for Whelan Field (80 Acres Spacing, 500,000 lb Proppant)

APPENDIX H

COMPLETE RESULTS OF FIELD APPLICATION PERCY WHEELER GAS FIELD

The material balance equation for dry gas volumetric reservoirs has been integrated to the results of DVS calculation to obtain the production performance behavior of Percy Wheeler gas field in East Texas, USA. This Appendix provides figures of the estimation of gas production rate, average reservoir pressure, and cumulative gas production of this field for an 80-acre spacing, development plan as a function of the completion scheme— Fracture and horizontal section produce together and production only from fractures—, number of transverse fractures, and the amount of propant (250,000 and 500,000 lb).). **Table H.1** Provides the reservoir and fluid properties used for the calculations

Table H.1 — Reservoir and Fluid Properties for Percy Wheeler Field Example

	Percy Wheeler
Net Pay (ft)	200
Hor. Permeability (md)	0.05
Porosity (%)	10.3
Initial Pressure (psia)	3000
Reservoir Temperature(°F)	245
Gas Gravity	0.62
Gas in Place(BCF)	11.495

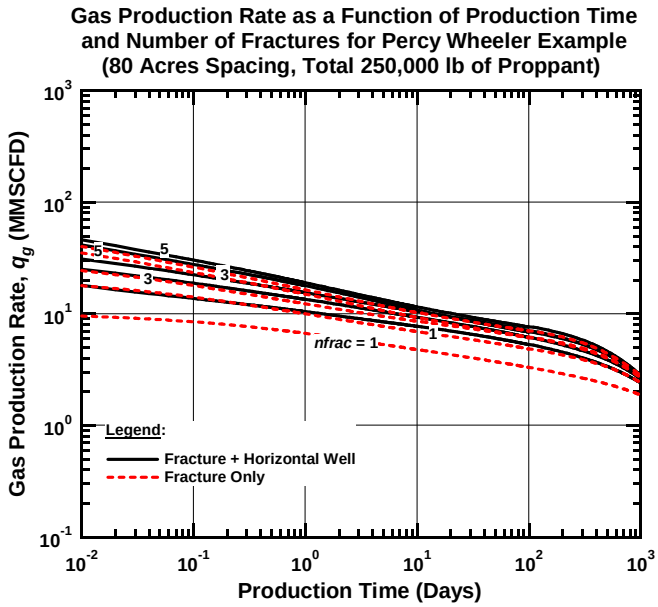

Figure H.1 — Gas Production Rate as a Function of Production Time, Number of Fractures, and Completion Scheme for Percy Wheeler Field (80 Acres Spacing, 250,000 lb Proppant)

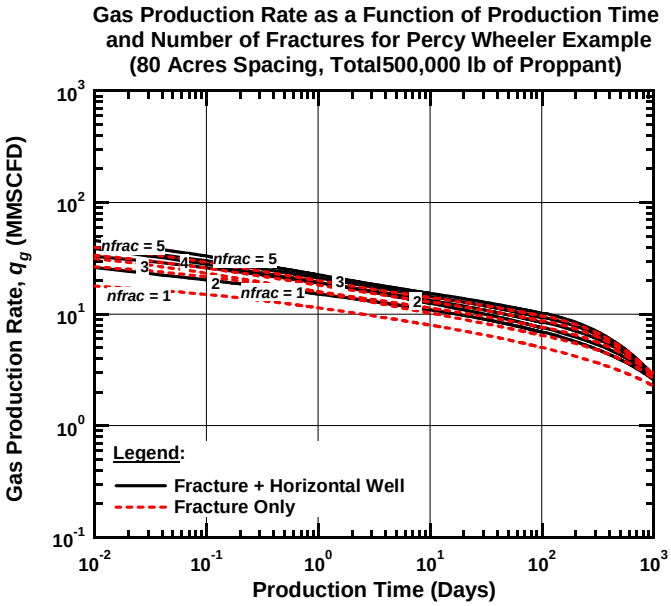

Figure H.2 — Gas Production Rate as a Function of Production Time, Number of Fractures, and Completion Scheme for Percy Wheeler Field (80 Acres Spacing, 500,000 lb Proppant)

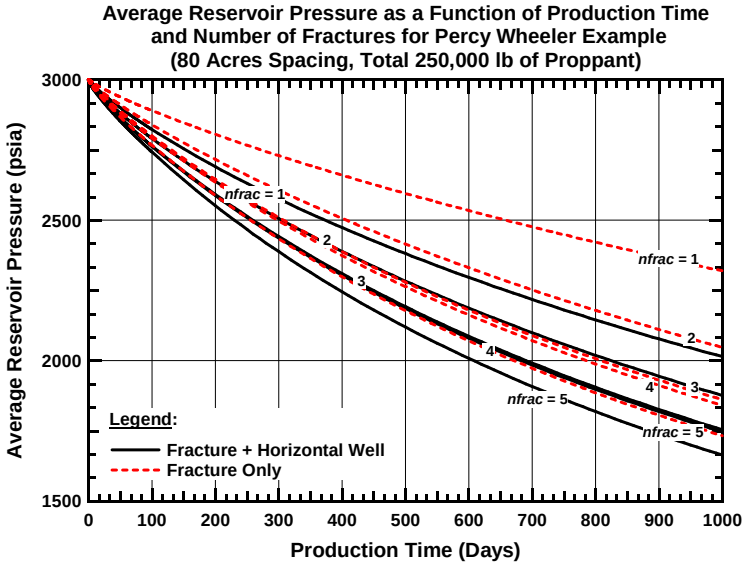

Figure H.3 — Average Reservoir Pressure as a Function of Production Time, Number of Fractures, and Completion Scheme for Percy Wheeler Field (80 Acres Spacing, 250,000 lb Proppant)

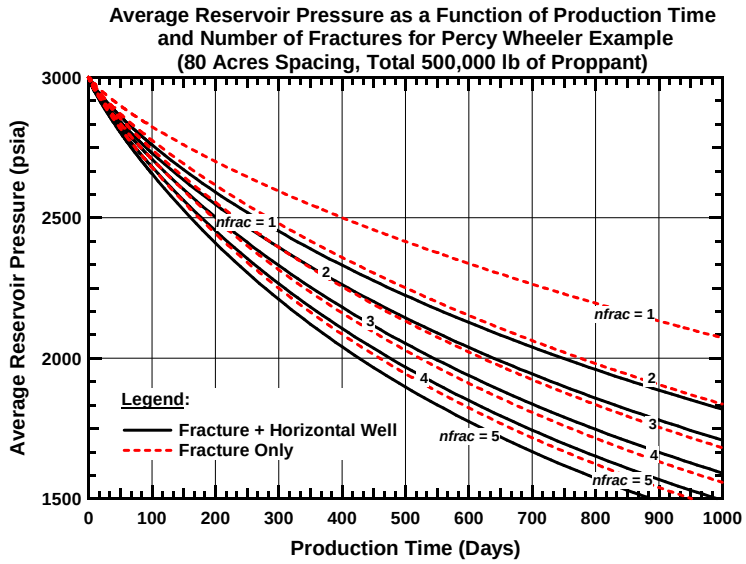

Figure H.4 — Average Reservoir Pressure as a Function of Production Time, Number of Fractures, and Completion Scheme for Percy Wheeler Field (80 Acres Spacing, 500,000 lb Proppant)

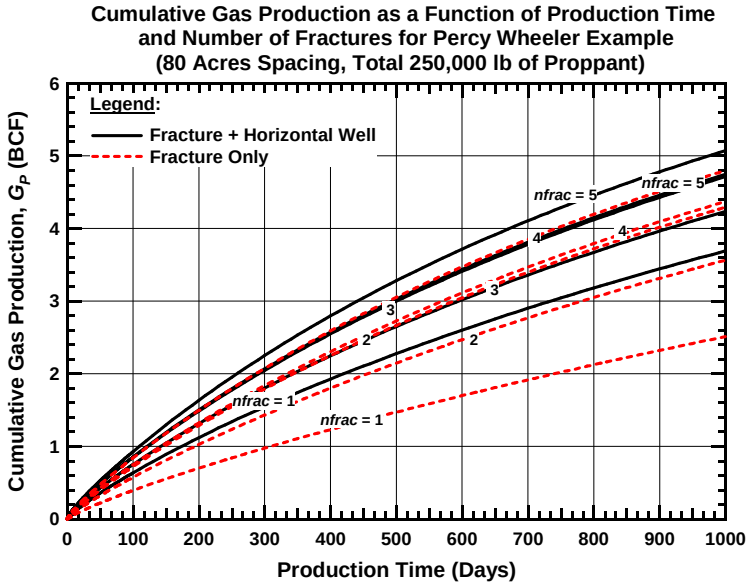

Figure H.5 — Cumulative Gas Production as a Function of Production Time, Number of Fractures, and Completion Scheme for Percy Wheeler Field (80 Acres Spacing, 250,000 lb Proppant)

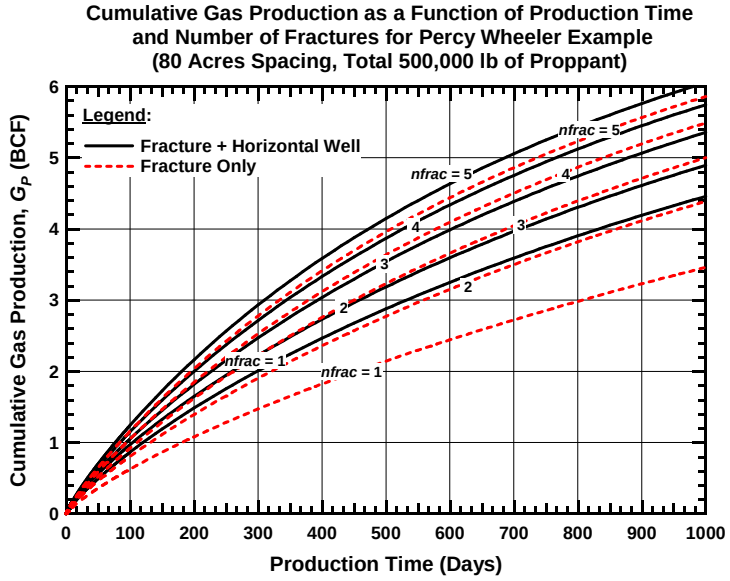

Figure H.6 — Cumulative Gas Production as a Function of Production Time, Number of Fractures, and Completion Scheme for Percy Wheeler Field (80 Acres Spacing, 500,000 lb Proppant)

APPENDIX I

COMPLETE RESULTS OF FIELD APPLICATION APPLEBY NORTH GAS FIELD

The material balance equation for dry gas volumetric reservoirs has been integrated to the results of DVS calculation to obtain the production performance behavior of Appleby North field in East Texas, USA. This Appendix provides figures of the estimation of gas production rate, average reservoir pressure, and cumulative gas production of this field for an 80-acre spacing, development plan as a function of the completion scheme— Fracture and horizontal section produce together and production only from fractures—, number of transverse fractures, and the amount of propant (250,000 and 500,000 lb).). **Table I.1** Provides the reservoir and fluid properties used for the calculations

Table H.1— Reservoir and Fluid Properties for Percy Wheeler Field Example

	Appleby North
Net Pay (ft)	60
Hor. Permeability (md)	0.01
Porosity (%)	8.8
Initial Pressure (psia)	2800
Reservoir Temperature(°F)	254
Gas Gravity	0.61
Gas in Place(BCF)	2.706

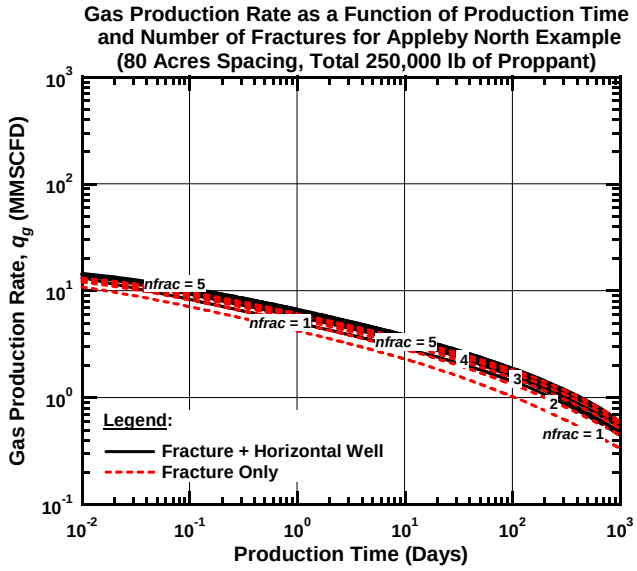

Figure I.1 — Gas Production Rate as a Function of Production Time, Number of Fractures, and Completion Scheme for Appleby North Field (80 Acres Spacing, 250,000 lb Proppant)

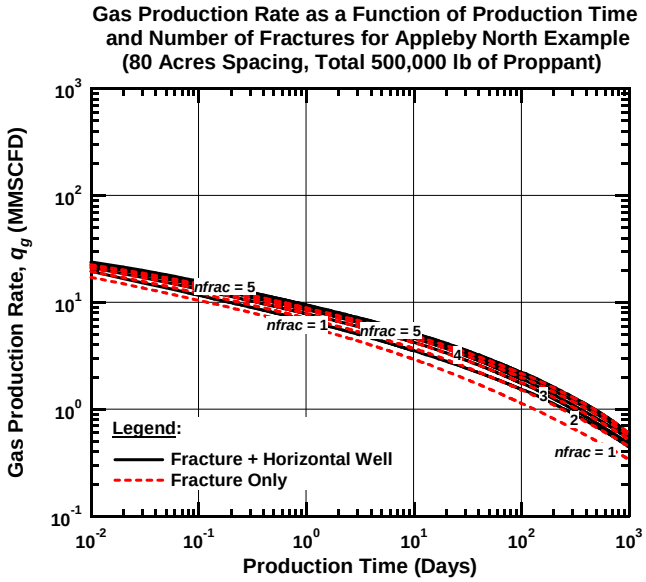

Figure I.2 — Gas Production Rate as a Function of Production Time, Number of Fractures, and Completion Scheme for Appleby Nprth Field (80 Acres Spacing, 500,000 lb Proppant)

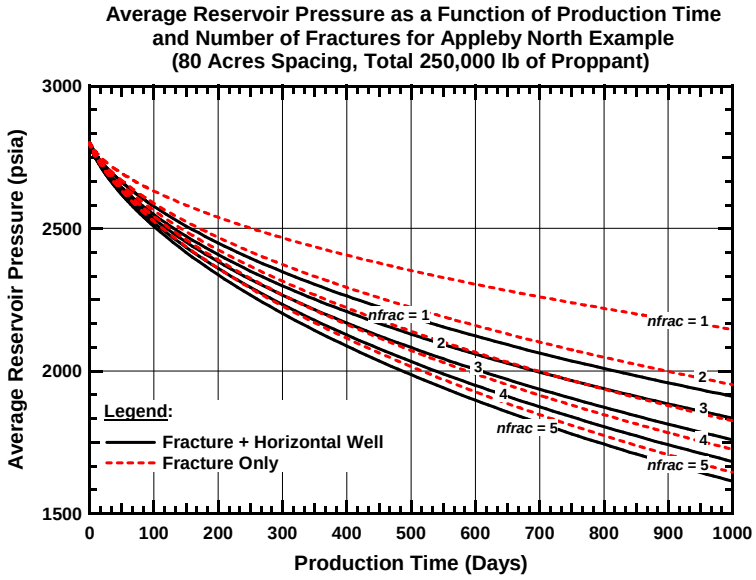

Figure I.3 — Average Reservoir Pressure as a Function of Production Time, Number of Fractures, and Completion Scheme for Appleby North Field (80 Acres Spacing, 250,000 lb Proppant)

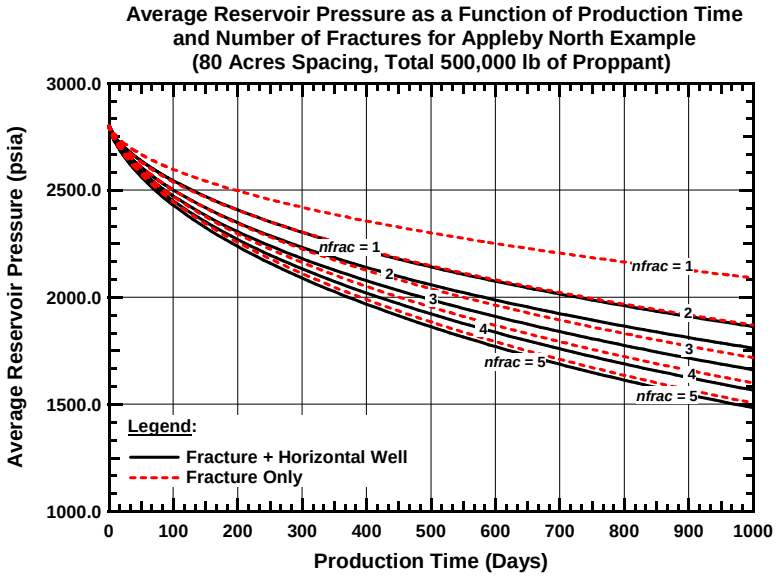

Figure I.4 — Average Reservoir Pressure as a Function of Production Time, Number of Fractures, and Completion Scheme for Appleby North Field (80 Acres Spacing, 500,000 lb Proppant)

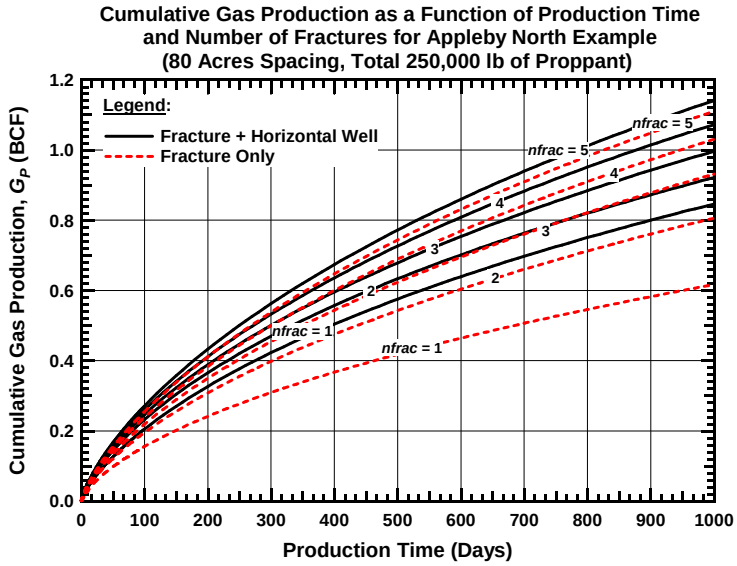

Figure I.5 — Cumulative Gas Production as a Function of Production Time, Number of Fractures, and Completion Scheme for Appleby North Field (80 Acres Spacing, 250,000 lb Proppant)

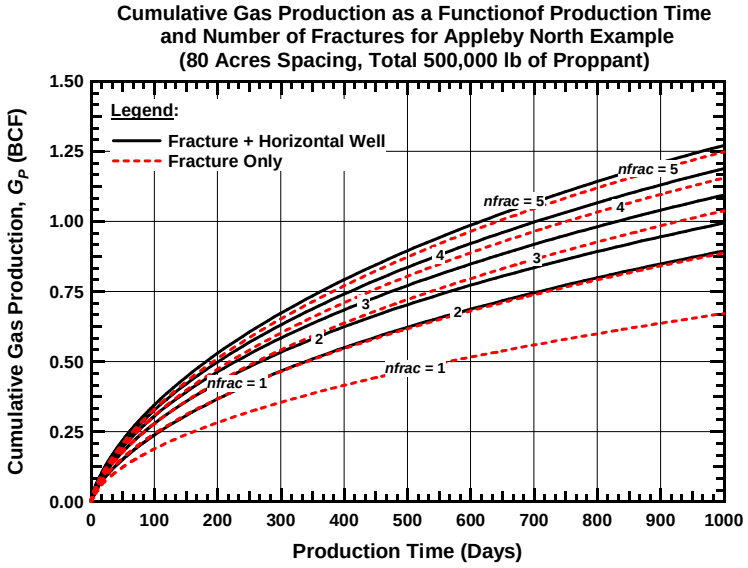

Figure I.6 — Cumulative Gas Production as a Function of Production Time, Number of Fractures, and Completion Scheme for Appleby North Field (80 Acres Spacing, 500,000 lb Proppant)

VITA

Name:	Shahram Amini
Mailing Address:	31 Ehsan Street Farahzadi Boulevard Shahrak E Gharb Tehran, 14689 83153 IRAN
E-mail Address:	Shahramamini@yahoo.com

Education:

Texas A&M University, College Station, Texas, USA
Doctor of Philosophy Degree in Petroleum Engineering
December 2007

IFP School (ENSPM), Rueil-Malmaison, France
Master of Science Degree in Reservoir Geosciences and Engineering
December 2000

University of Tehran, Tehran, Iran
Master of Science Degree in Chemical Engineering
June 1996

University of Tehran, Tehran, Iran
Bachelor of Science Degree in Chemical Engineering
September 1993

Affiliations: Society of Petroleum Engineers